GEOS 28600

The science of landscapes:
Earth & Planetary Surface Processes

Lecture 17

Wednesday 4 March 2020

(1) Count layers (tree rings, varves).
(2) Optically stimulated luminescence.
(3) Radiocarbon - ^{14}C.
(4) Spike of radioactive elements (e.g. tritium) associated with atmospheric nuclear testing.
(5) Cosmogenic dating.
(6) Fission track.
(7) (U-Th)/He & other exhumation methods.
(8) Shared event of known age.
(9) The sedimentary record.

(1) Count layers (tree rings, varves)

Varves: annual layers, most commonly in strongly-seasonal lakes

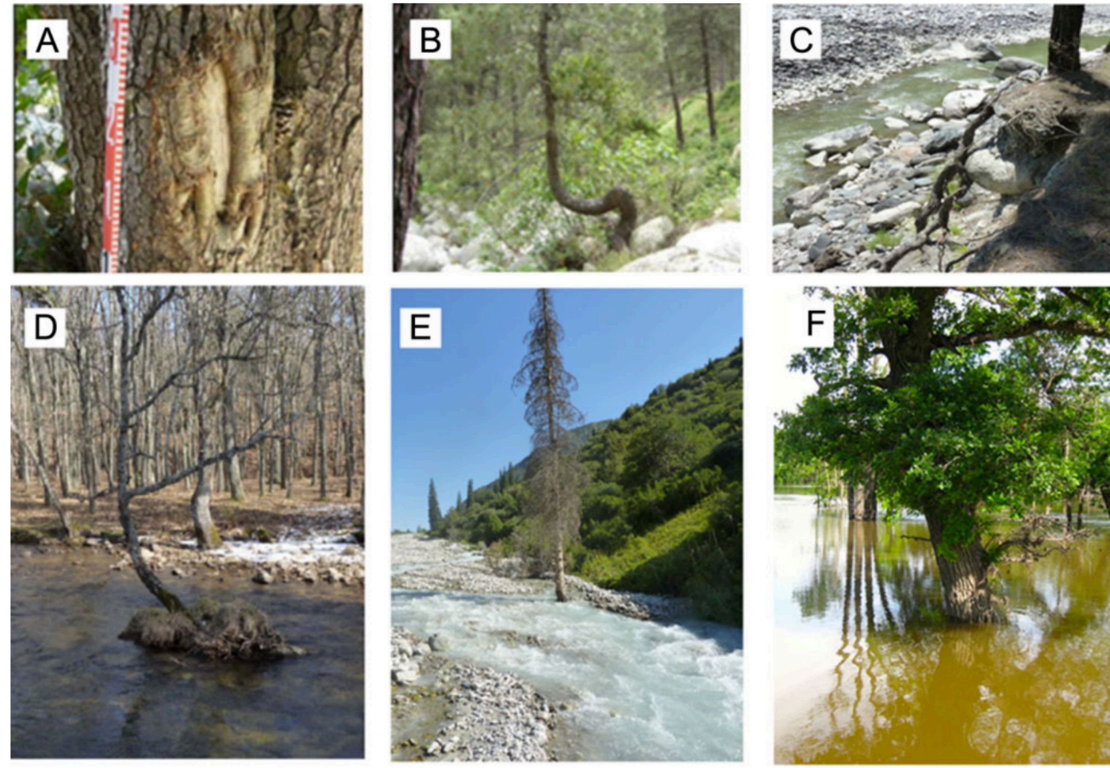

Figure 2. Types of botanical evidence used to identify paleofloods using tree rings. (A) Trees can be injured by the impact or abrasion of boulders or course woody debris transported by flood waters. (B) Flood debris may break the main stem, causing trees do adopt unusual stem morphologies after regrowth. (C) Bank erosion caused by flooding can cause tree roots to become sub-aerially exposed. (D) The hydraulic pressure of floodwaters can tilt tree stems. (E) Changes in channel position or pattern can kill trees growing within the riparian zone. (F) Flooding during the early growing season can cause inundated oak trees to form abnormal anatomical structures within the newly formed wood.

Tree rings – when found embedded in e.g. flood deposits

Ballesteros-Cavenos, Prog. Phys. Geogr. 2015

Example application: mass movements and debris flows → tree death in Southern Alps
Strengths: Well-established, interlocked chronologies for most continents.
Weaknesses: Requires wood preservation (for tree rings). Rarely, tree ring years are “missing” in individual trees.
Time range of application: to 15 Kyr (tree rings); to ~14 Kyr (Cariaco varves); out to 30 Kyr (“floating” varve chronologies, e.g. Lake Suigetsu)

(2) Optically Stimulated Luminescence (OSL)

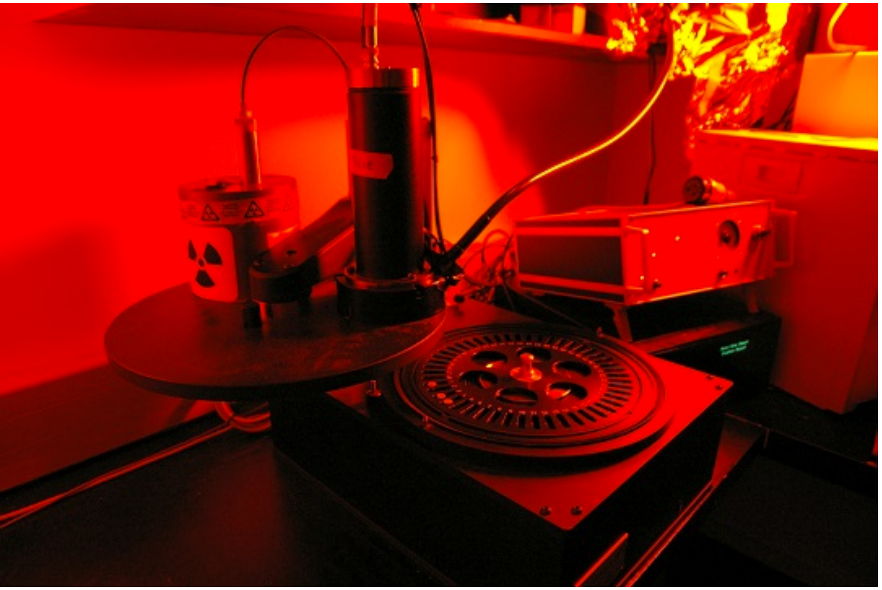

Rhodes et al. Annual Reviews 2011

Strengths: date sand dune overturn, beach sands …

Weaknesses: 5-10% uncertainty; usually requires quartz; collection can be difficult (age reset by 1s of light).

Age range of validity: 0.1-350 Kyr with quartz (out to 1 Myr with feldspar)

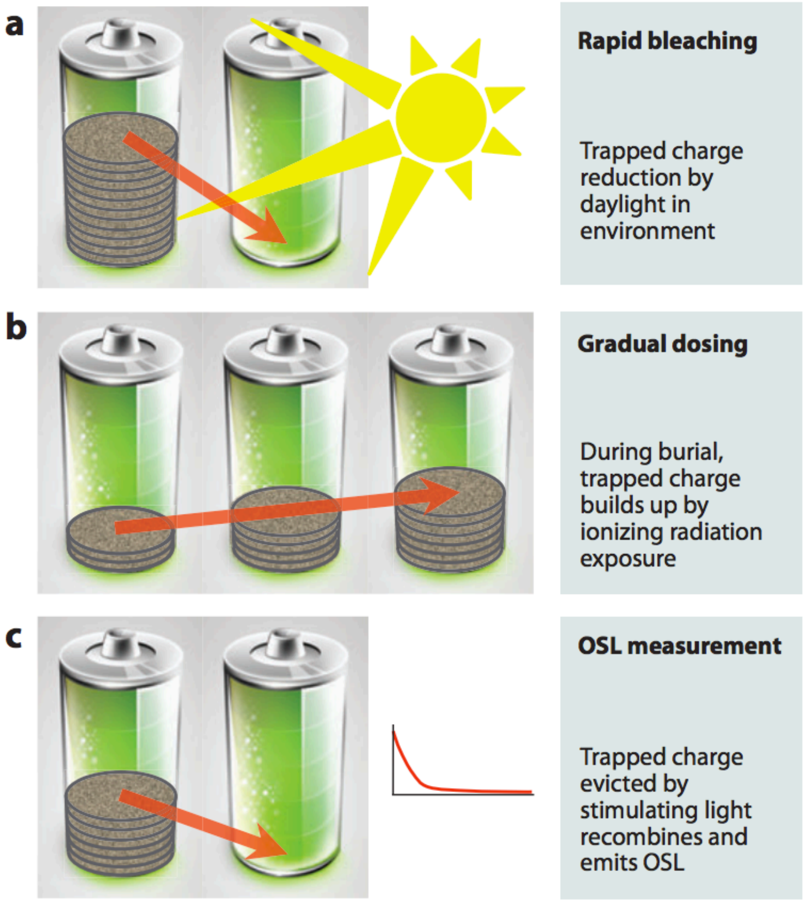

Figure 4

The rechargeable battery forms a useful analogy to help understand optically stimulated luminescence (OSL) dating; gray circles show charge level. (*a*) Daylight releases trapped charge during grain movement over periods of seconds to minutes. (*b*) Charge is slowly built up as a small fraction of electron-hole pairs produced by low levels of environmental radiation are trapped at defects. (*c*) After sample collection and preparation, intense stimulating light releases charge from light-sensitive traps, which recombines emitting UV luminescence, in the form of an OSL decay (shown). Based on an illustration by Duller (2008).

Mechanism of OSL:

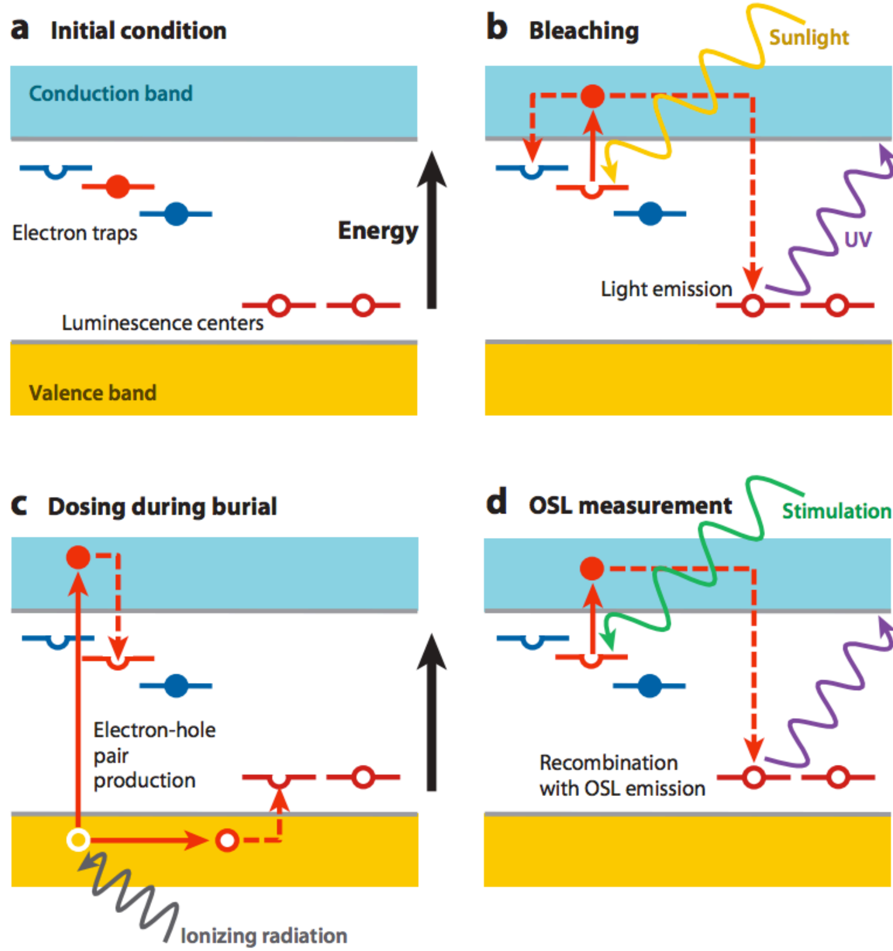

Figure 2

Simple band gap energy model of optically stimulated luminescence (OSL). Light-sensitive (OSL) electron traps are shown in red, light-insensitive (thermoluminescence) traps in blue. (*a*) Under typical initial conditions, low thermal stability traps close to the conduction band are kept empty by thermal eviction at ambient temperature, but other traps are filled; luminescence centers are available. (*b*) On light exposure, electrons in OSL traps are evicted and may become trapped in other available trapping sites or may recombine at hole centers (luminescence centers). After brief light exposure, all OSL traps are emptied. (*c*) During subsequent burial, ionizing radiation gradually produces electron-hole pairs, some of which may become trapped, increasing the OSL trap population. (*d*) Following collection and mineral separation, intense blue-green stimulating light is directed at the sample. Electrons are evicted from OSL traps and recombine at luminescence centers, emitting UV luminescence, detected through glass filters with a photomultiplier tube. As the remaining OSL trap populations falls, the emission rapidly decays to a low level.

(3) Radiocarbon - ^{14}C.

Atmosphere contains ^{14}C (half-life 6 Kyr) due to cosmic-ray bombardment
Plants/soil organisms take up ^{14}C from atmosphere and isolate it upon burial
Isolation date can be constrained by measuring present-day ^{14}C concentration.

$$\frac{N_o}{2} = N_o e^{-\lambda t_{1/2}}$$
$$\frac{1}{2} = e^{-\lambda t_{1/2}} \quad (6.5)$$
$$t_{1/2} = -\frac{1}{\lambda} \ln\left[\frac{1}{2}\right]$$

New method: Accelerator Mass Spectroscopy
Eliminates molecular isobars (e.g. ^{13}CH) by accelerating sample to >>KeV and passing through a thin graphite foil.

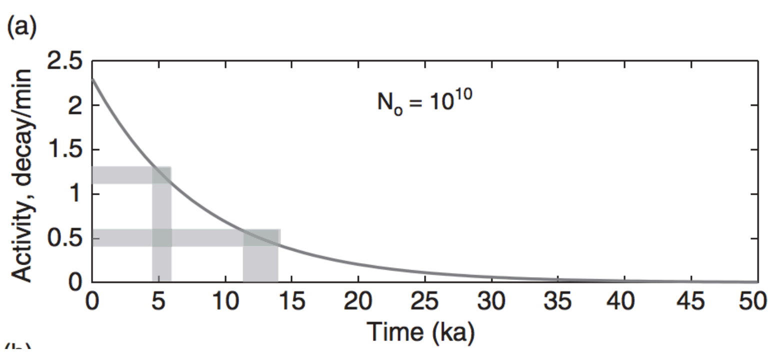

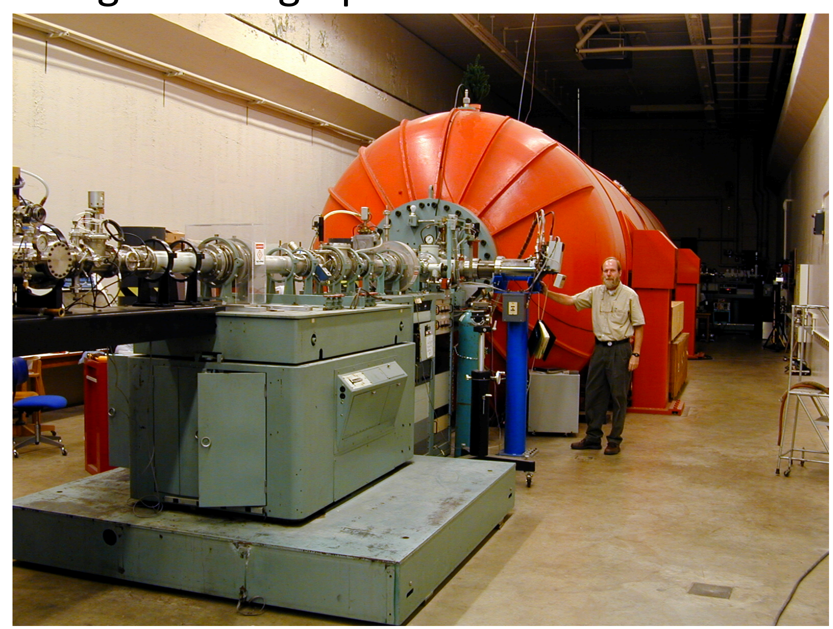

Mark Chaffee (Purdue)

Strengths: Precise, widely used,
can date soil profiles & fluvial deposits.
Example weaknesses: Reworking of old wood,
decay of ancient organic matter.
Time range of validity: 50+ Kyr

^{14}C measurements are very precise, but are affected by several systematic biases. "^{14}C age" is not equal to actual age. Ages are reported this way to allow for future improvements in ^{14}C de-biasing.

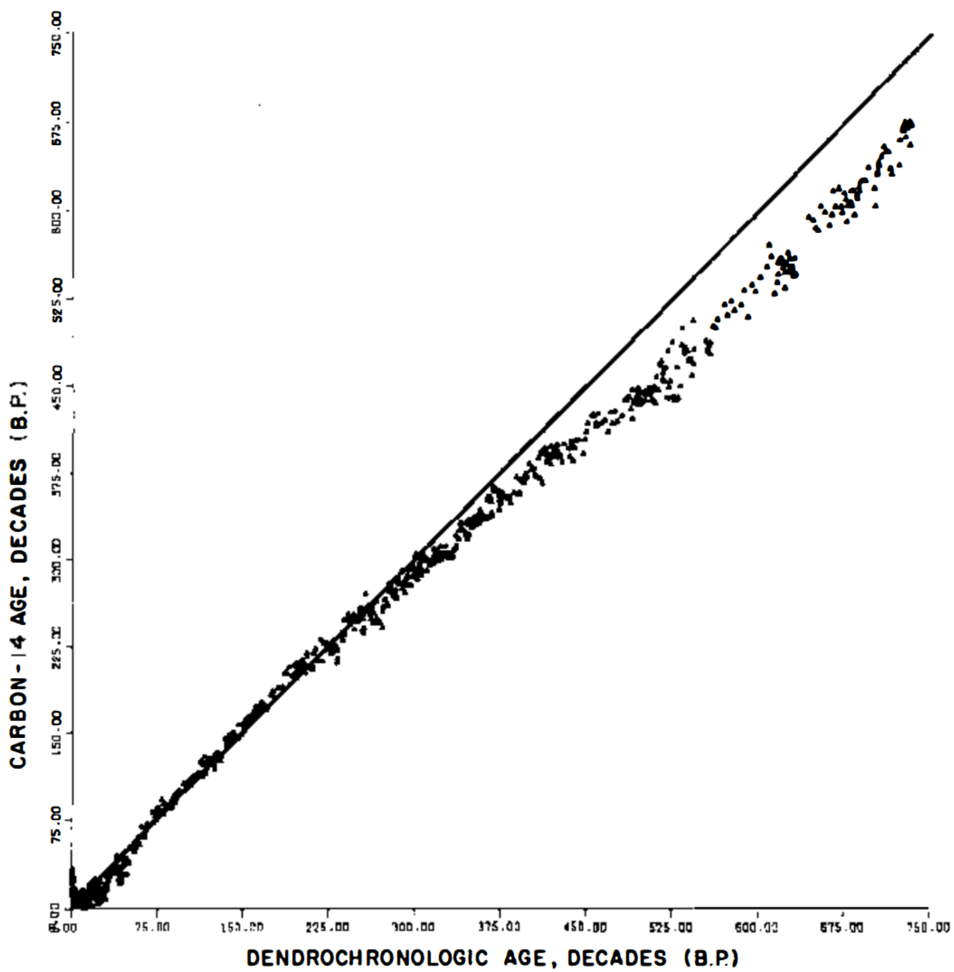

Past atmosphere contained more radiocarbon

Damon et al. Annual Reviews 1978

^{14}C uncertainty is affected by variations in the rate of production (& atmospheric content) of ^{14}C.

Varying magnetic field on Earth:

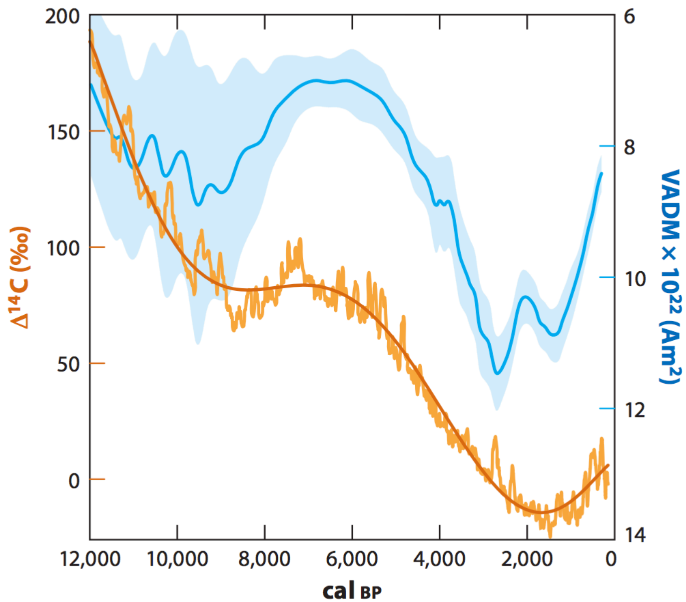

VADM = Virtual Axial Dipole Moment (Strength of Earth's magnetic field)

Varying solar activity (De Vries effect):

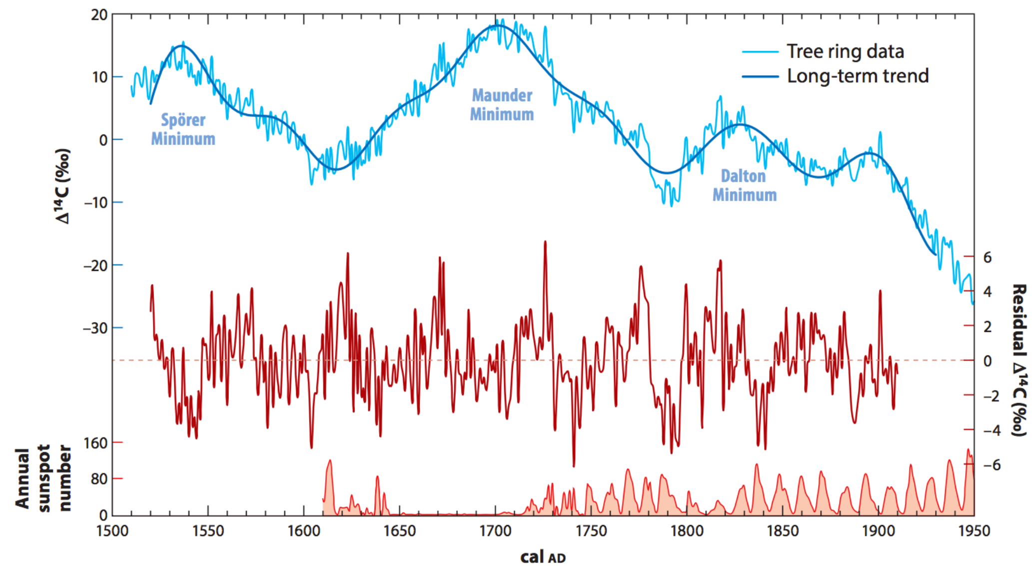

Figure 7

University of Washington Single Year (UWSY; Stuiver & Braziunas 1993b) $\Delta^{14}C$ data in tree rings from the Pacific Northwest (*thin light blue line*) showing the long-term trend (*thick dark blue line*). Periods of major minima (Spörer, Maunder, and Dalton) of solar activities over the last five centuries correspond to higher levels of atmospheric $\Delta^{14}C$. The addition of fossil fuel CO_2 after the onset of the Industrial Revolution lowered levels of atmospheric $\Delta^{14}C$ between 1900 and 1950. The middle curve (*dark red*) represents residuals of $\Delta^{14}C$, obtained by subtracting the long-term trend from the single-year data. The annual sunspot numbers observed since AD 1610 are indicated by the filled red curve at the bottom.

Also: Varying rates of atmosphere-ocean exchange.

(4) Spike of radioactive elements (e.g. tritium) associated with atmospheric nuclear testing

Also: fossil-fuel burning dilutes atmopsheric C with radioactively-inert C

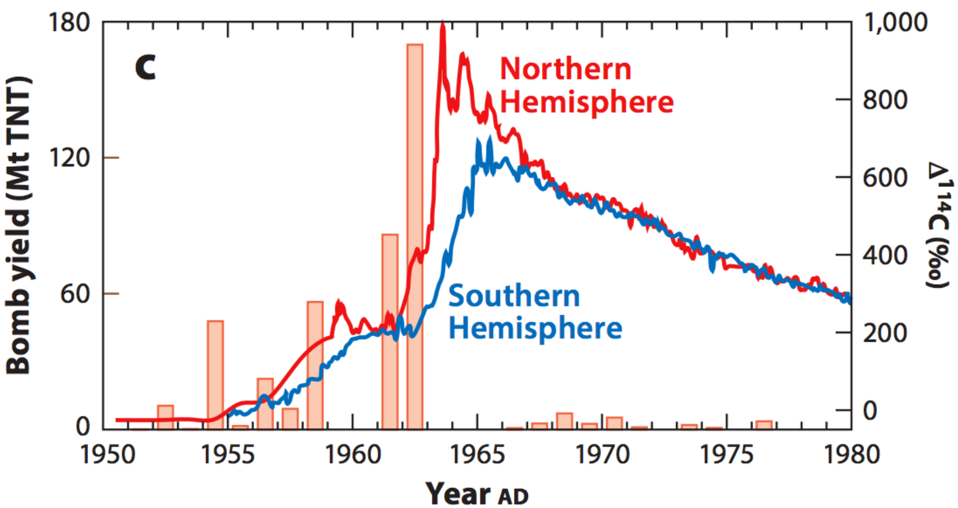

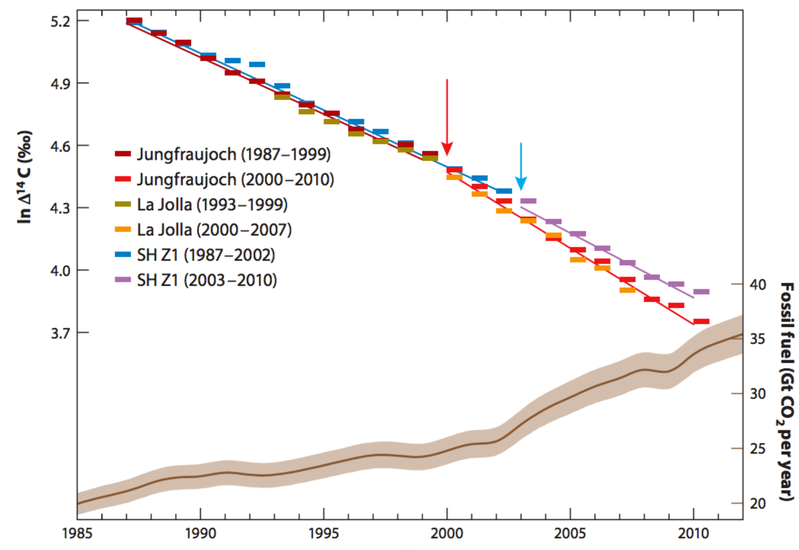

Dutta, Annual Reviews, 2016

(5) Cosmogenic dating

Alongside LIDAR, one of the two most important innovations in geomorphology in the last 20 years

- Produced within rock (not absorbed from atm.), mostly by neutrons
- 10Be, 26Al, 36Cl are radioactive
- Depth profiles allow correction for inheritance

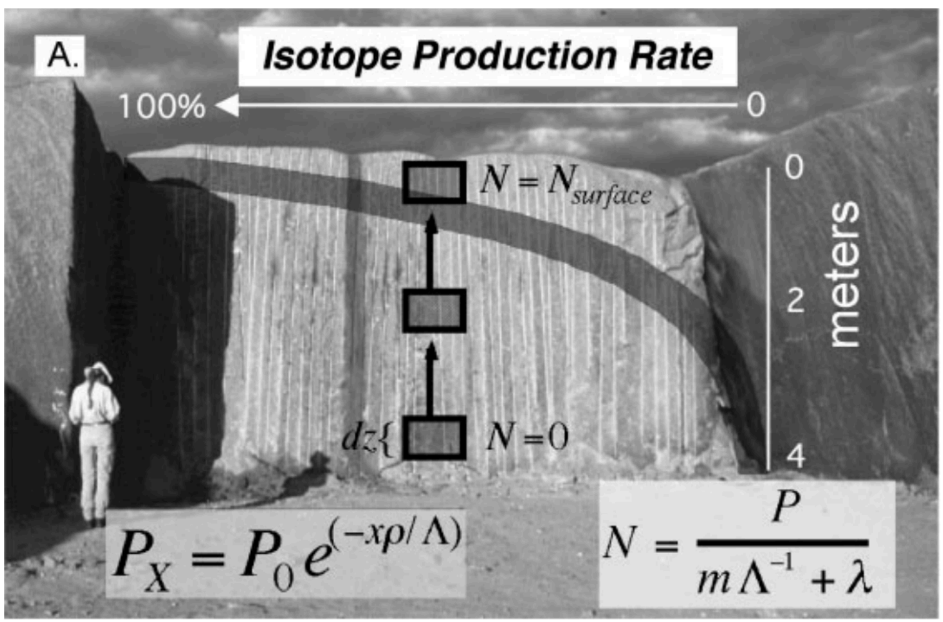

Bierman & Nichols Annual Reviews 2004

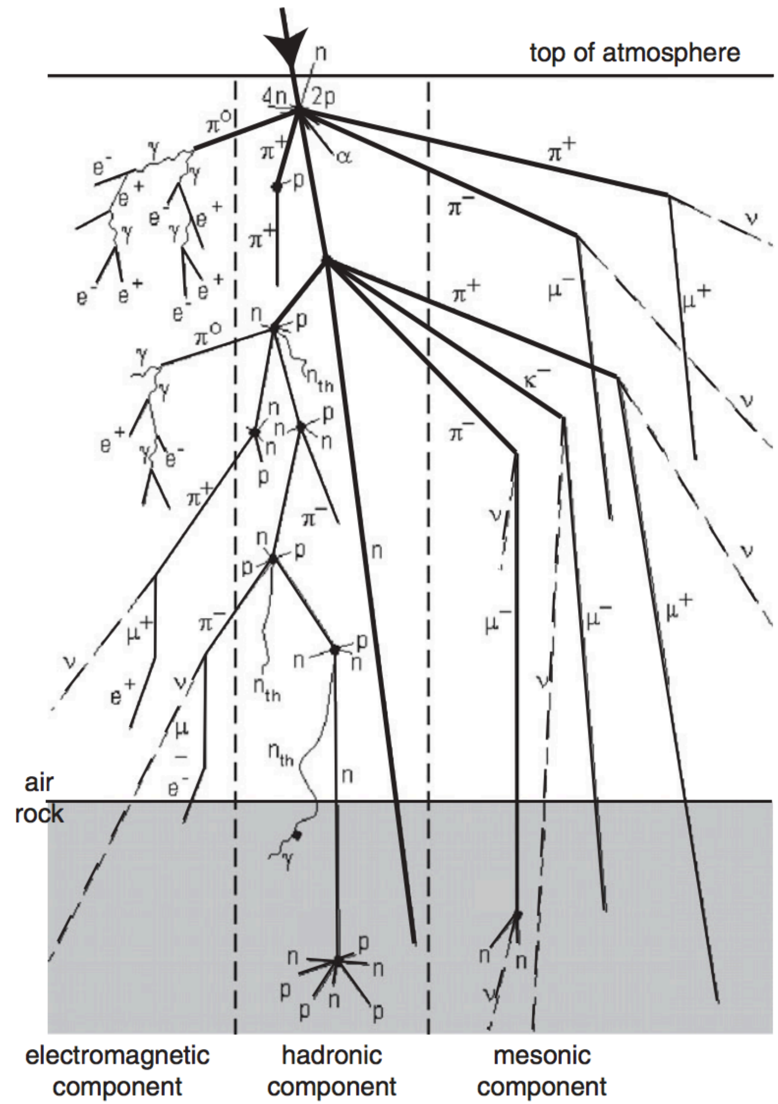

Figure 6.12 Cascade of particle interactions generated by the entrance of a high-energy particle at the top of the atmosphere. Cosmogenic nuclides produced both in the atmosphere and in the top few meters of rock most commonly result from at least secondary particles.

Anderson & Anderson, ch. 6

Equilibrium between production and decay for cosmogenic radionuclides with no erosion

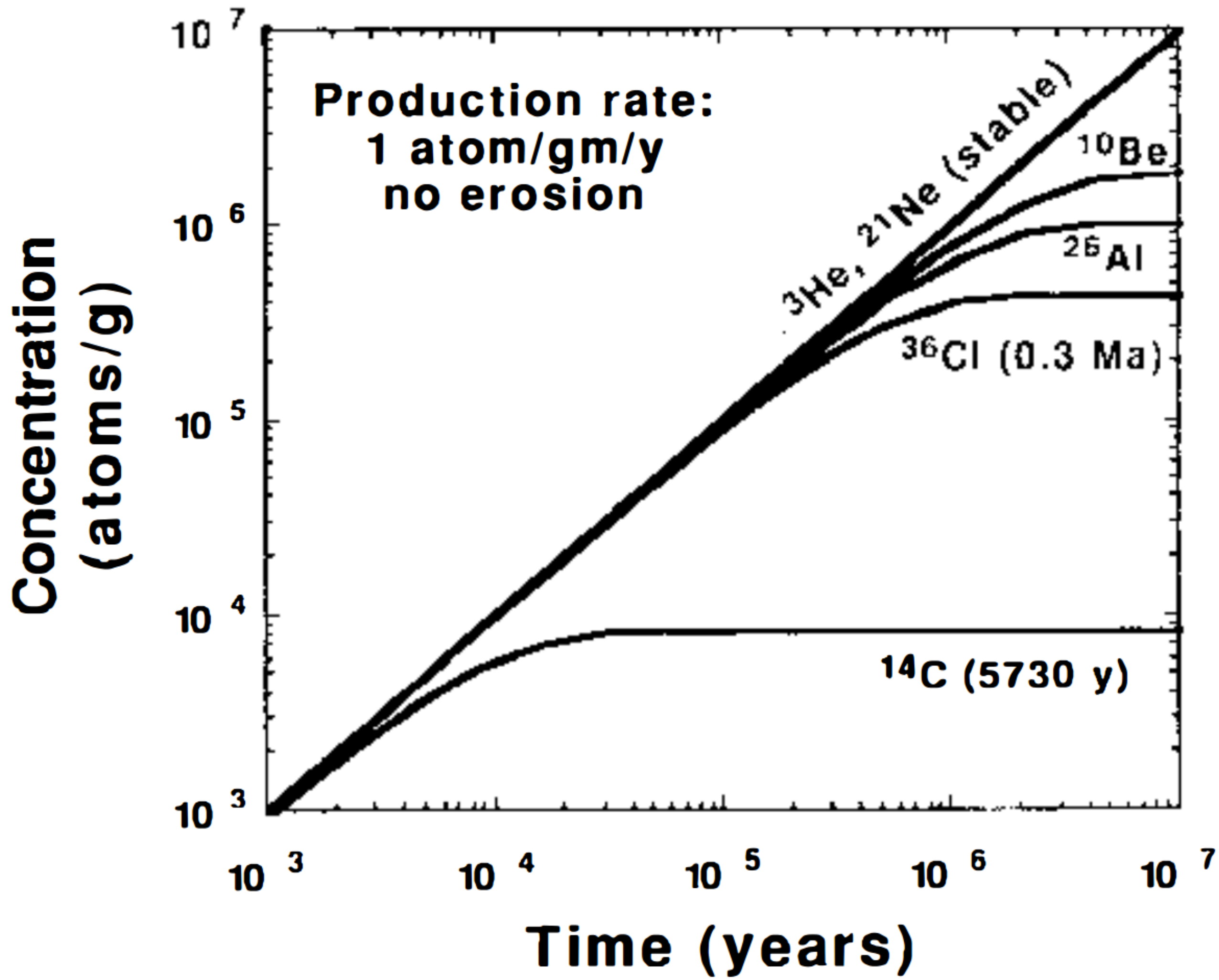

Figure 8 Concentration of in-situ cosmogenic isotopes for a sample with a constant production rate for the case with no erosion. Radioactive cosmogenic isotopes approach a steady-state concentration after about 5 half-lives.

Equilibrium between production and erosion for a stable cosmogenic isotope (e.g., 3He)

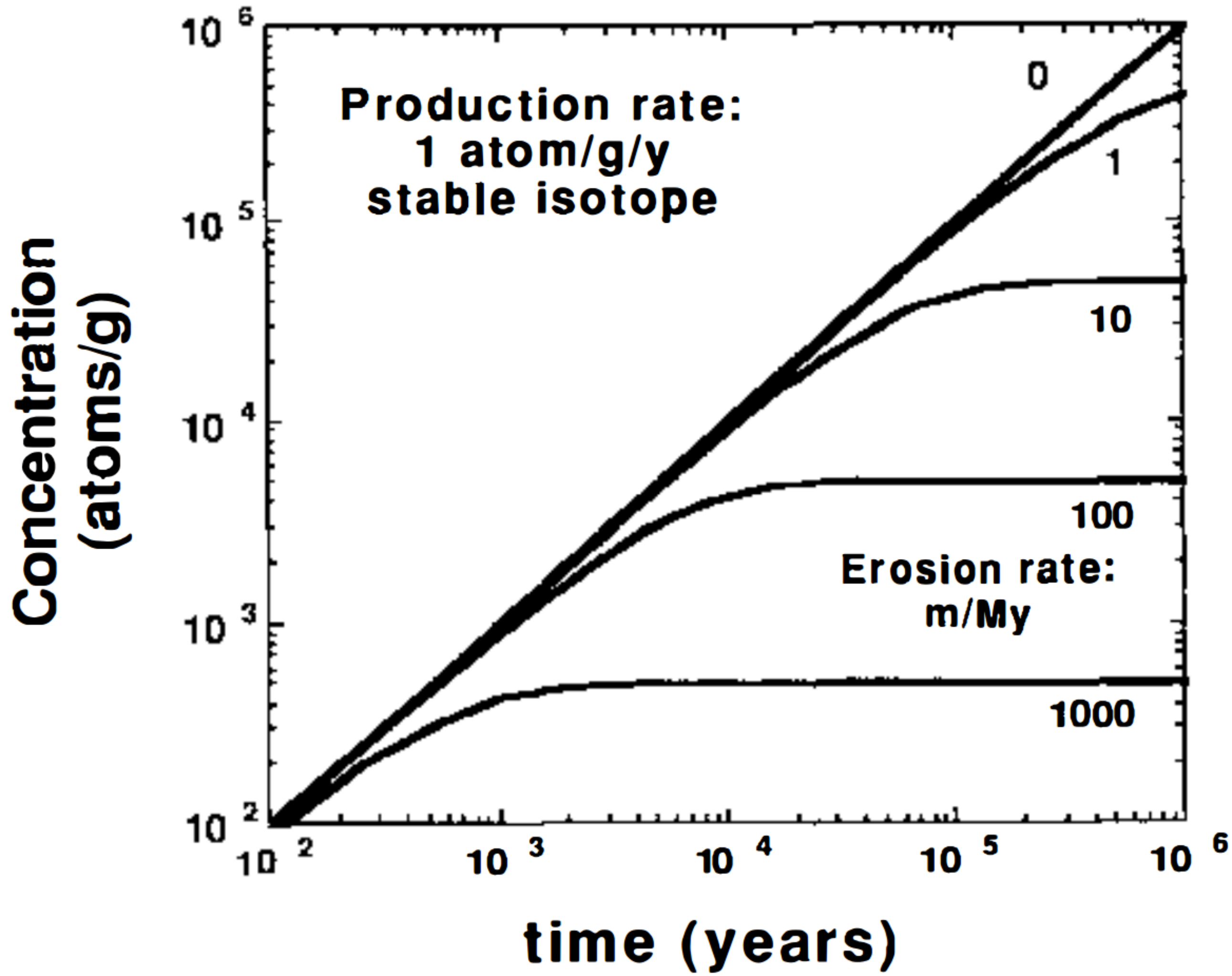

Figure 9 Concentrations of in-situ stable isotopes for samples with erosion rates ranging from 0 to 1000 m/My.

Softer cosmic ray energy spectrum
at high latitudes (due to Earth's magnetic field)

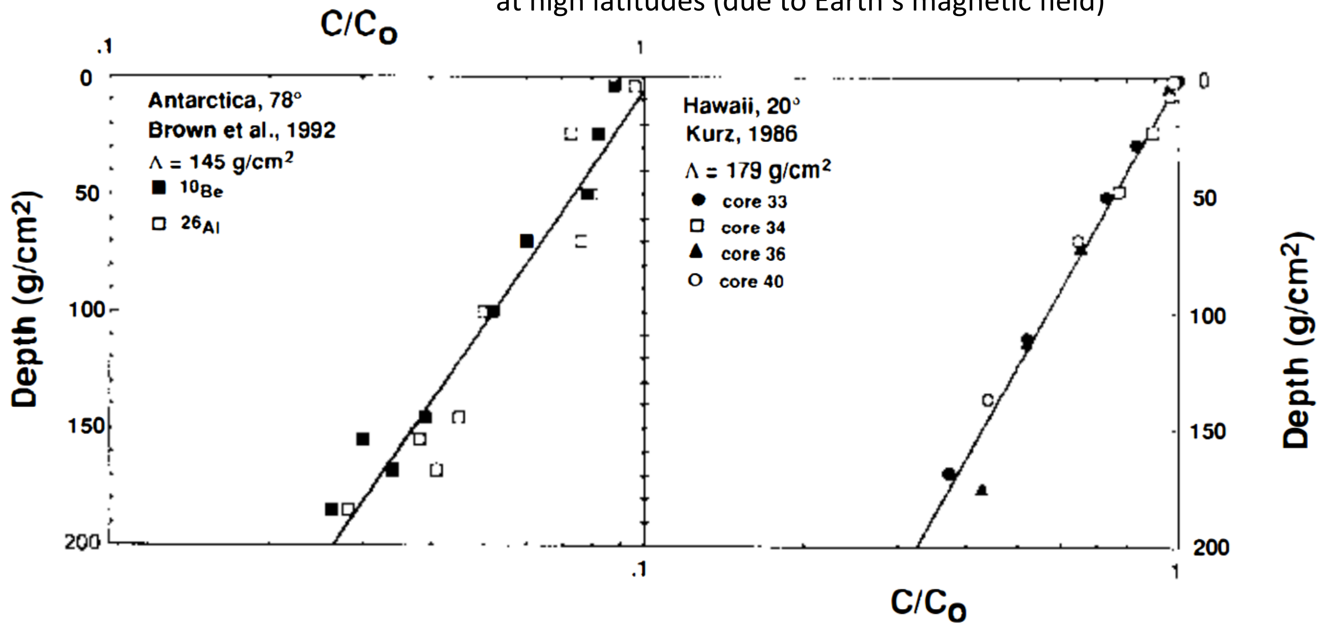

Cerling & Craig,
Annual Reviews 1994

Figure 2 Mass attenuation effects for samples from high latitude and from low latitude. Data from Brown et al (1992) and Kurz (1986b) for rock sample depths less than 200 g/cm^2. Concentrations are normalized to the Earth's surface.

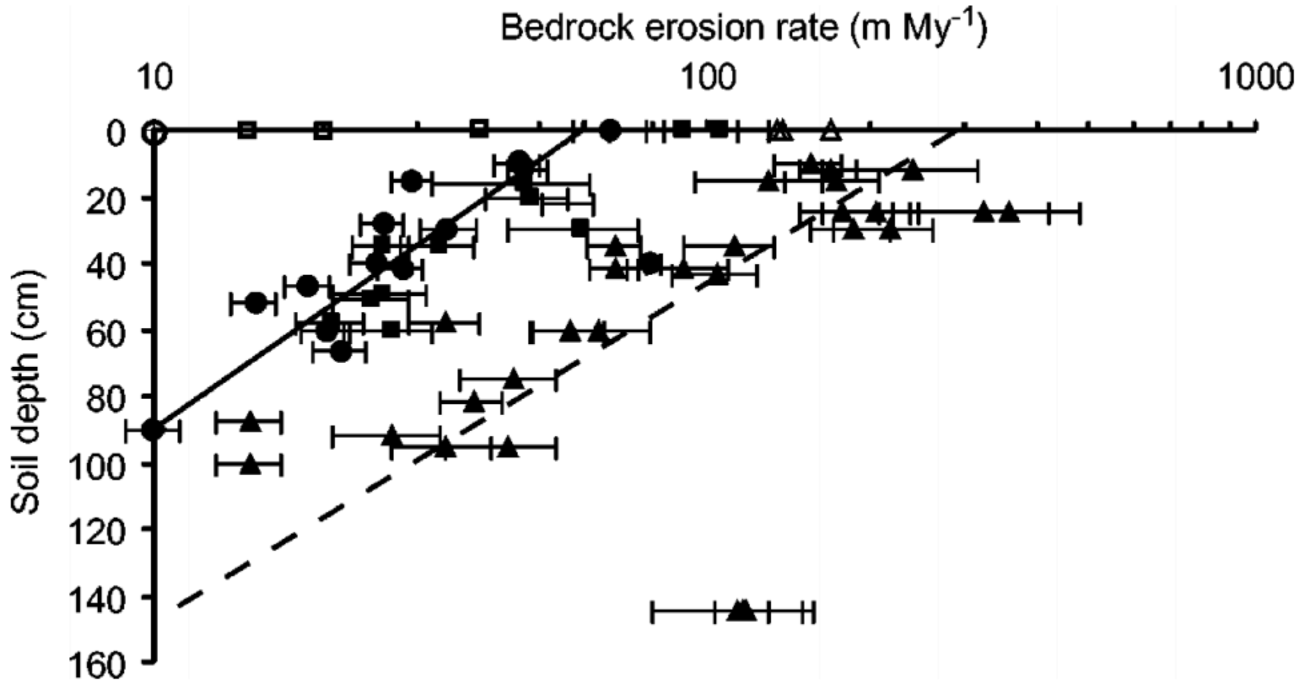

Figure 12 Compilation of soil production rates versus soil depth showing that bedrock erosion rates decrease as soil cover depth increases. Exposed outcrop samples are shown as open symbols and soil production rates are shown as filled symbols for southeastern Australia (*circles*); for Tennessee Valley, California (*squares*); and for Sullivan Creek, Oregon (*triangles*). Modified from Heimsath et al. (1997, 2000, 2001).

Bierman et al. Annual Reviews 2012

(6) Fission track dating

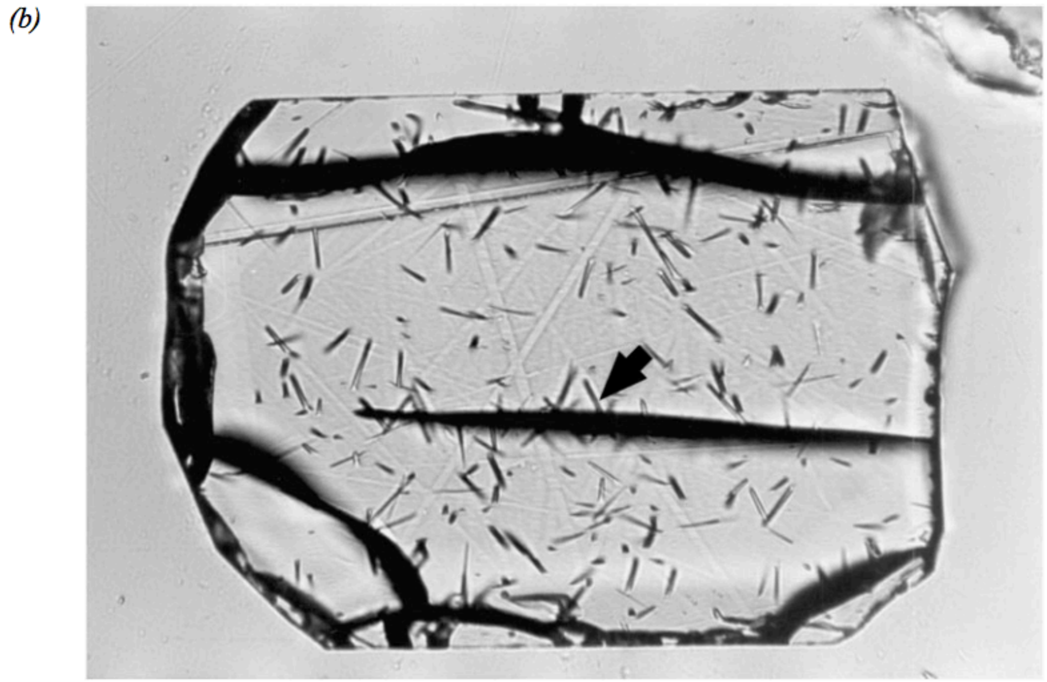

Figure 2 (*a*) Transmission electron microscope images of an unetched fission track in fluorapatite (from Paul & Fitzgerald 1992; reproduced with permission from the Mineralogical Society of America). (*b*) Photomicrograph of a polished and etched prismatic section through an apatite crystal, showing etched surface intersecting tracks and a horizontal confined track (*arrow*). The acid etchant reached the confined track through a large fracture. The long axis of the grain is ~150 μm.

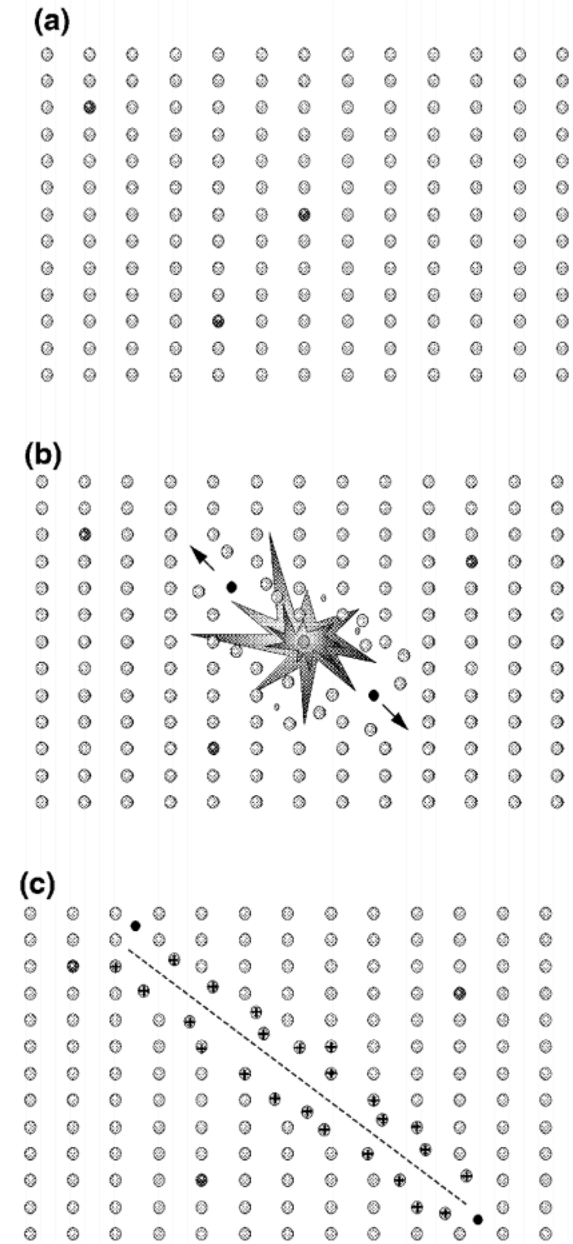

Gallagher et al. Annual Reviews 1998

The meaning of "closure temperature"

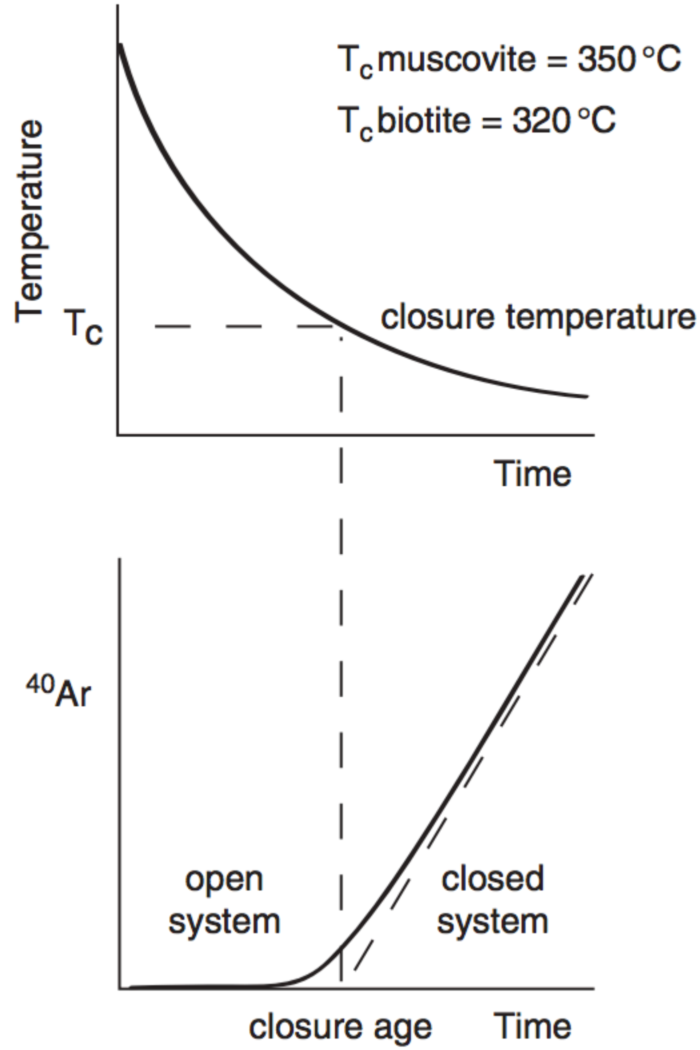

Closure temperature varies depending on what's escaping, and on what mineral it's escaping from.

Figure 6.35 $^{40}Ar/^{39}Ar$ system. The system is open to diffusive loss of ^{40}Ar at high temperatures, becoming progressively more closed and retentive of ^{40}Ar as temperature cools during exhumation.

(6) Fission track.

why are these
not straight lines?

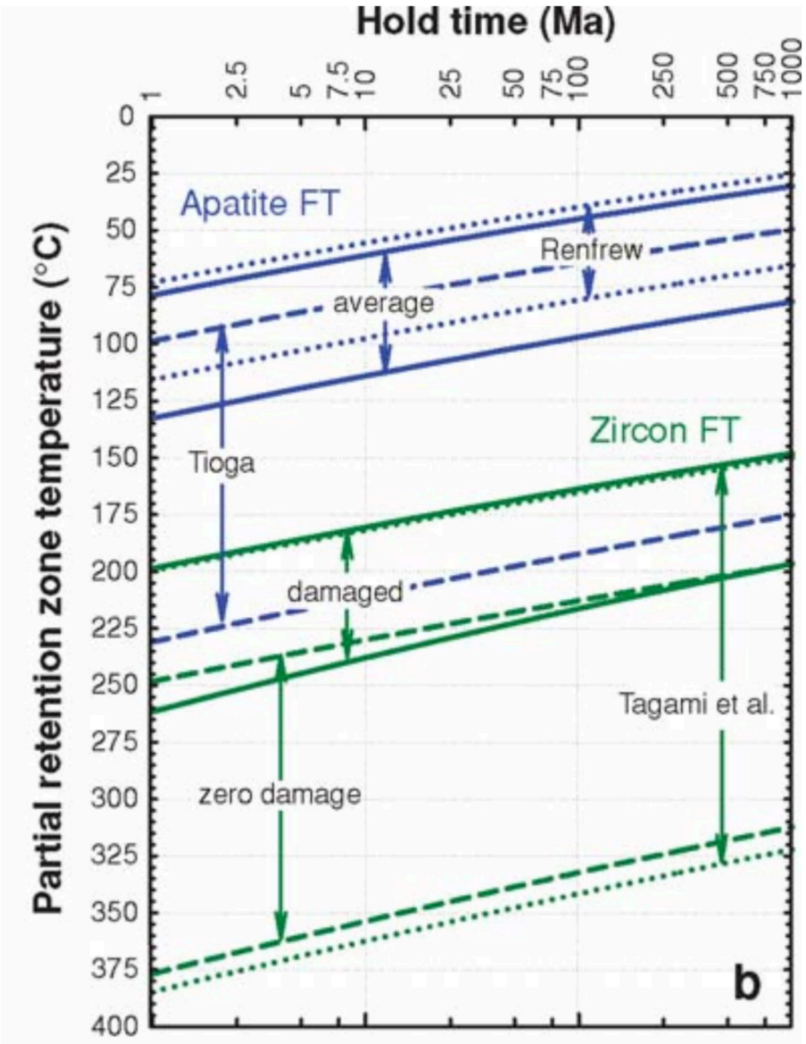

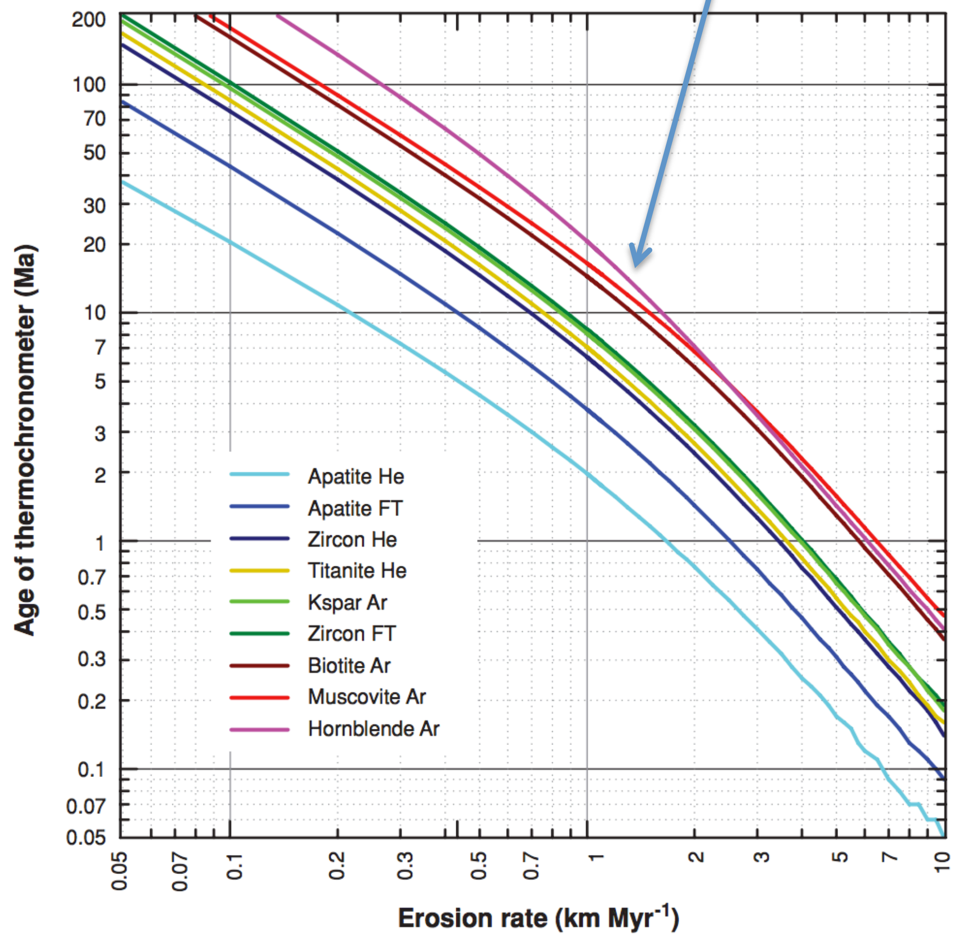

Mountain belt uplift:
Pe = L*u/kappa ~ 30 km*(1 mm/yr)/10^{-6} m^2s^{-1} ~ 1

Reiners & Brandon,
Annual Reviews 2006

Example application: Olympic Peninsula

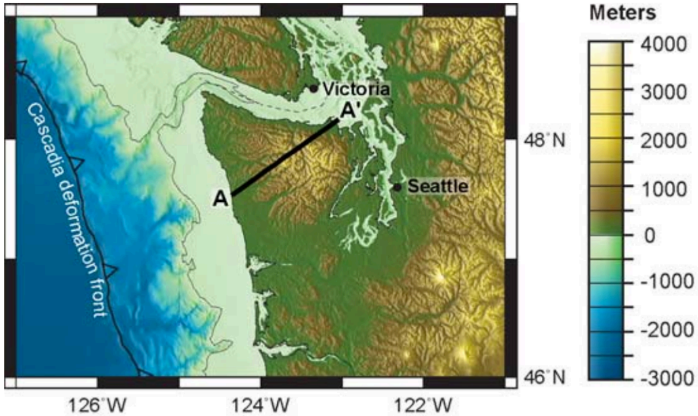

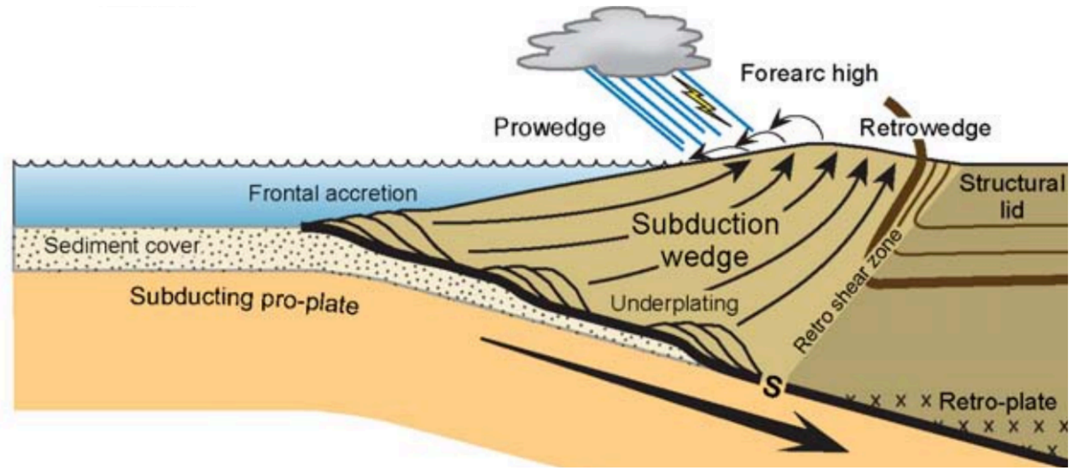

“strath” rates: uplift
of dated marine terraces

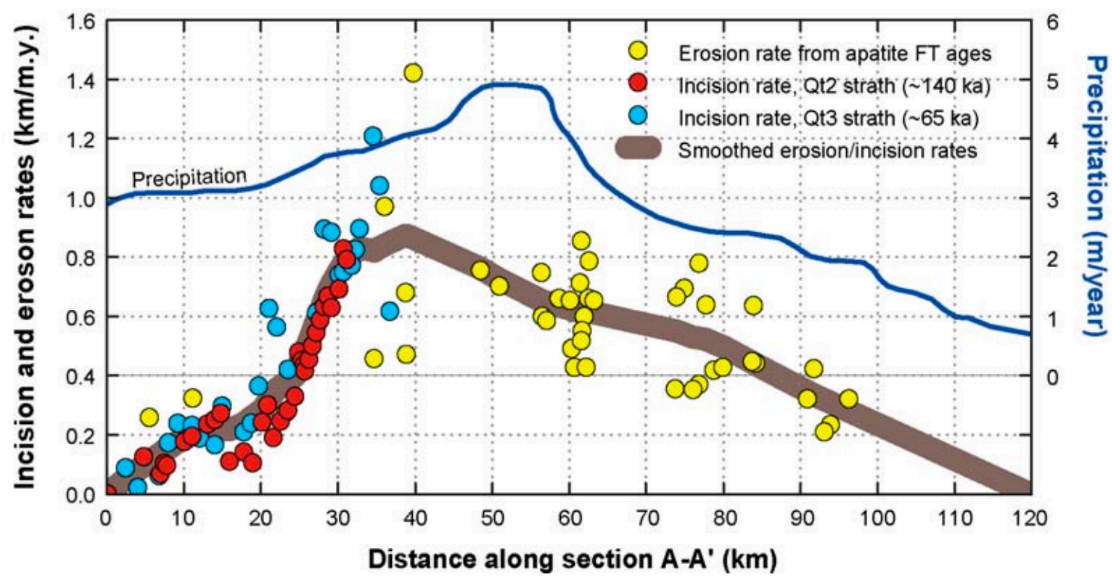

(7) (U-Th)/He & other exhumation methods.

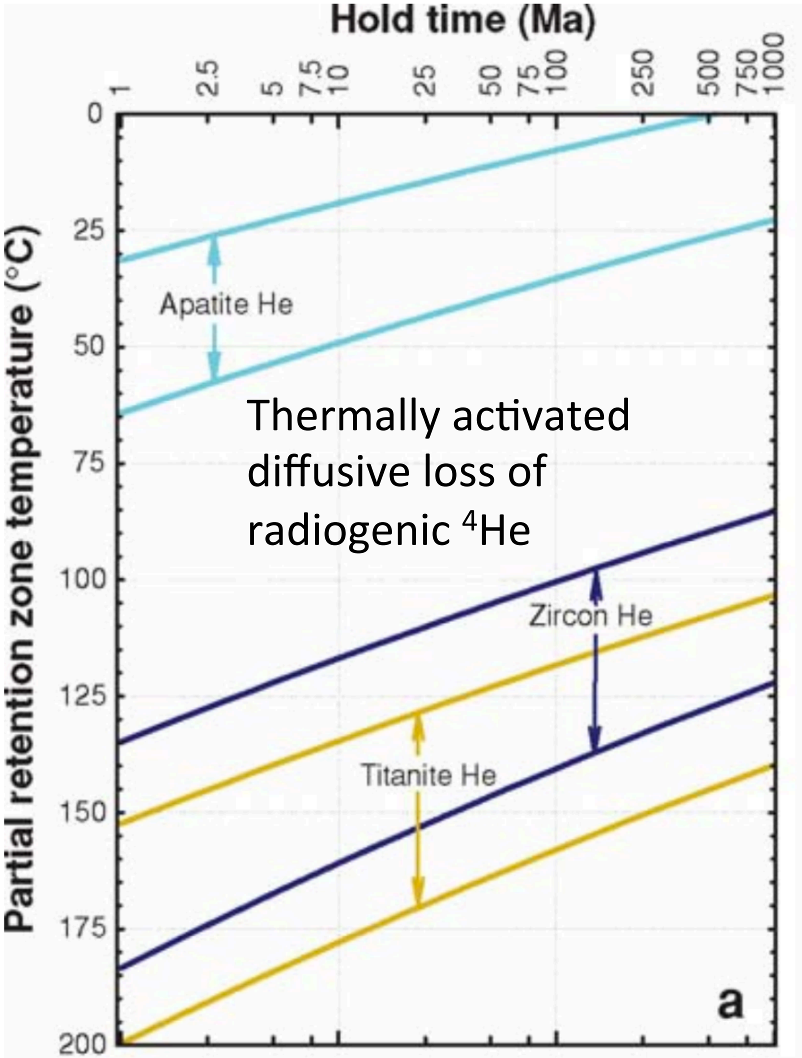

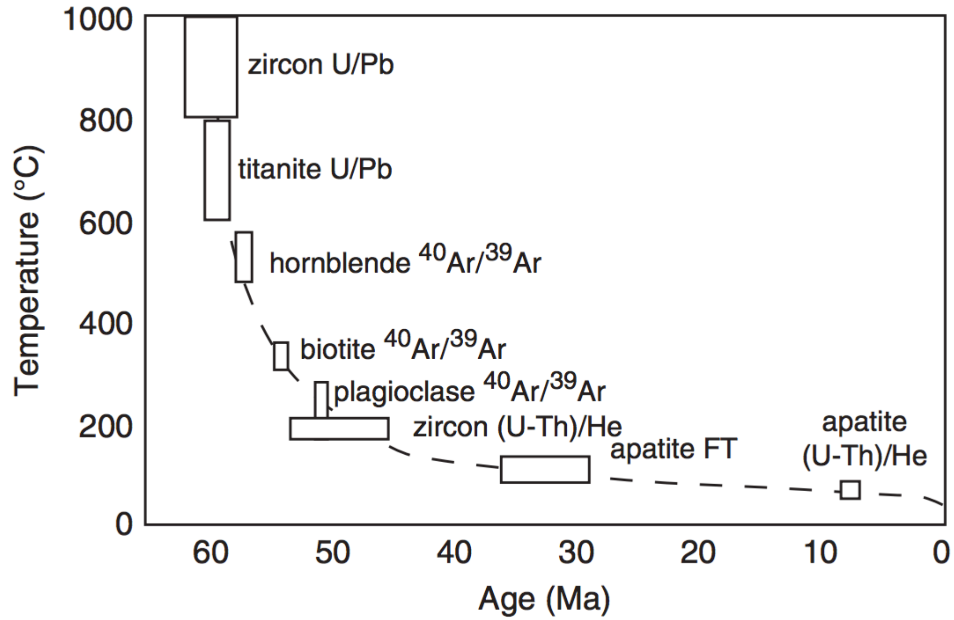

Figure 6.33 Temperature history of the Speel pluton, Alaska, derived from several thermochronometers. The data reveal rapid cooling after emplacement, followed by rapid cooling caused by exhumation after 10 Ma (after Reiners, 2005, Figure 3A and references therein, with permission from the American Geophysical Union).

(7) - Detrital thermochronology

Enabling technology: $^{40}Ar/^{39}Ar$ ages of <u>individual grains</u>

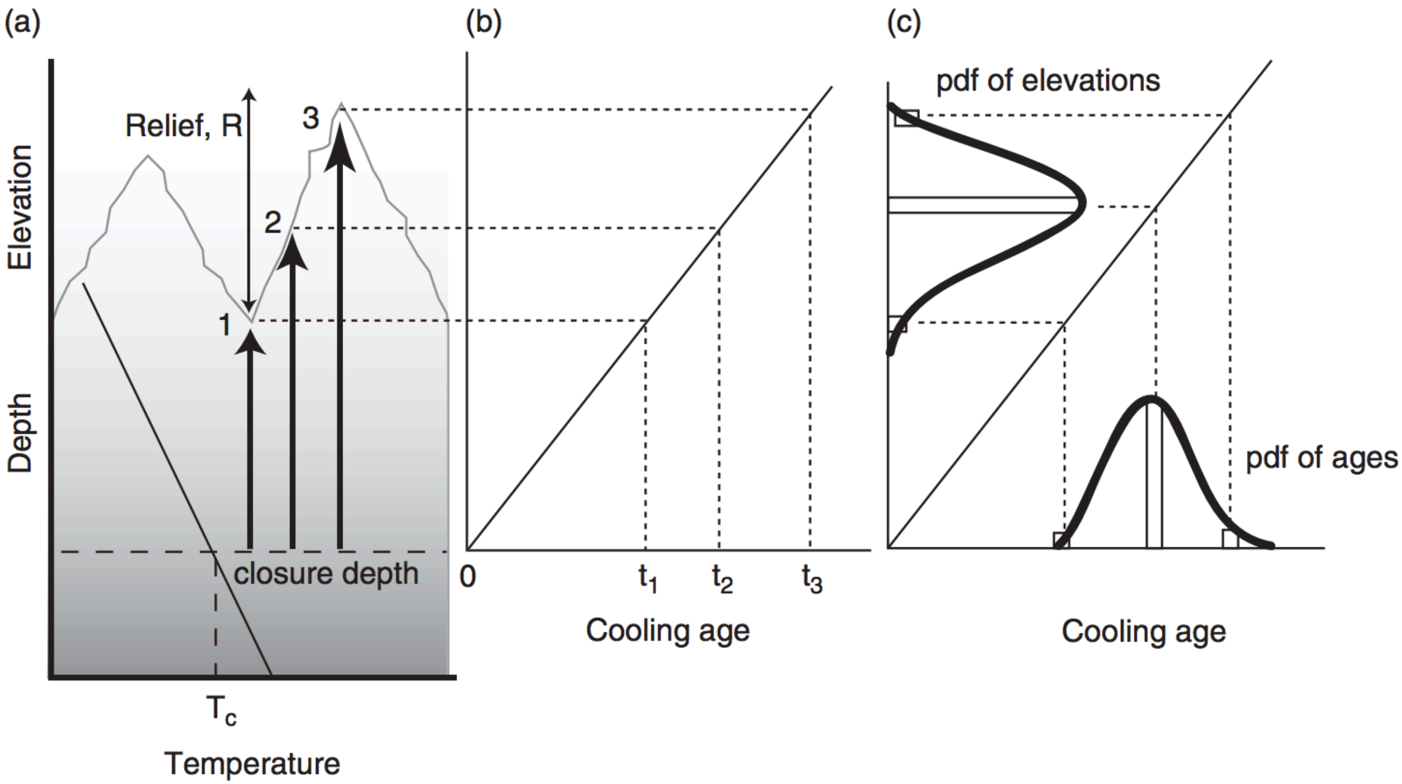

Figure 6.36 (a) Use of elevation profiles to infer exhumation rate in a steady-state landscape. (b) Expected age-elevation distribution in a uniformly eroding landscape such that the rate of erosion in the valley bottom is identical to that at the crest of the mountain. The long-term erosion rate can then be determined to be $R/\Delta t$, where Δt is the difference between ages at the mountain crest and valley trough. (c) The detrital method in which the pdf of ages from a sediment sample in a stream draining this landscape is interpreted in the light of the pdf of elevations in the catchment (its hypsometry). In a uniformly eroding landscape and steadily eroding landscape the pdf of elevations should map directly onto the pdf of cooling ages. Note that the interpretation of the cooling ages depends upon one's assumption about the geothermal gradient, which dictates the assumed cooling depth (after Brewer *et al*., 2003, Figure 2, with permission from Blackwell Publishing).

(8) Shared event of known age.

Berlin et al. JGR-Earth Surface, 2007

Example: Roan Plateau, NW Colorado:

8 Ma incision
by Colorado River

Test of streampower incision model

See also Crosby & Whipple JGR 2006.

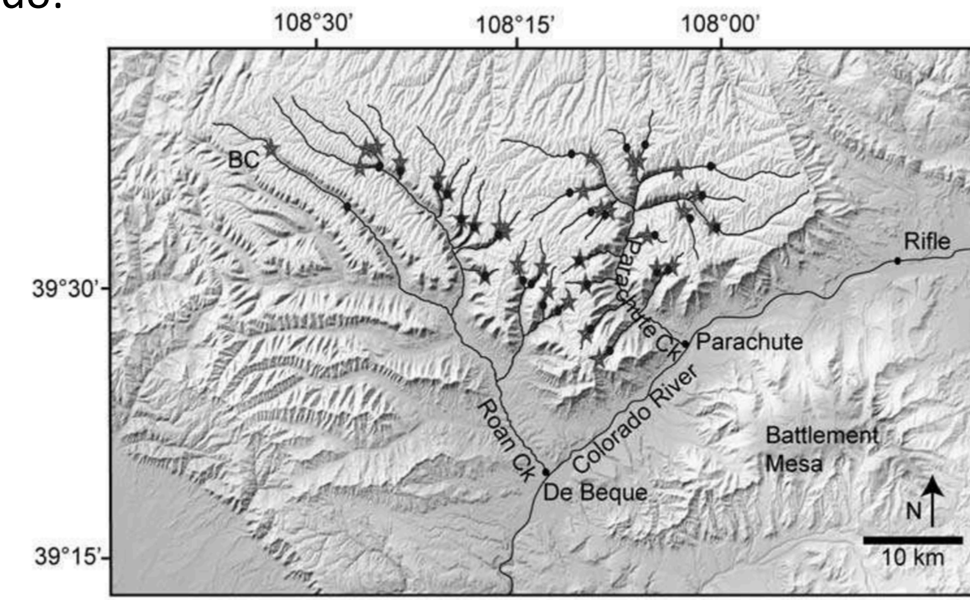

Figure 8. Modeled and observed knickpoint locations on the Roan Plateau. Solid circles indicate the modeled knickpoint positions and stars indicate observed knickpoint locations obtained from DEM analysis. BC–Brush Creek.

Strengths: Natural experiment.
Weaknesses: Relative, not absolute method (though can be calibrated by other methods)
Age range of applicability: Unrestricted in principle; in practice, post-180 Ma
(for which ~complete plate reconstructions are available).

Gondwana rifting

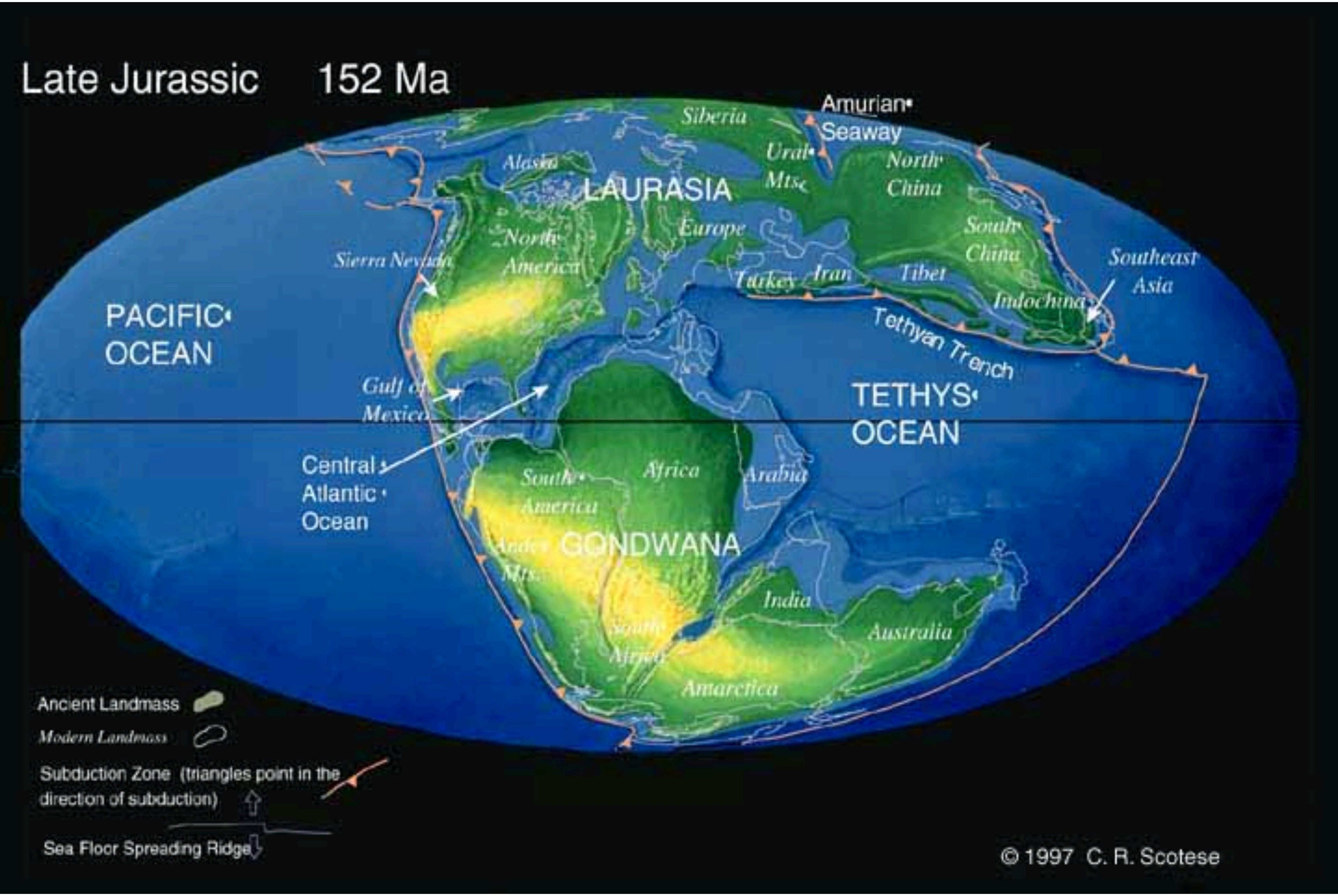

(8) Shared event of known age

Other example: Gondwana Scarp,
known as "Great Escarpment" in S. Africa

South Africa: rifting ~160 Ma
(plate tectonic reconstruction)
Scarp retreat rate: ~1 km/Myr

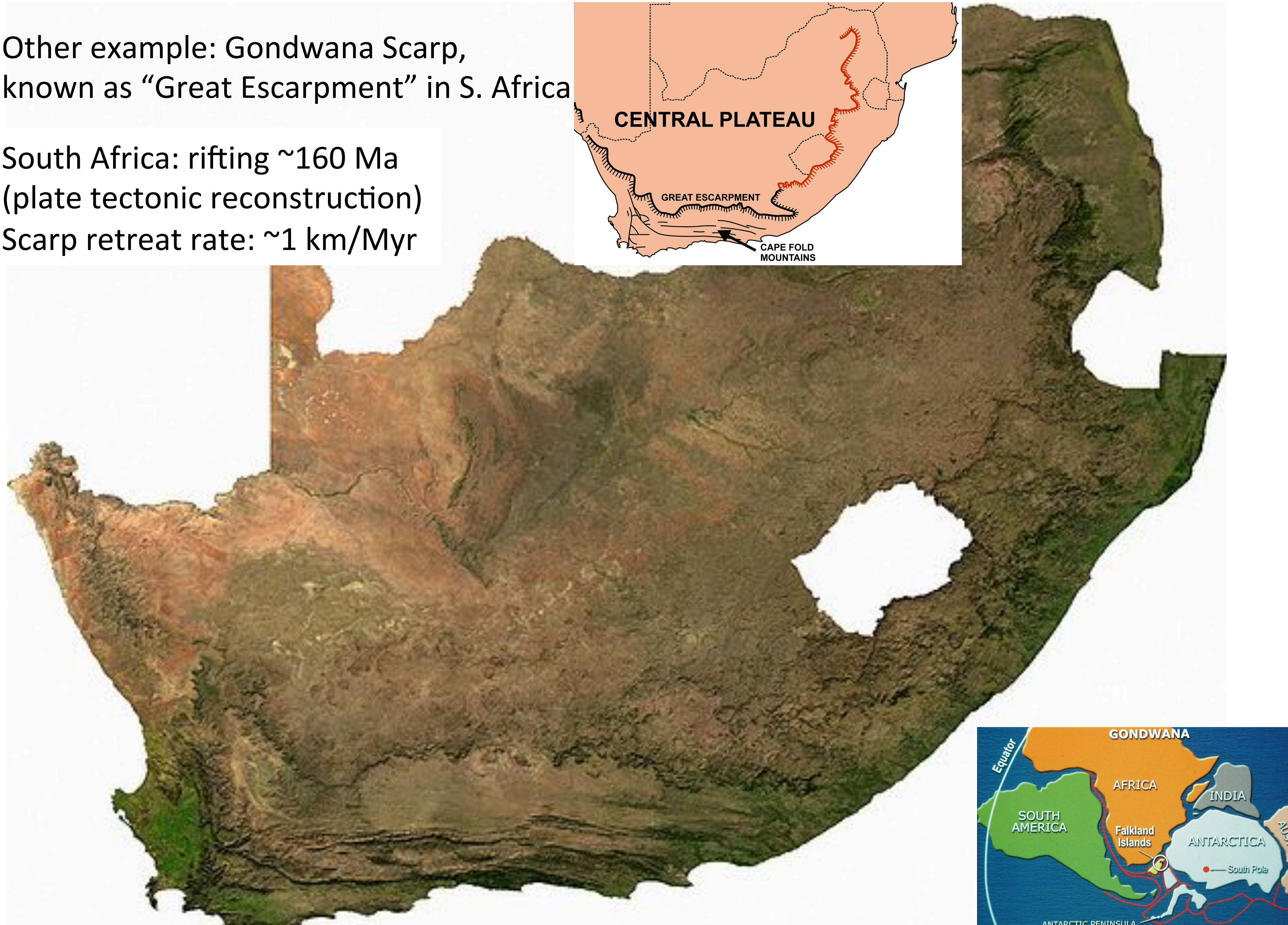

Gondwanaland reconstruction c.400 million years ago

Scarp retreat following continental break-up is constrained by apatite fission-track data

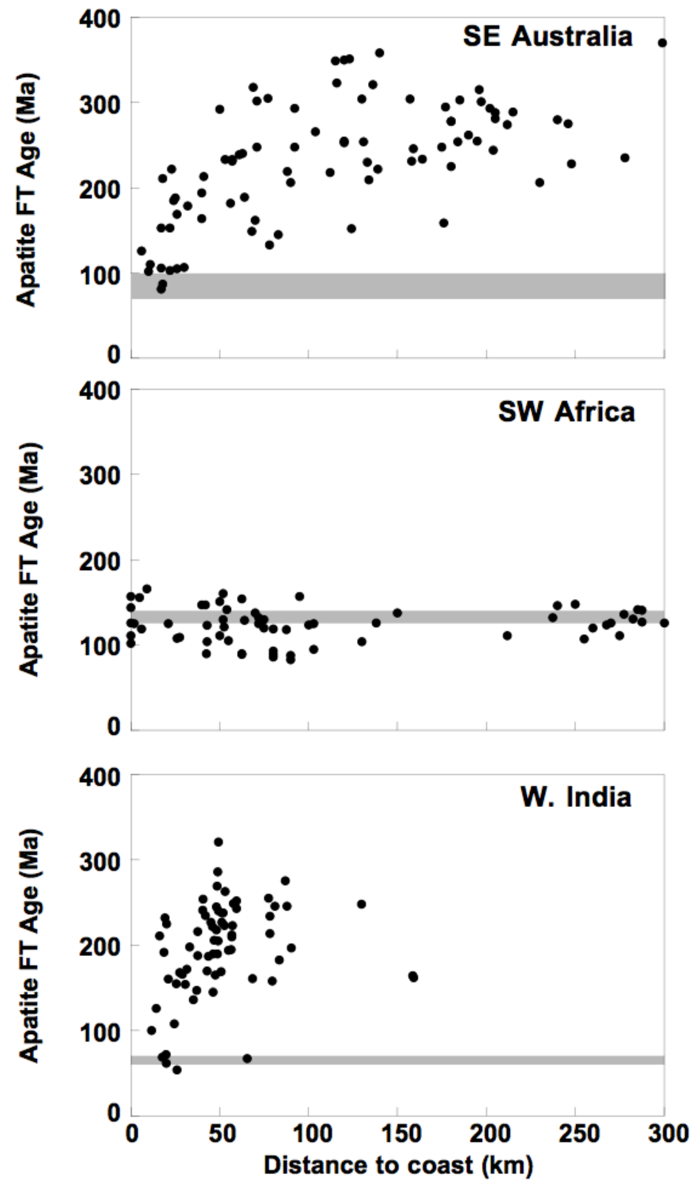

(9) The sedimentary record.

method with great promise for the future; see required reading Allen 2008

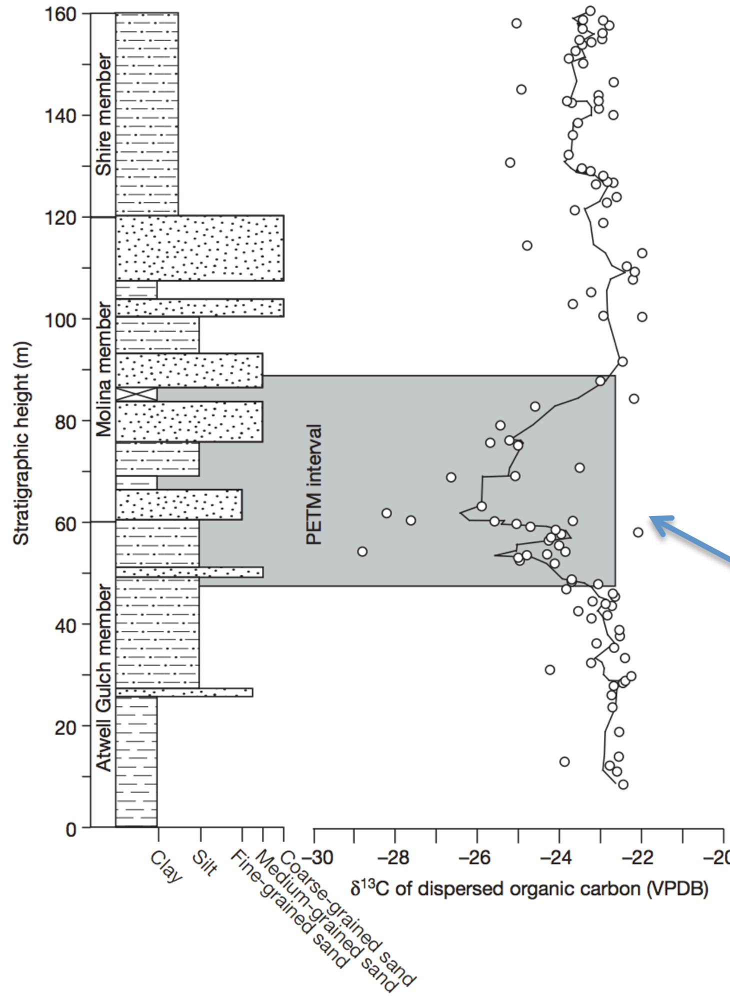

Foreman et al. Nature 2012

4-6 deg C increase in global T accompanied by 2x-4x increase in pCO_2

Strengths: Records information about fully-vanished landscapes.
Weaknesses: Changes in grain size + channel dimensions have multiple possible explanations.
Age range of application: < 3.5 Ga on Earth; <4.1 Ga on Mars (for orbiter methods)

Example (idealized model):

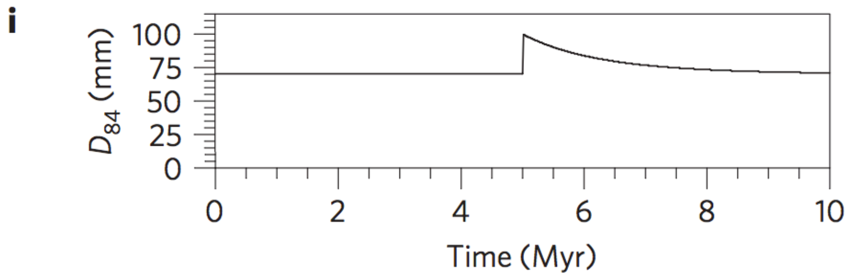

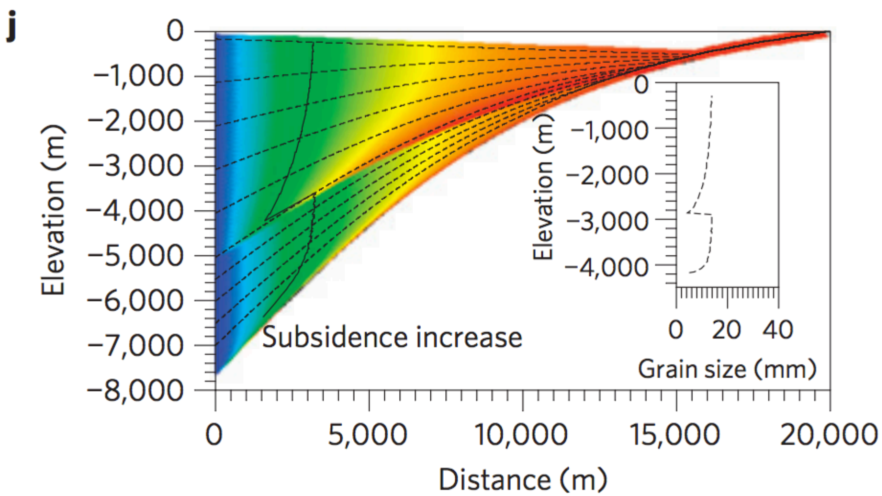

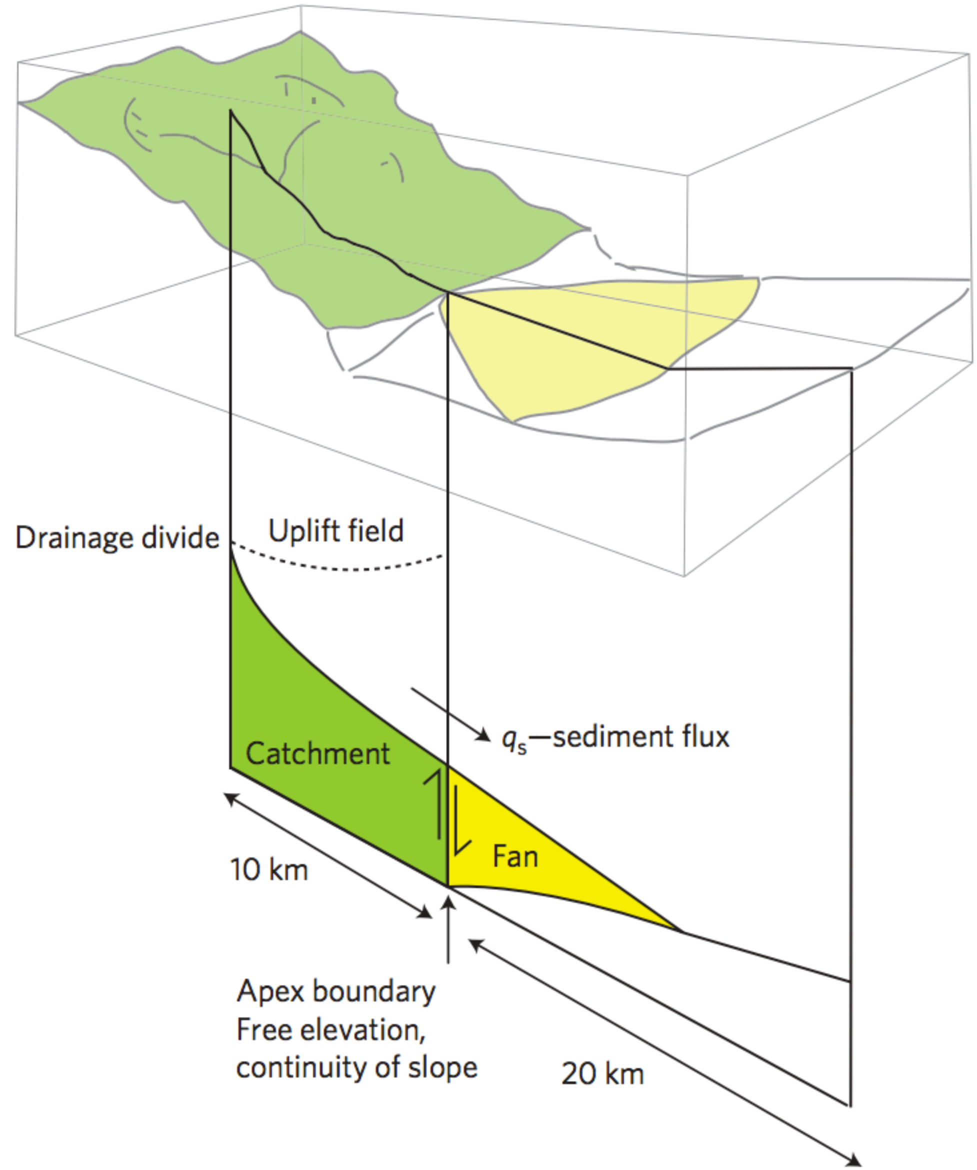

Figure 1 | Diagram of model domain. The uplifting catchment (green) is bounded by a vertical normal fault. The fault marks the transition from catchment to fan (yellow). In this idealized model domain, we maintain a continuity of slope and elevation across the apex[15,29].

Armitage et al. Nature Geoscience 2011

Integration and cross-checking of methods.

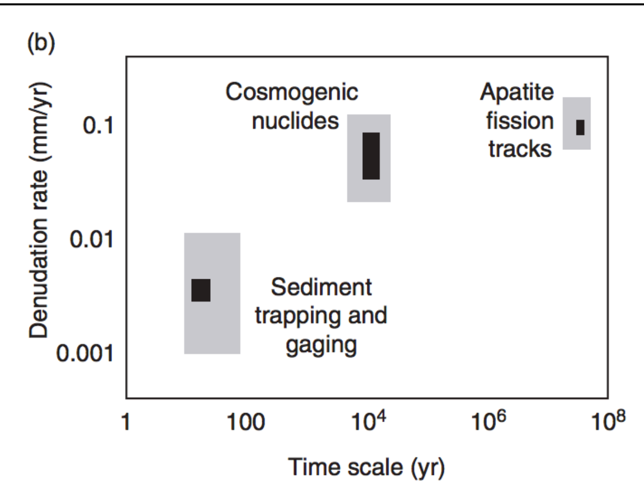

Anderson & Anderson, ch. 6

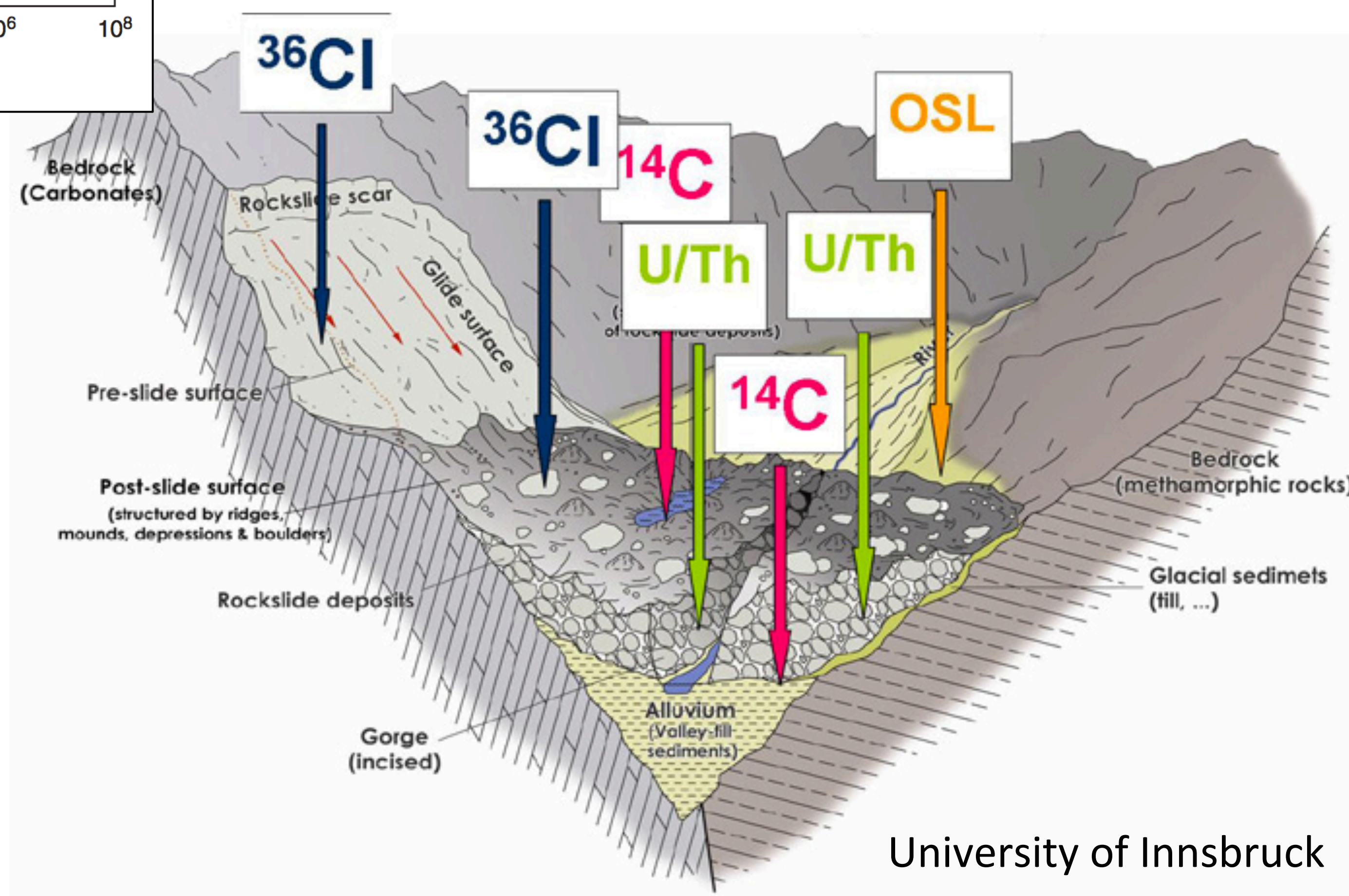

University of Innsbruck

Landscape evolution: sources of data

SOME MAJOR LANDSCAPE EVOLUTION PROBLEMS

DATE/RATE DATA ON EARTH

DATE/RATE DATA ON OTHER PLANETS

(P1) Crater-density constraints on burial and exhumation.

CONCEPT:

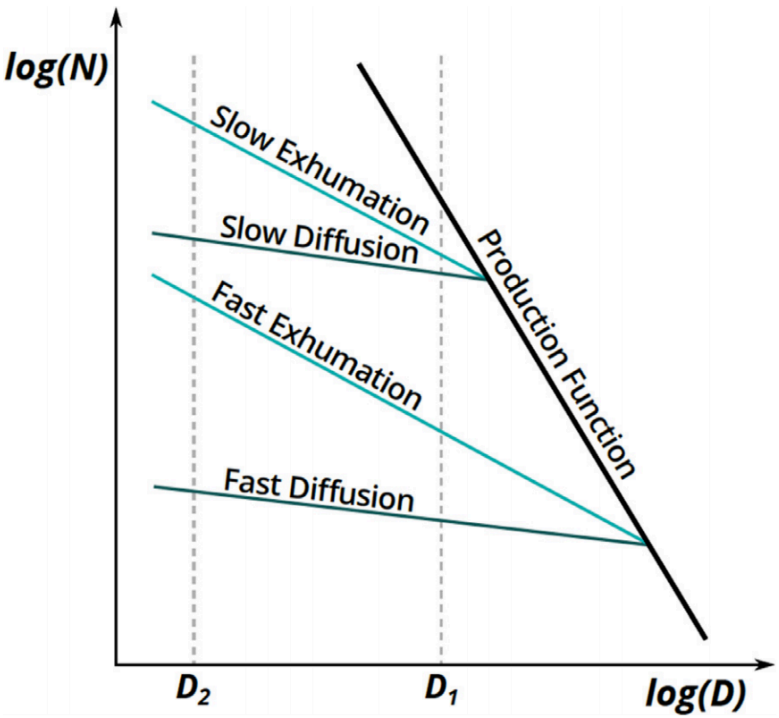

DATA:

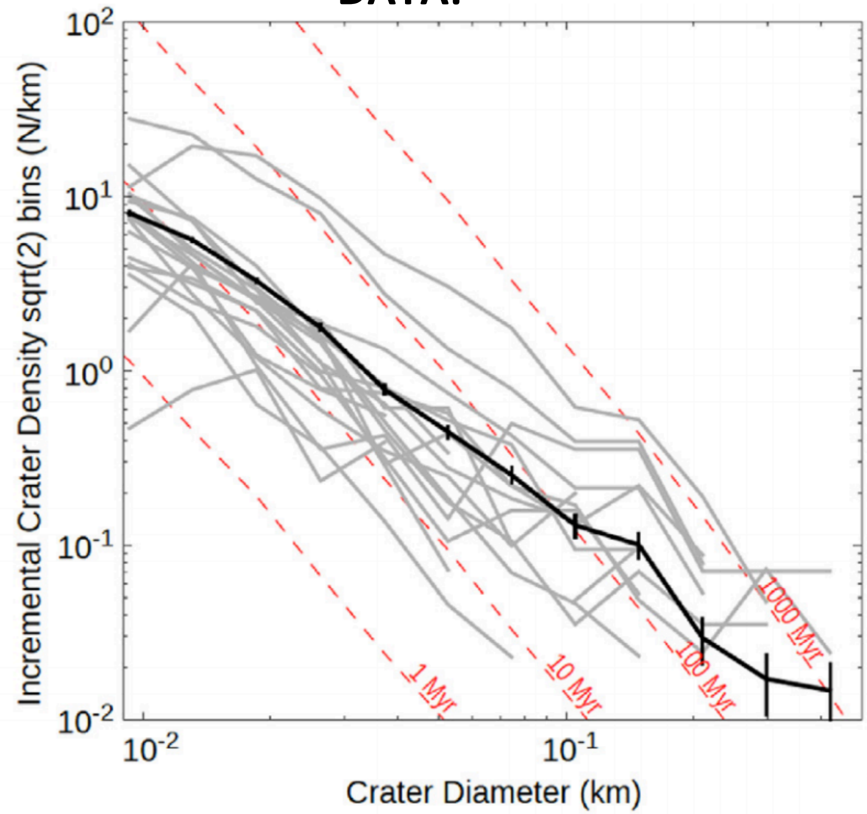

Kite & Mayer 2017

Strengths: Can be applied anywhere on Mars;
Can give past sedimentation rates.

Weaknesses: Difficult to date steep slopes (small area, distorted craters)

Age range of validity: In principle, applies to all timescales.
In practice, restricted to 1-100 Myr for erosion rates

(P2) Statistical approaches (e.g. crater modification)

Fassett & Thomson, JGR-Planets, 2014 – Goal:measure crater degradation on the moon vs. time. Plot the diffusional degradation of individual craters as a function of the crater density of the terrains that host them. Map the crater density to absolute age using Apollo radiometric dates.

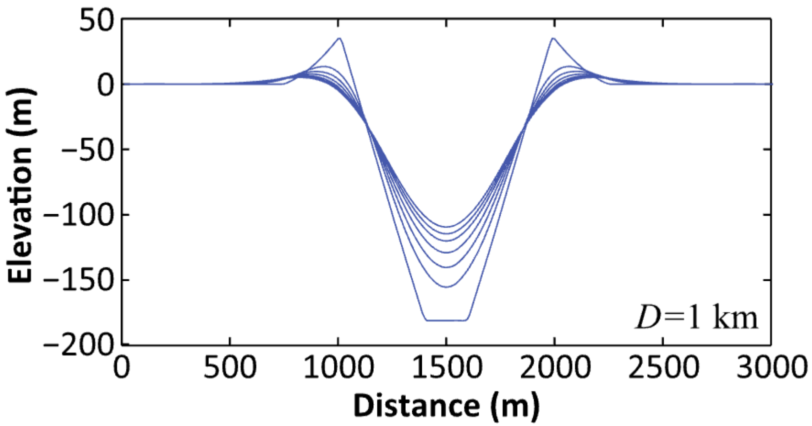

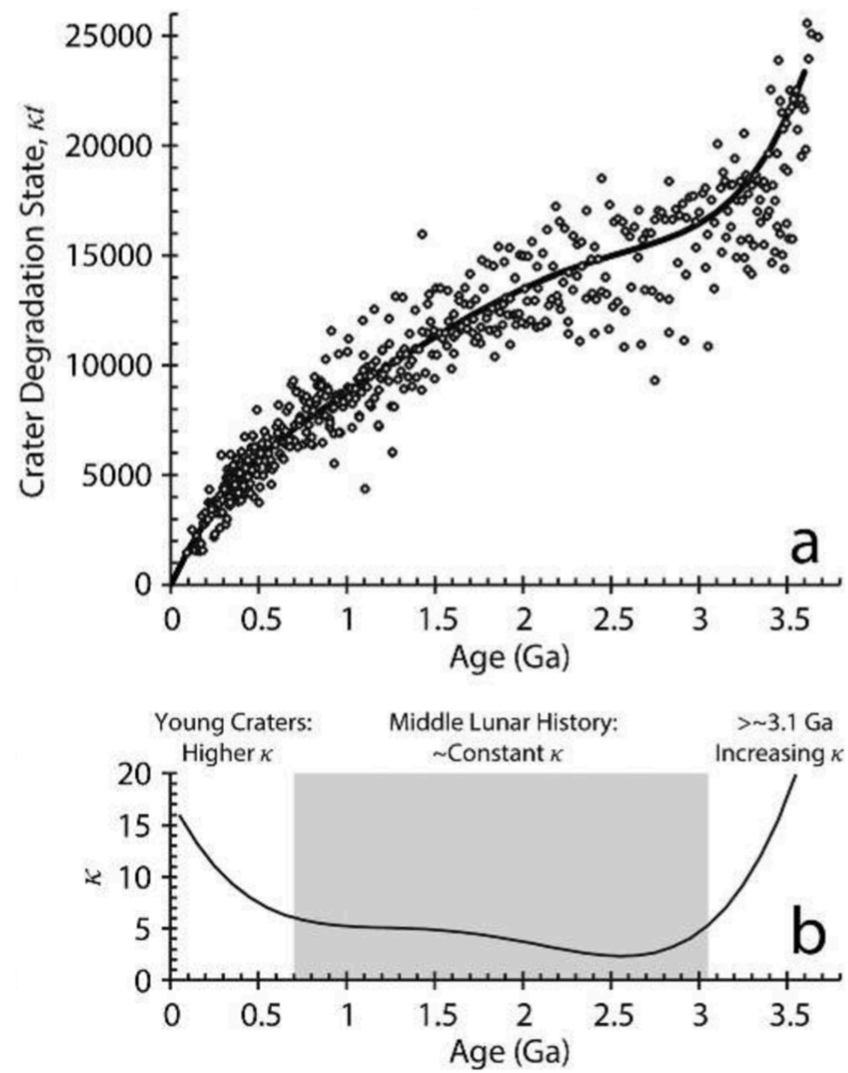

Key points

- For each Earth-based dating method, know the principle, advantages, disadvantages, example application, age range of application, for each technique.
- Explain the evidence for and against a Pleistocene uptick in global erosion on Earth (two arguments for and two arguments against, plus geographic context)

Natural environmental radiation causes charge (electrons and holes) to become trapped when grains are buried in the ground, as bonding electrons are excited from their valence positions, and a small fraction become trapped within the crystal lattice (**Figure 2**). Electron and hole traps are formed at point defects such as those formed by elemental substitution, for example, where Ti replaces Si in quartz. Charge may be compensated by the presence of alkali ions, for example, species such as an electron trap $[TiO_4/Li^+]^\circ$, or the hole center $[AlO_4]^\circ$, known from electron paramagnetic resonance studies (e.g., Weil 1984). Although several models have been proposed (e.g., Itoh et al. 2002), the detailed structure of the OSL electron traps in quartz continues to be explored; the Al hole center mentioned above is likely responsible for the quartz OSL emission in the UV region around 360–380 nm (Martini et al. 2009).

Surface processes as a record of climate: Titan

EXPLORATION OF TITAN

CLIMATE DRIVERS

SURFACE PROCESS RESPONSE

EXPLORATION OF TITAN

CLIMATE DRIVERS

SURFACE PROCESS RESPONSE

Titan is a moon of Saturn (10x Earth's separation from the Sun, 29 years orbital period)
5^{th}-largest solid-surface object in the Solar System (bigger than Mercury, smaller than Mars)

Titan is in a 16-day orbit around Saturn ($e = 0.03$) & always keeps the same face pointed to Saturn.

Low density → ½ H_2O, ½ rock

10^2 less sunlight
→ $(10^2)^{1/4} = 3x$ less temperature from $L(1-\alpha) = \varepsilon\sigma T4$
→ $T_{surf} \sim 100K$
→ H_2O will behave as rock; **<u>CH_4 close to its triple point</u>**

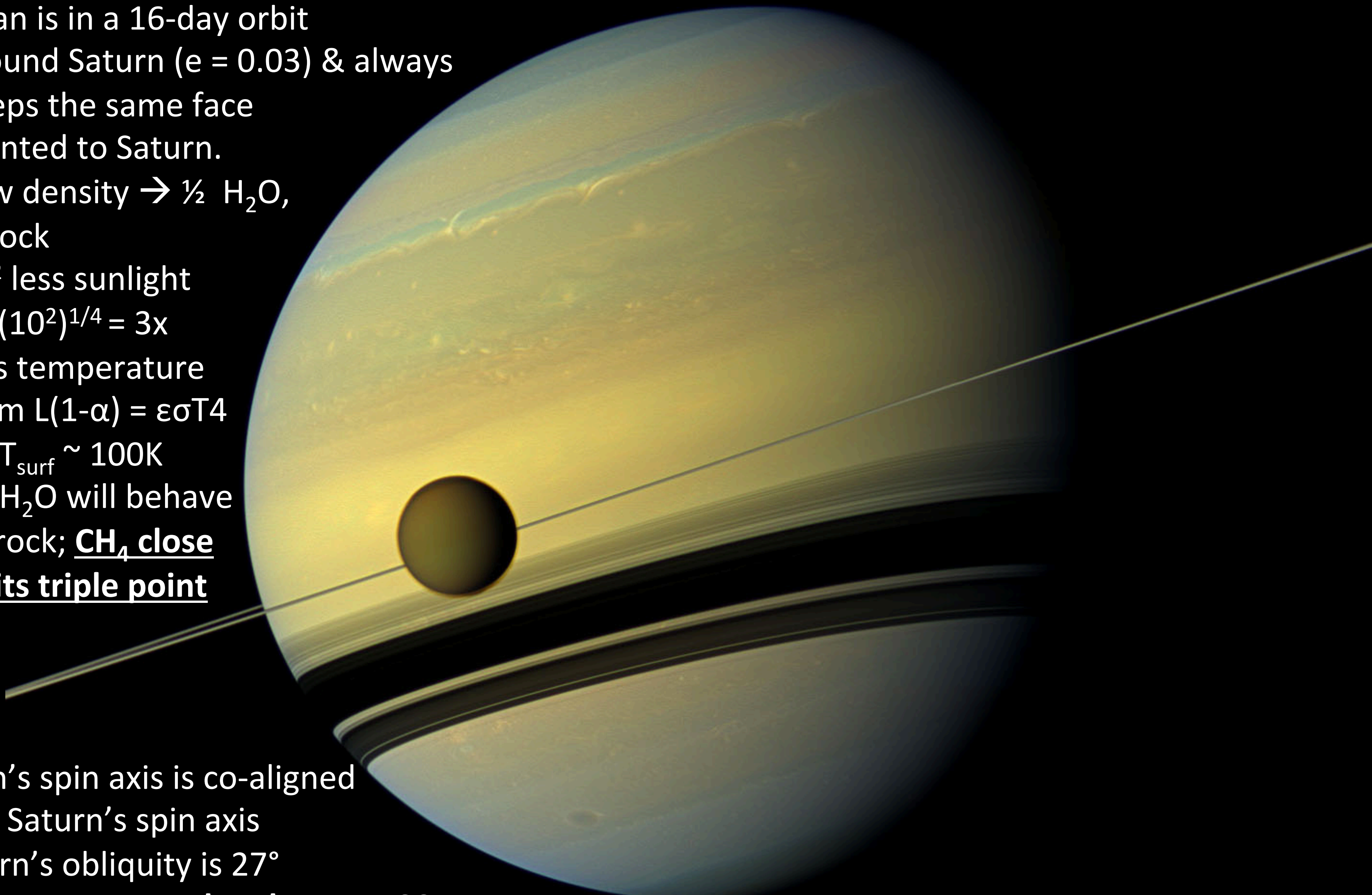

Titan's spin axis is co-aligned with Saturn's spin axis
Saturn's obliquity is 27°
→ **strong seasonal cycle every 29 years**

Titan's hazy atmosphere was discovered by G. Kuiper (University of Chicago)

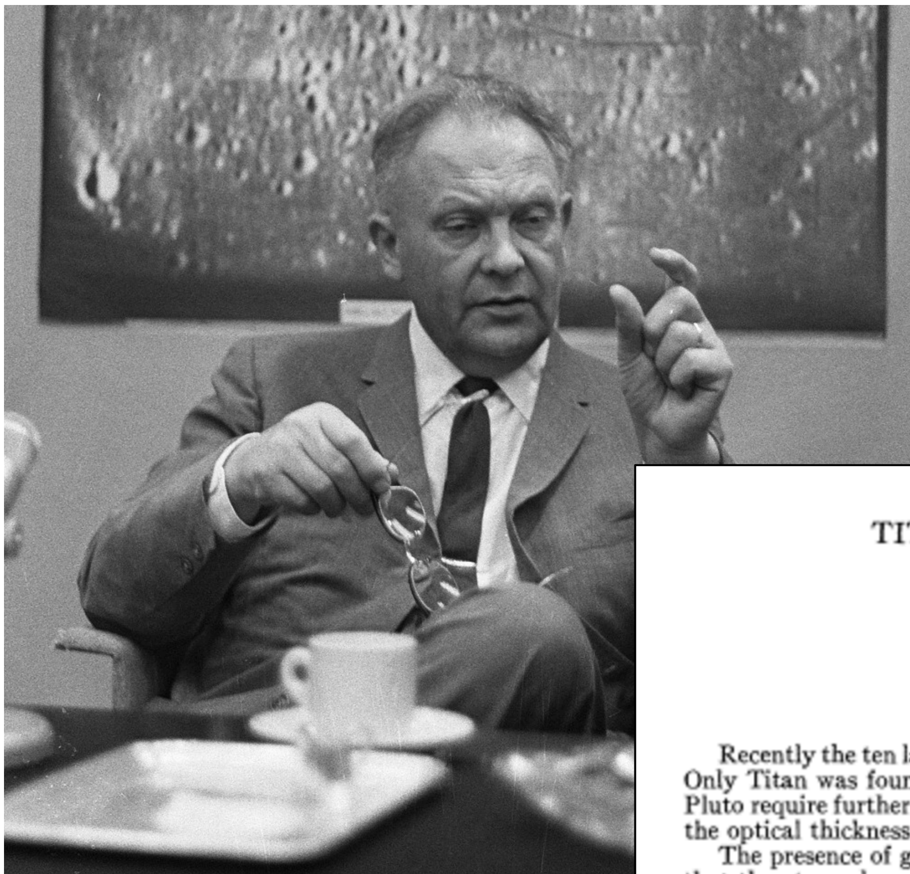

1.5 bars surface pressure
(kg/m^2 equivalent to 11 bars on Earth)

98.4% N_2 (always a gas on <u>modern</u> Titan)
1.4% CH_4 (liquid and gas on modern Titan)

UV light from the Sun fragments CH_4 near the top of the atmosphere. The fragments recombine and further react to form C_2H_6, C_3H_8, HCN, eventually forming solid soot particles that sink.
… H escapes to space.

TITAN: A SATELLITE WITH AN ATMOSPHERE*

GERARD P. KUIPER[1]
McDonald and Yerkes Observatories
Received August 21, 1944

ABSTRACT

Recently the ten largest satellites in the solar system, as well as Pluto, were observed spectroscopically. Only Titan was found to have an atmosphere of sufficient prominence to be detected, but Triton and Pluto require further study. The composition of Titan's atmosphere is similar to that of Saturn, although the optical thickness is somewhat less.

The presence of gases rich in hydrogen atoms on a small body like Titan is surprising and indicates that the atmosphere was formed after Titan had cooled off. Similar arguments, though less compelling, may be advanced for analogous conclusions in regard to the formation of the atmospheres of Mars, Venus, and the earth.

Astrophysical Journal, 1944

In 1980, Voyager 1’s trajectory permitted a close encou
with Titan (at the expense of a flyby of Pluto), but Voyag
was unable to see through the haze

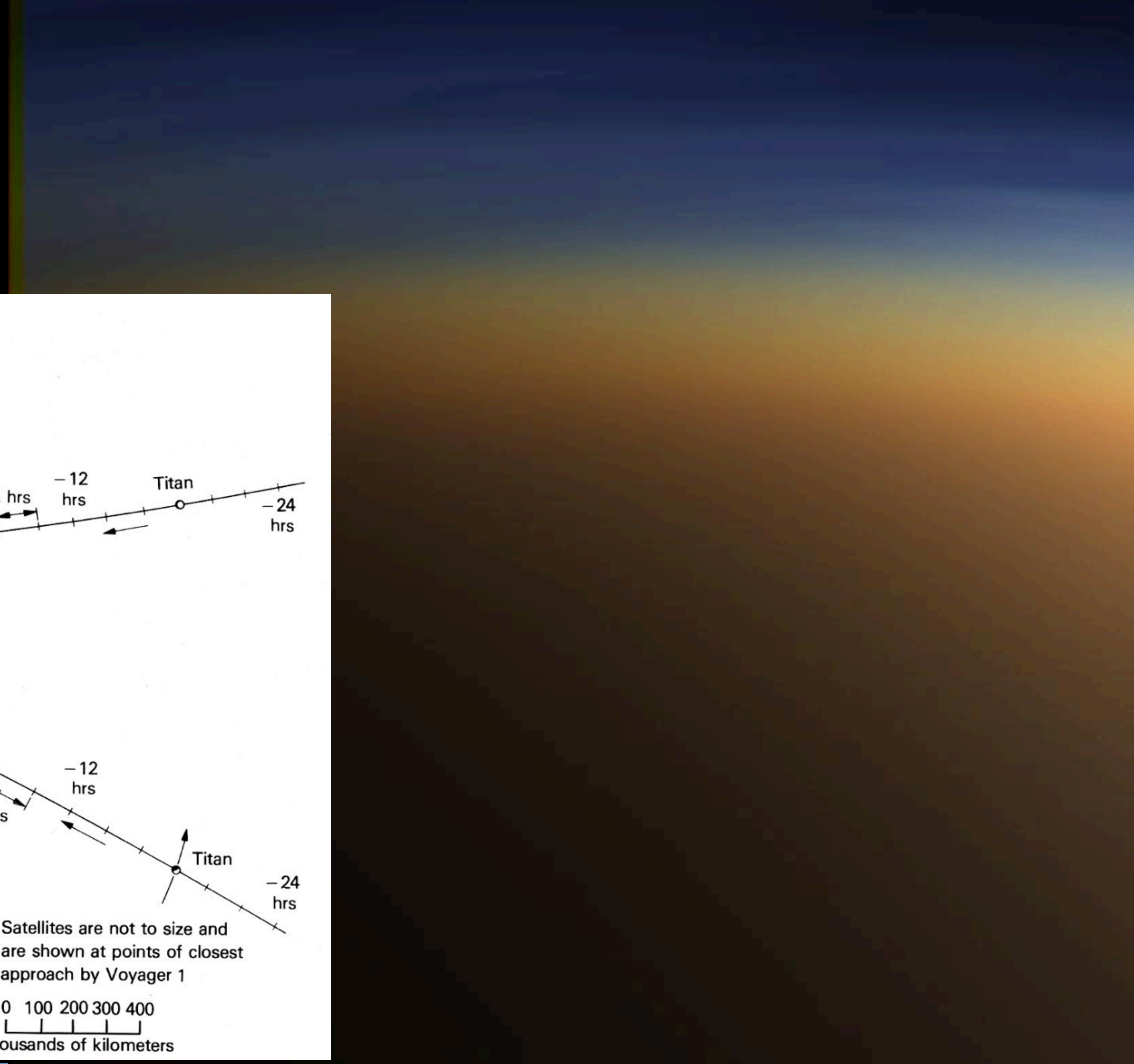

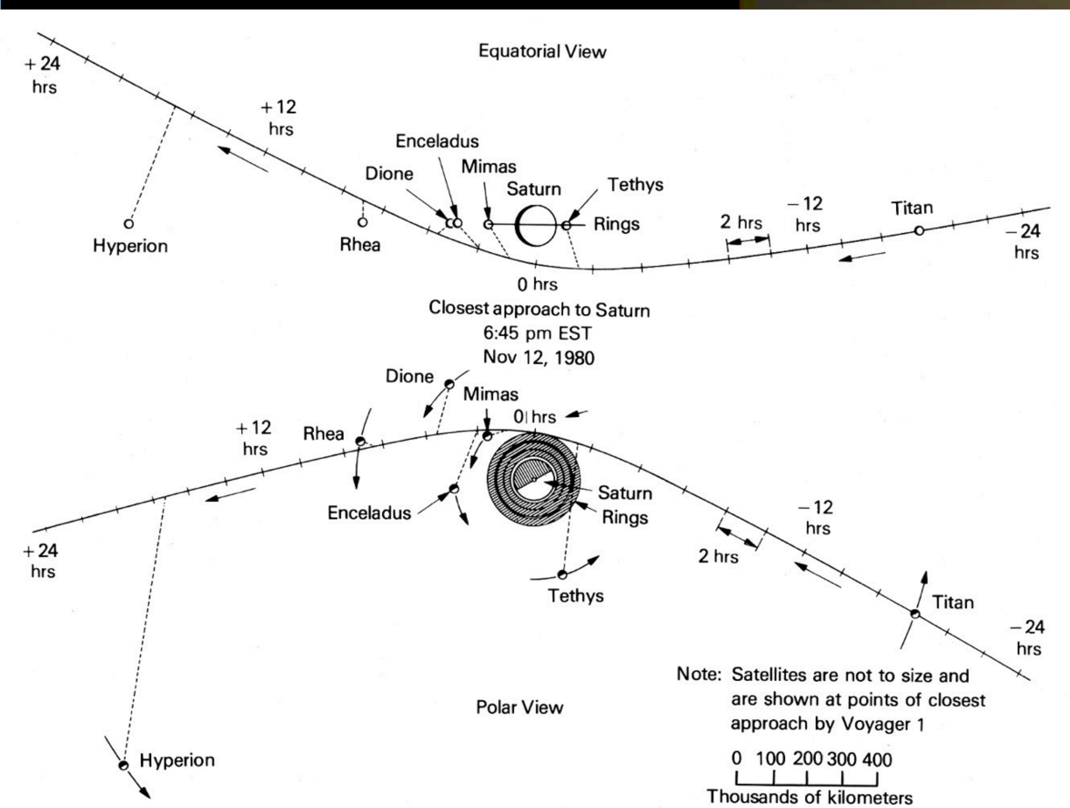

The Cassini-Huygens mission (launch 1997, Saturn orbit 2004-2017) was designed to see beneath Titan's haze

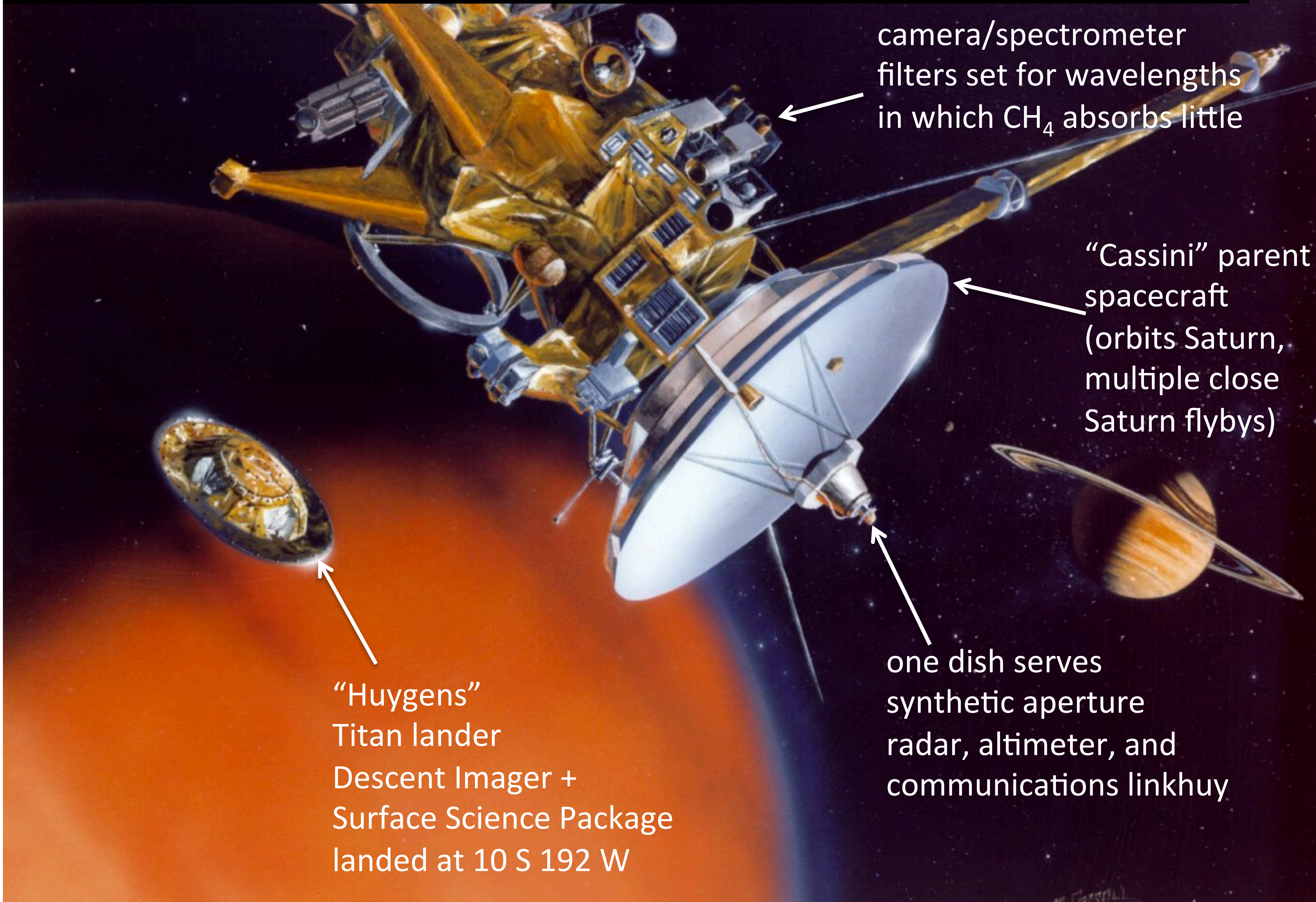

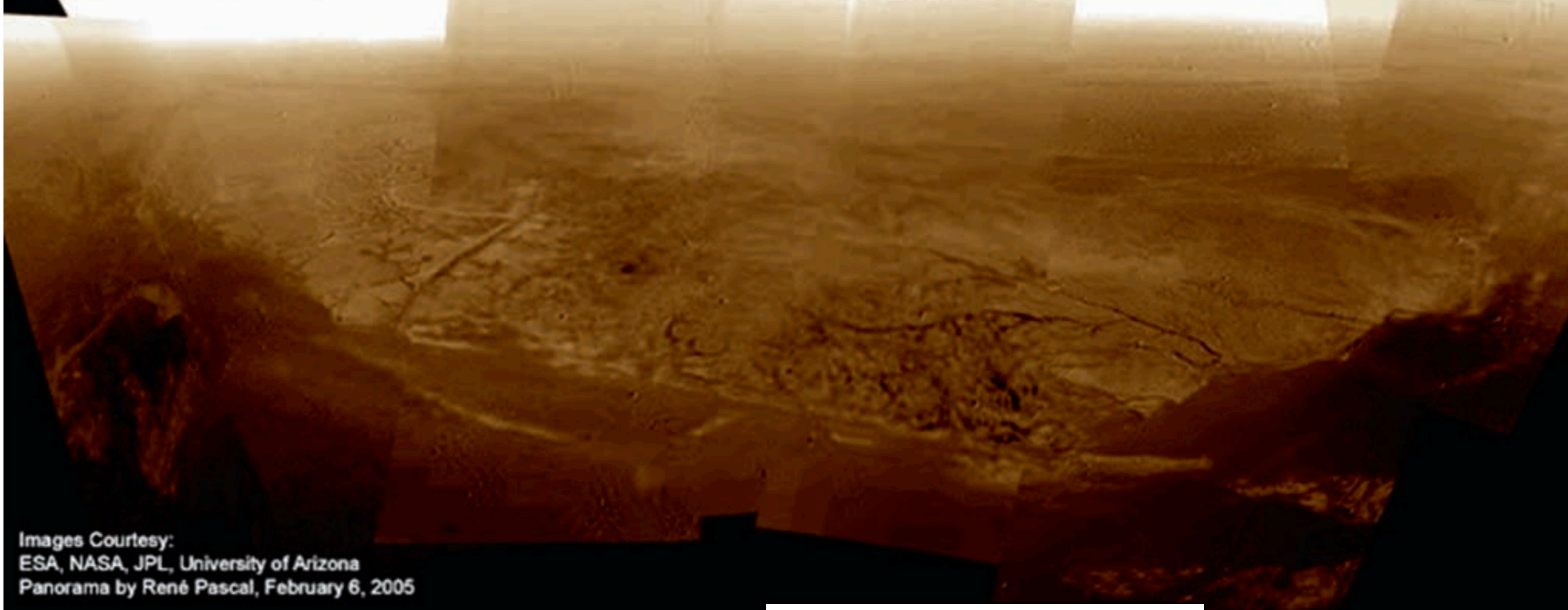

Fig. 5.20 Panorama view taken by the DISR cameras during decent.

Jaumann et al. 2009

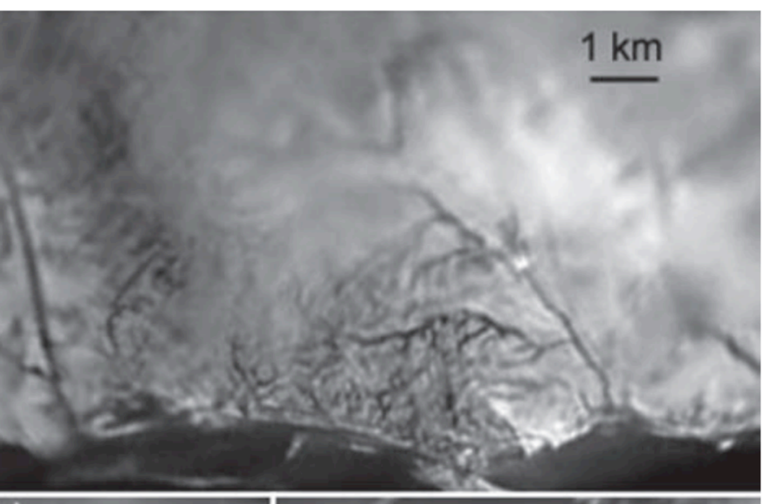

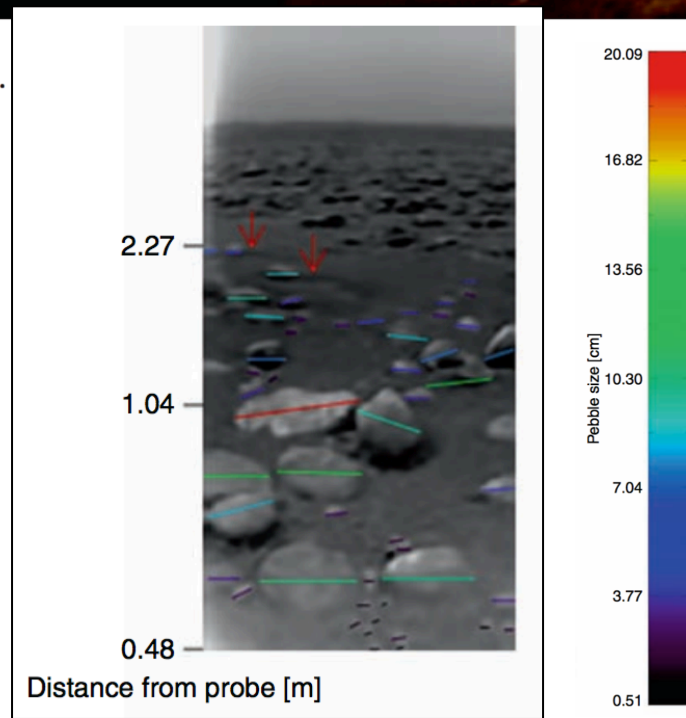

Titan has a buried global ocean, almost certainly liquid water
The surface is mostly solid hydrocarbons

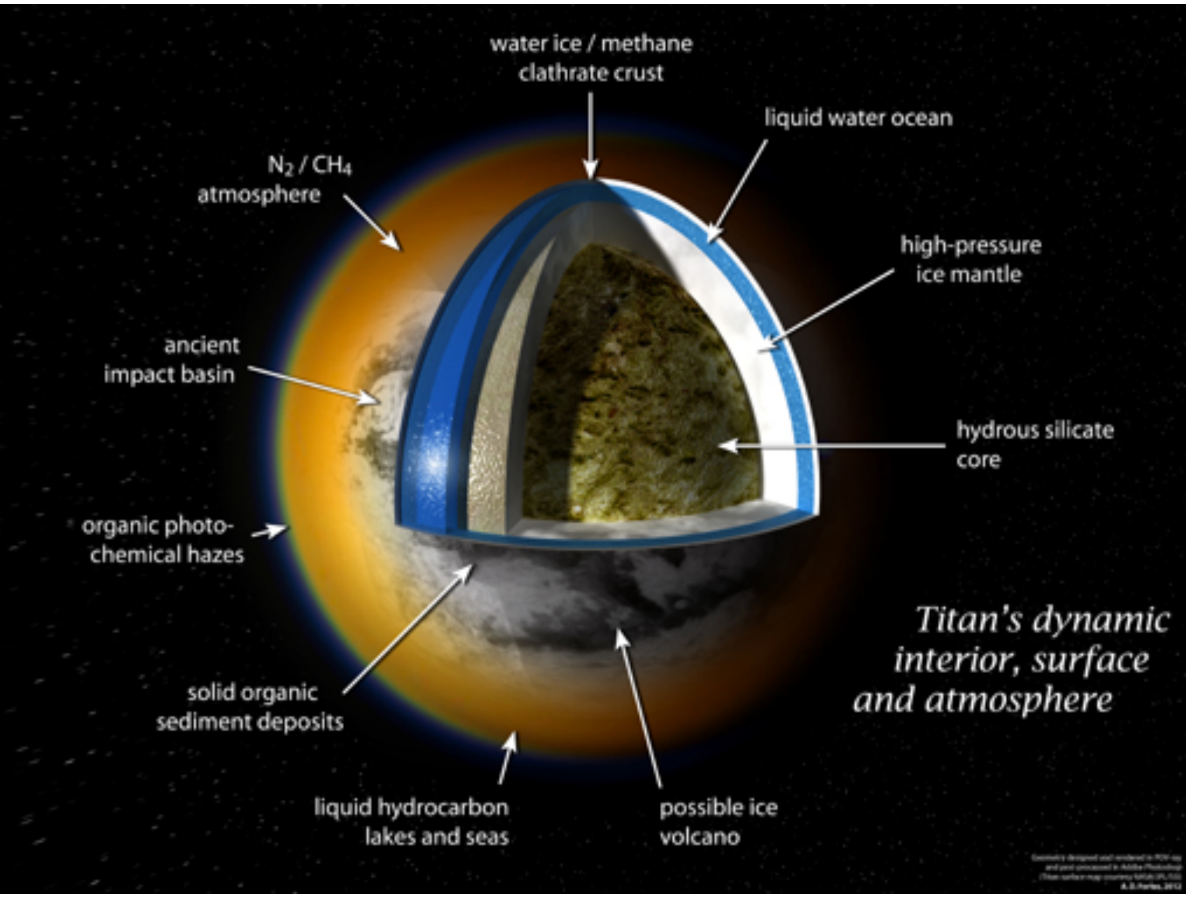

Diurnal tide measured in the degree-2 gravity of Titan

Amplitude of gravity tide corresponds to a diurnal surface shape bulge of ~10 m amplitude

A solid moon would show a bulge of ~1 m amplitude → Titan's outer water ice shell is mechanically fully decoupled from the interior on 16-day timescales

Speculative models of atmosphere-interior coupling: CH4 released to atmosphere from cryovolcanoes

Low latitudes: sand dunes

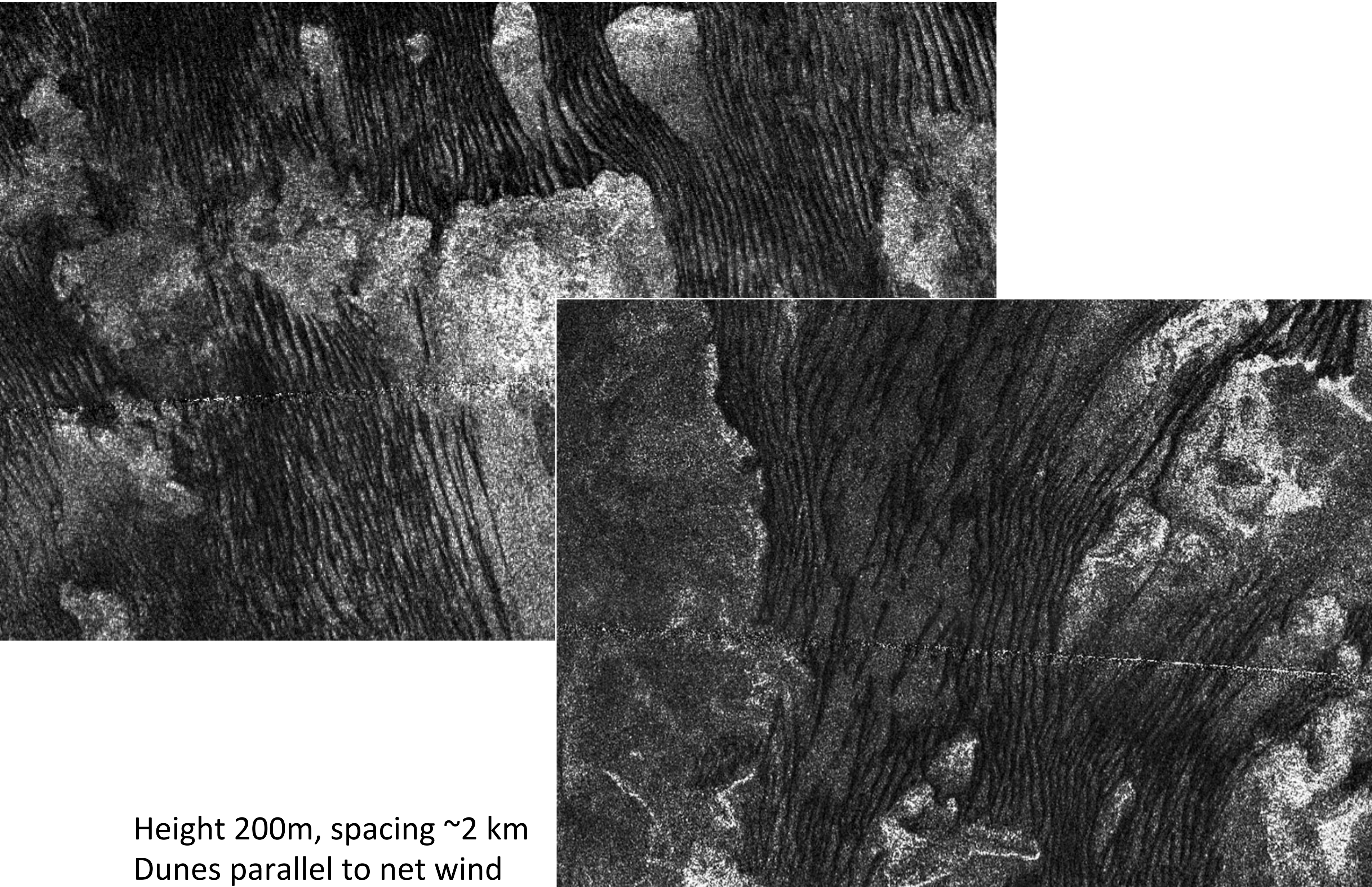

Height 200m, spacing ~2 km
Dunes parallel to net wind

Sources of elevation data for Titan: radar altimetry, radar stereogrammetry, and "SARTopo"

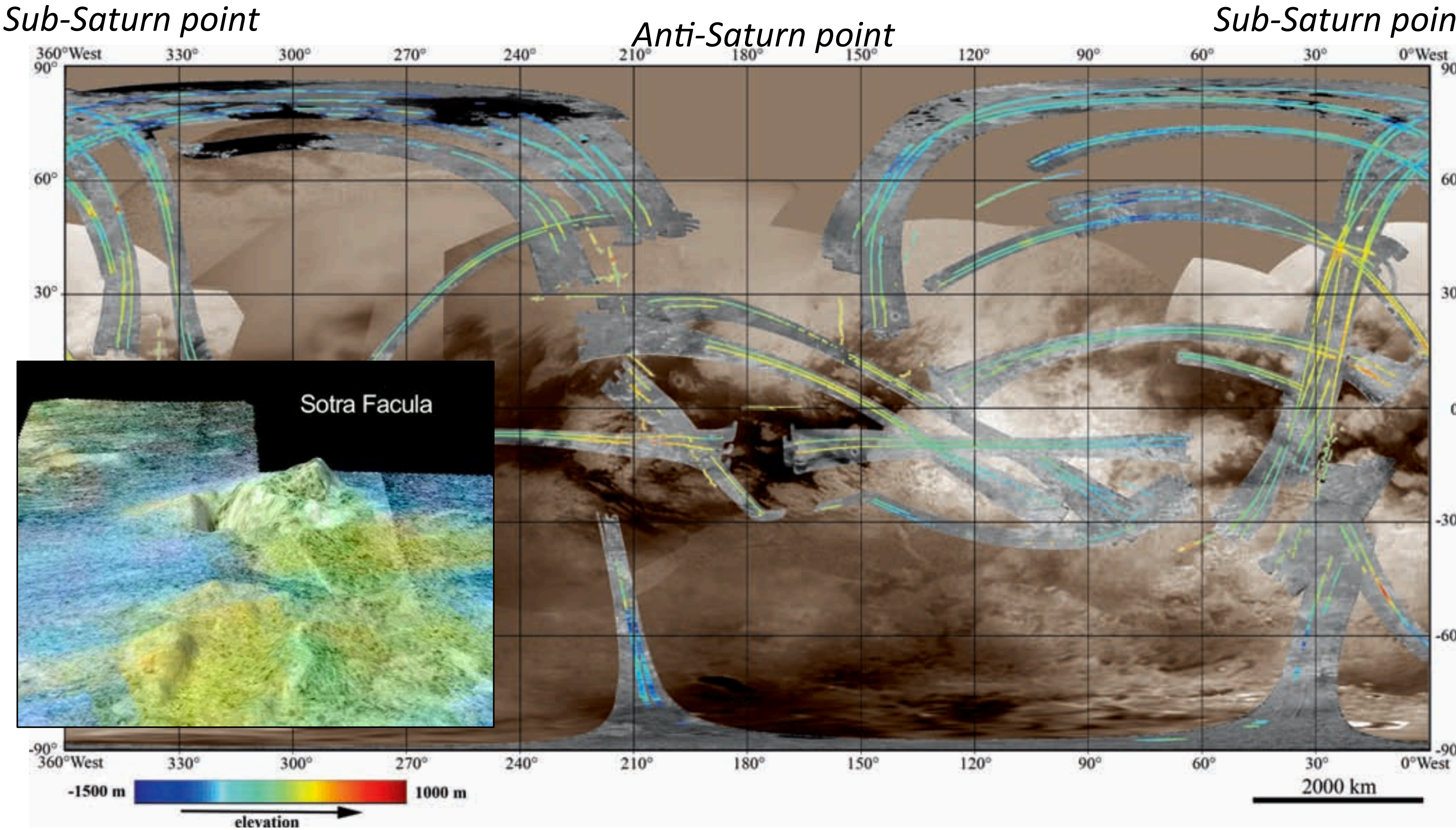

Fig. 5.14 Global mosaic of RADAR images through T29 with color-coded elevation profiles obtained by 'SARTopo' processing (Stiles et al. 2009) as described in text. Simple cylindrical projection, north at top, centered on 180° longitude

Serendipitous stereo photogrammetry from Huygens as it spun under parachute (1/2)

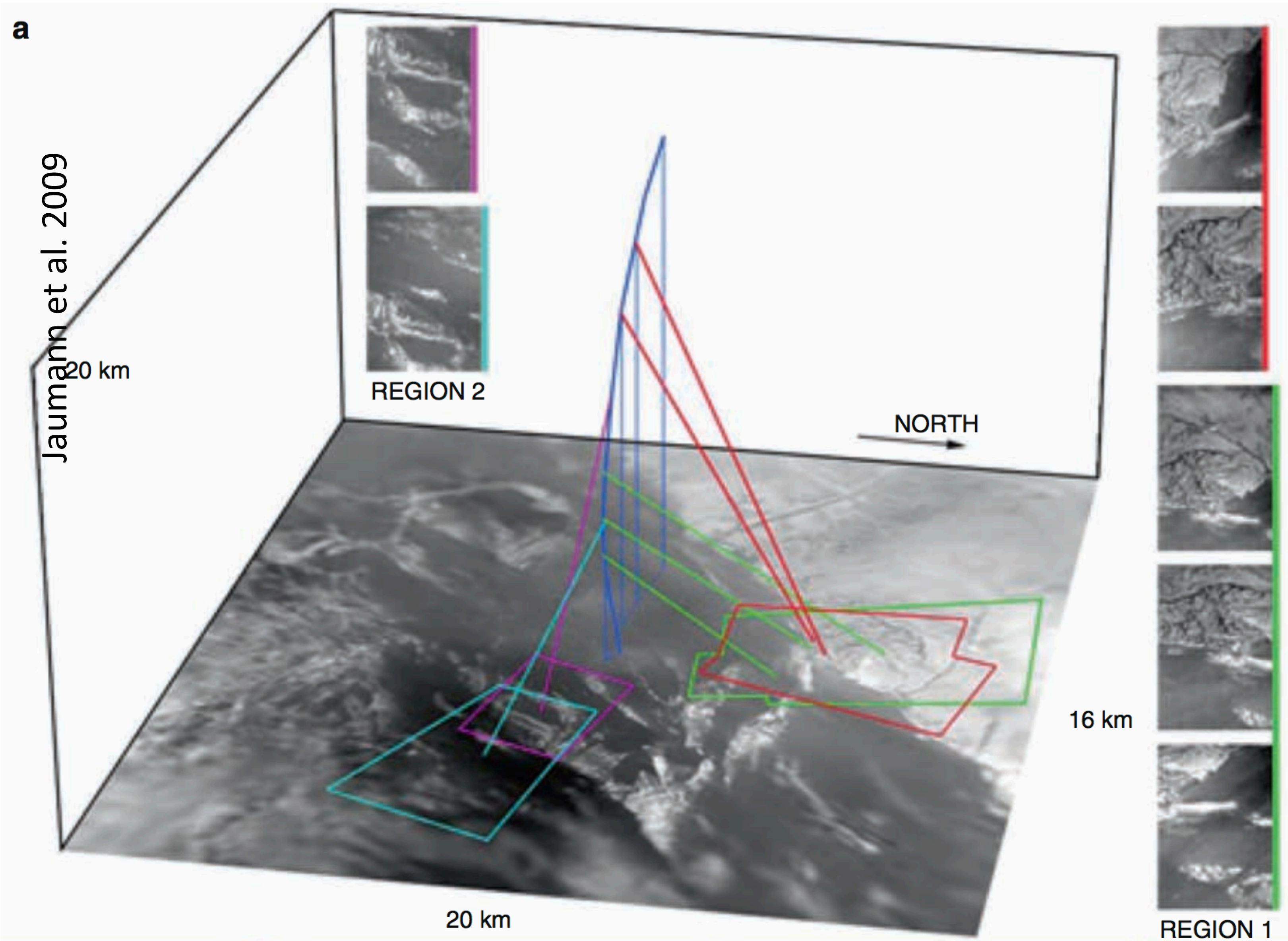

Jaumann et al. 2009

Serendipitous stereo photogrammetry from Huygens as it spun under parachute (2/2)

Jaumann et al. 2009

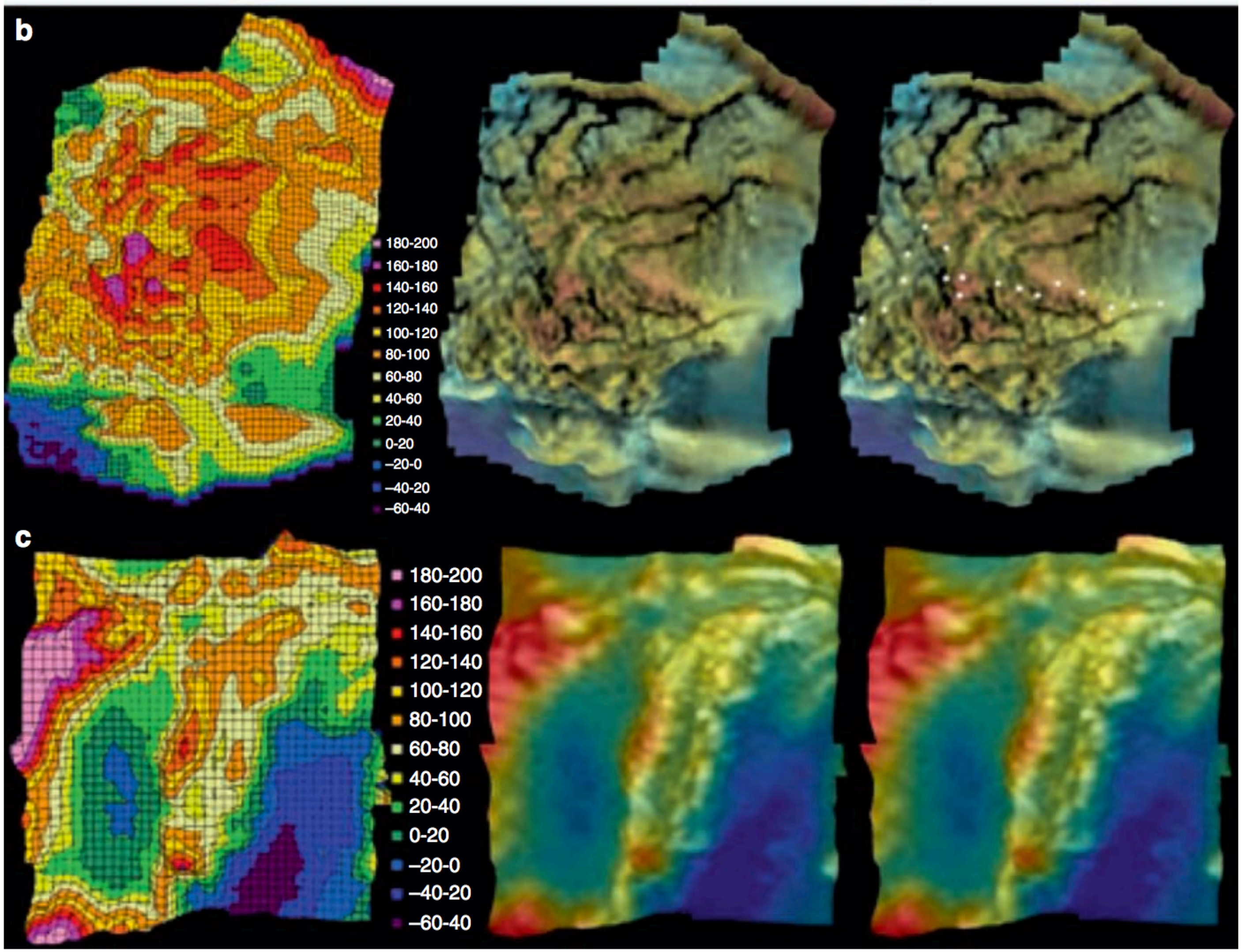

Fig. 5.10 Topographic models of bright and dark areas near the Huygens landing site, based on stereo analysis of DISR images. View is from the east. (**a**) Descent trajectory showing the acquisition geometry of the images used. (**b**) Region 1 in bright terrain. (**c**) Region 2 in dark terrain. For each region, a color-coded topographic map is shown, accompanied by a synthetic stereo pair showing an oblique view of the images with color-coding according to elevation added (adapted from Soderblom et al. 2007b)

Titan geography: Low latitude soot dunes, polar methane lakes and seas.
Few impact craters → 0.1-1 Gyr surface age (similar to Earth)

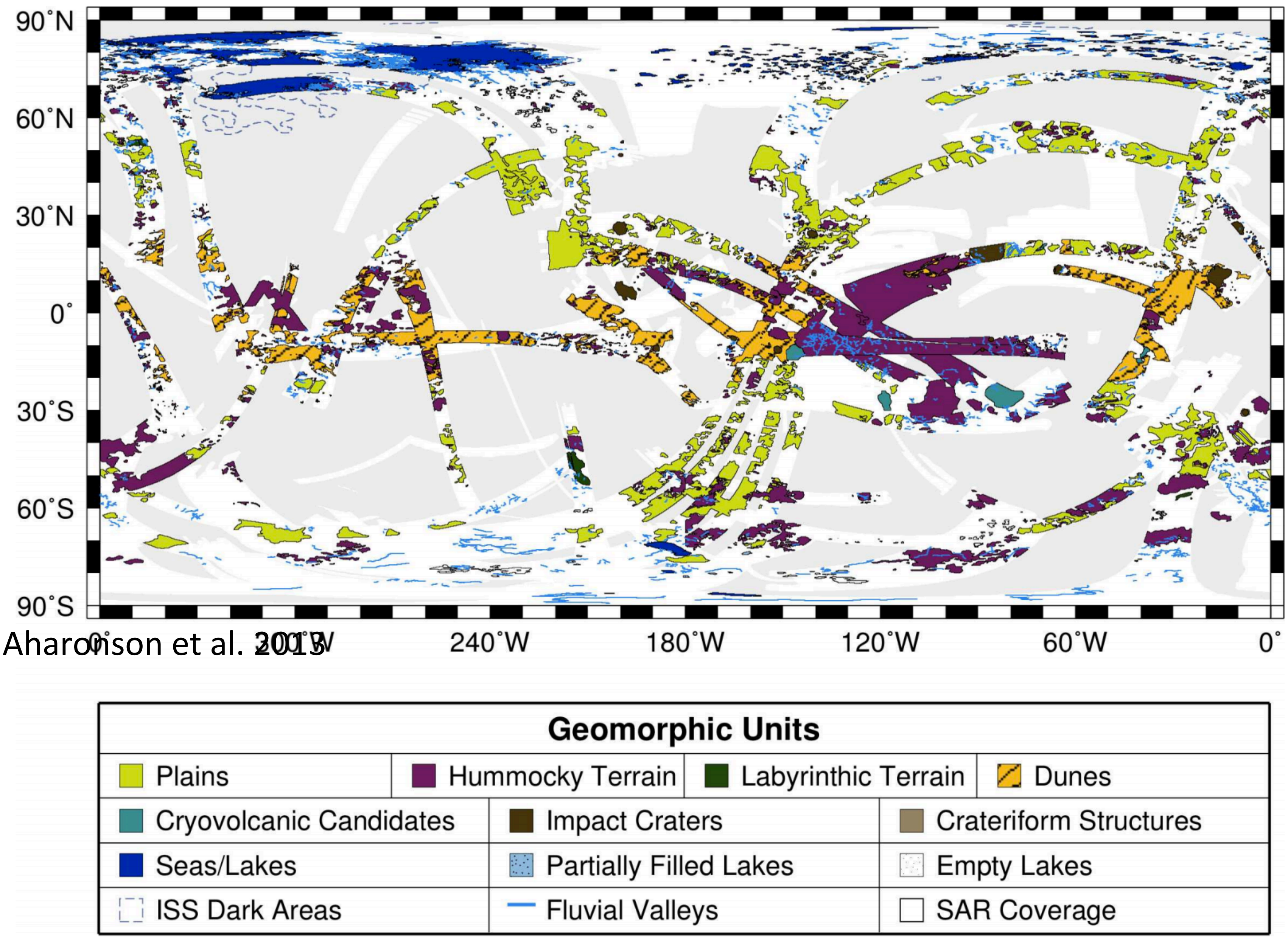

Aharonson et al. 2013

High latitudes: lakes and seas

Liquid coverage is ~1% of planet surface area (not including ephemeral lakes); >10% in North Polar region.

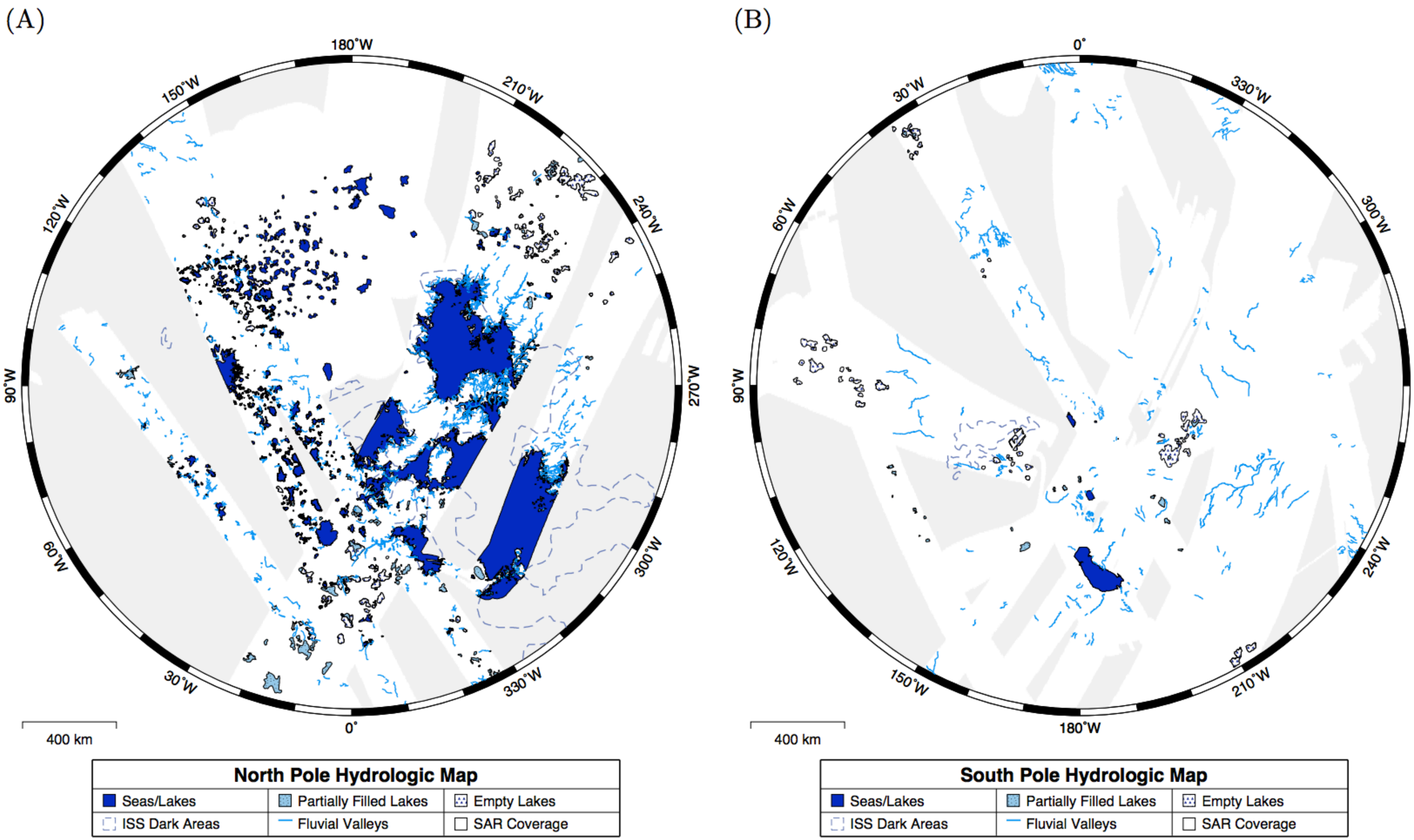

Lakes are mostly in the N hemisphere

Evidence for lakes and seas includes spectrum consistent with liquid methane, extreme smoothness (minimal radar return, specular reflection), radar reflections from both seabed+(sea surface), translucency in visible light, shoreline morphology, uniform topographic elevation, & location in topographic lows.

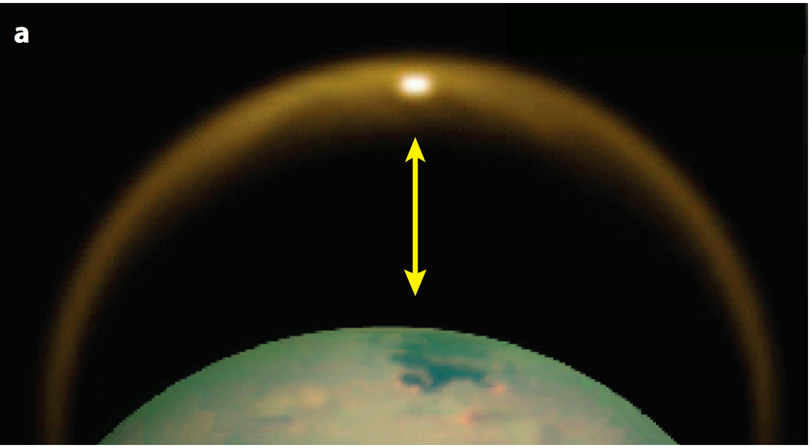

Specular reflection

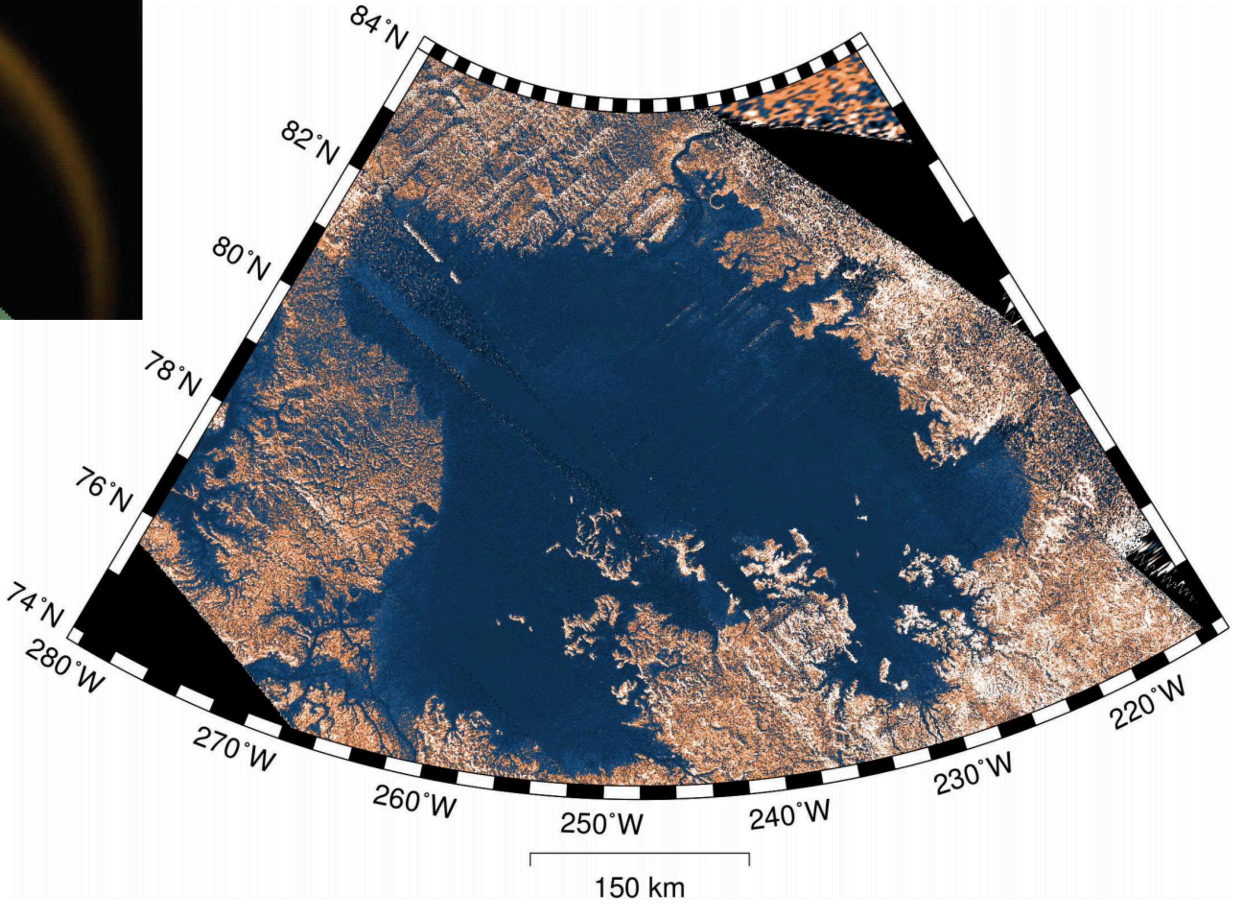

Surface processes as a record of climate: Titan

EXPLORATION OF TITAN

CLIMATE DRIVERS

SURFACE PROCESS RESPONSE

Seasons on Titan (= Seasons on Saturn)

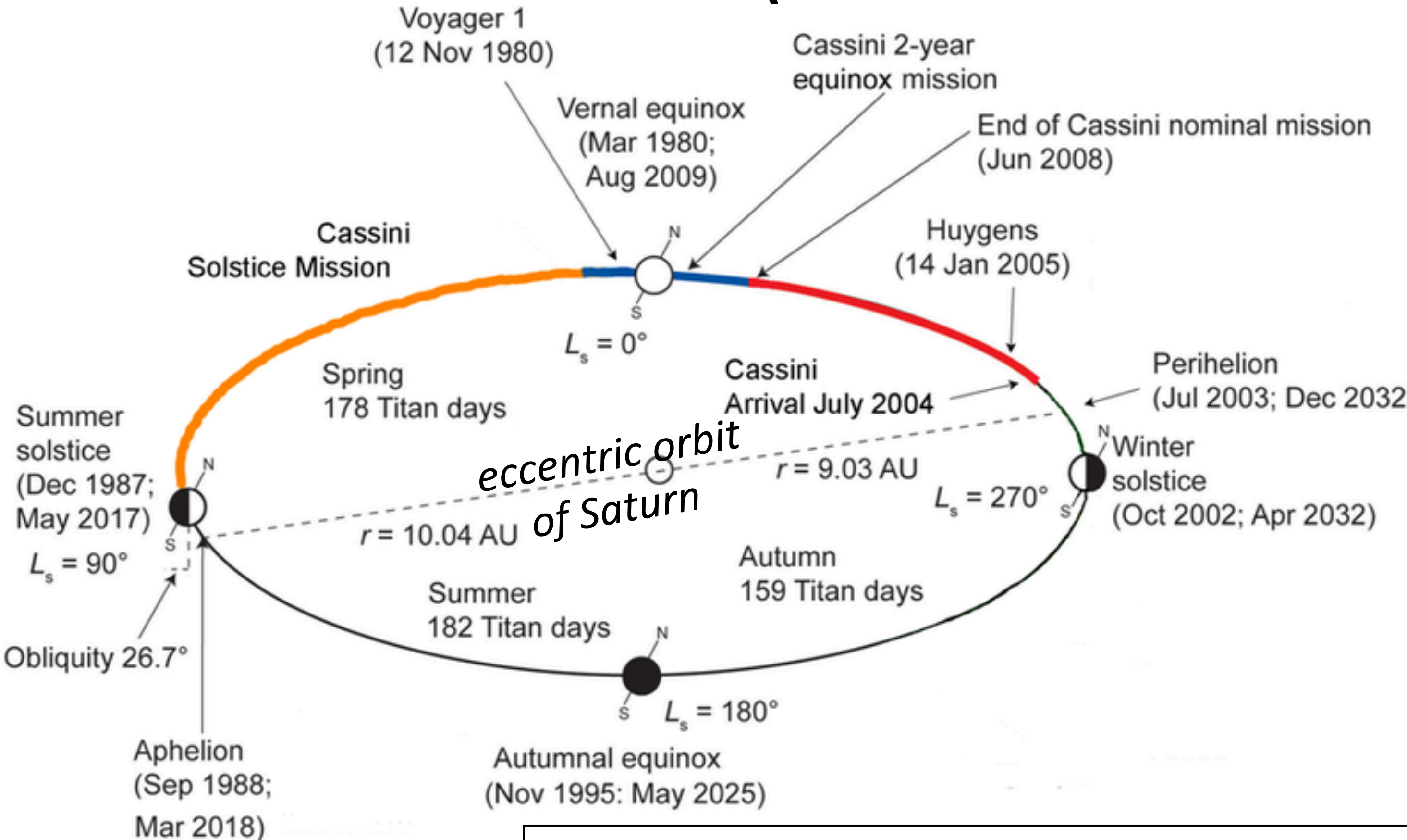

MODEL:
consistent
with very limited data
(presence/absence of waves)

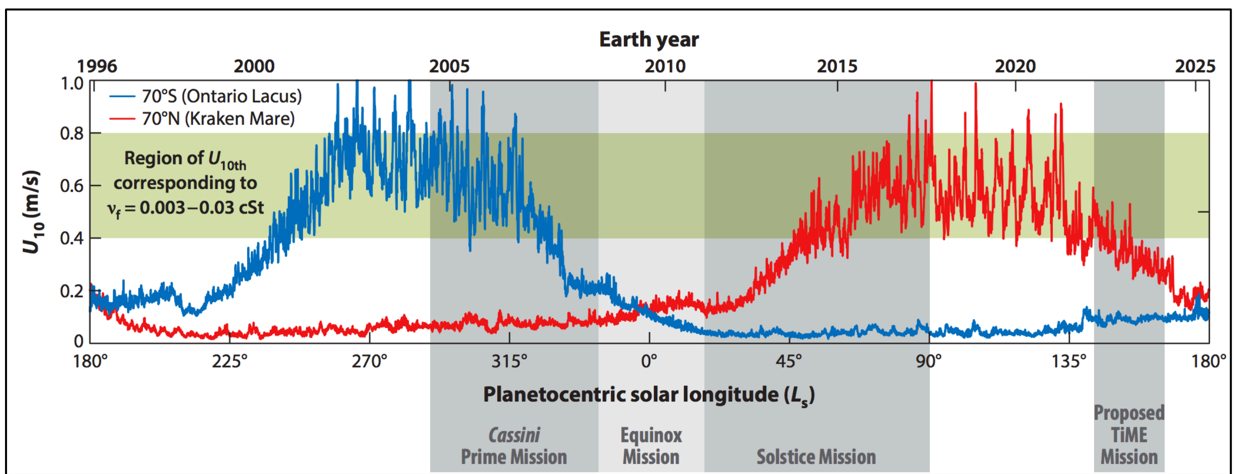

Because Titan is small and spins slowly, its atmospheric circulation has weak horizontal temperature gradients (Coriolis force is less important than on Earth).

Annual mean:
S = Sunlight
OLR = Outgoing Longwave Radiation

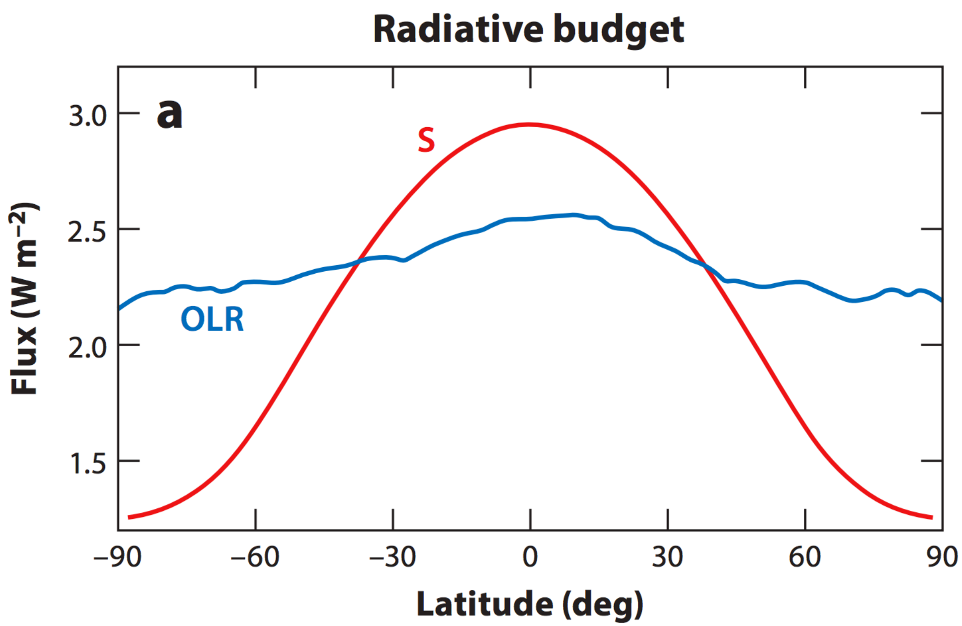

CH4 humidity 100% between 40 km and 8 km altitude; below saturation closer to the ground.

Mitchell & Lora 2016

Table 3 Radius of deformation on Earth and Titan

Parameter	Earth	Titan
Brunt-Väisälä frequency, N (s^{-1})	10^{-2}	5×10^{-3}
Scale height, H (km)	7	20
Coriolis parameter, f (s^{-1})	10^{-4}	10^{-5}
Deformation radius, L_D (km)	700	10^4
Confinement height, H_c (km)	NA	5

Titan's thick atmosphere (high column heat capacity) and weak insolation allow winds to cause a weak equator-pole gradient in surface temperature

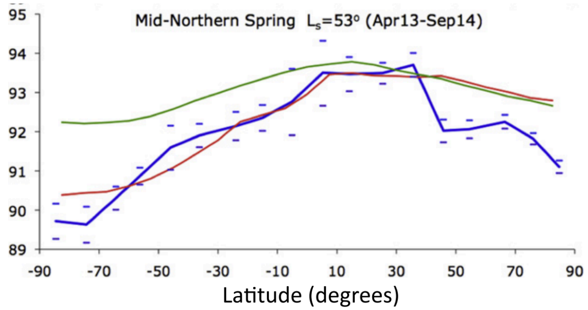

Figure 1. Measured surface brightness temperatures (blue) on Titan compared with GCM predictions, for five approximately two-year periods during the *Cassini* mission. The error bars are two standard deviations, calculated from the

Jennings et al.
Astrophysical Journal 2016

Table 2 Climate timescales ordered by increasing value

Mitchell & Lora 2016

Description	Equation or reference	Value (years)
Boundary layer radiative	$\tau_{\text{rad,BL}} \simeq \tau_{\text{IR,BL}} \frac{C_p \Delta p_{\text{BL}}}{4 g \sigma T^3_{\text{BL}}}$	~7
Shallow overturning	$\tau_{\text{dyn,BL}} \simeq \frac{H_{\text{BL}}}{\dot{T}_{\text{rad}}} \left(\frac{g}{C_p} - \frac{\Delta T_{\text{BL}}}{H_{\text{BL}}} \right)$	~10
Liquid infiltration	Hayes et al. 2008	~10–20
Annual period	$2\pi/\omega_{\text{orbit}}$	~29.5
Troposphere radiative	$\tau_{\text{rad,tropo}} \simeq \tau_{\text{IR,tropo}} \frac{C_p \Delta p_{\text{tropo}}}{4 g \sigma T^3_{\text{tropo}}}$	~200
Tropospheric overturning	$\tau_{\text{dyn,tropo}} \simeq H_{\text{tropo}}/w \simeq \frac{H_{\text{tropo}}}{\dot{T}_{\text{rad}}} \left(\frac{g}{C_p} - \frac{\Delta T_{\text{tropo}}}{H_{\text{tropo}}} \right)$	~500
Methane residence time	$\tau_{\text{CH}_4\text{,res}} \simeq \frac{L_v \times 2{,}250 \text{ kg m}^{-2}}{R}$	~900
Milankovitch cycles	Aharonson et al. 2009	~10^4

Strong seasonal cycle in winds (“single Hadley cell”)

Streamfunction (kg/sec) $\psi = \int_A^P (u\,\mathrm{d}y - v\,\mathrm{d}x)$

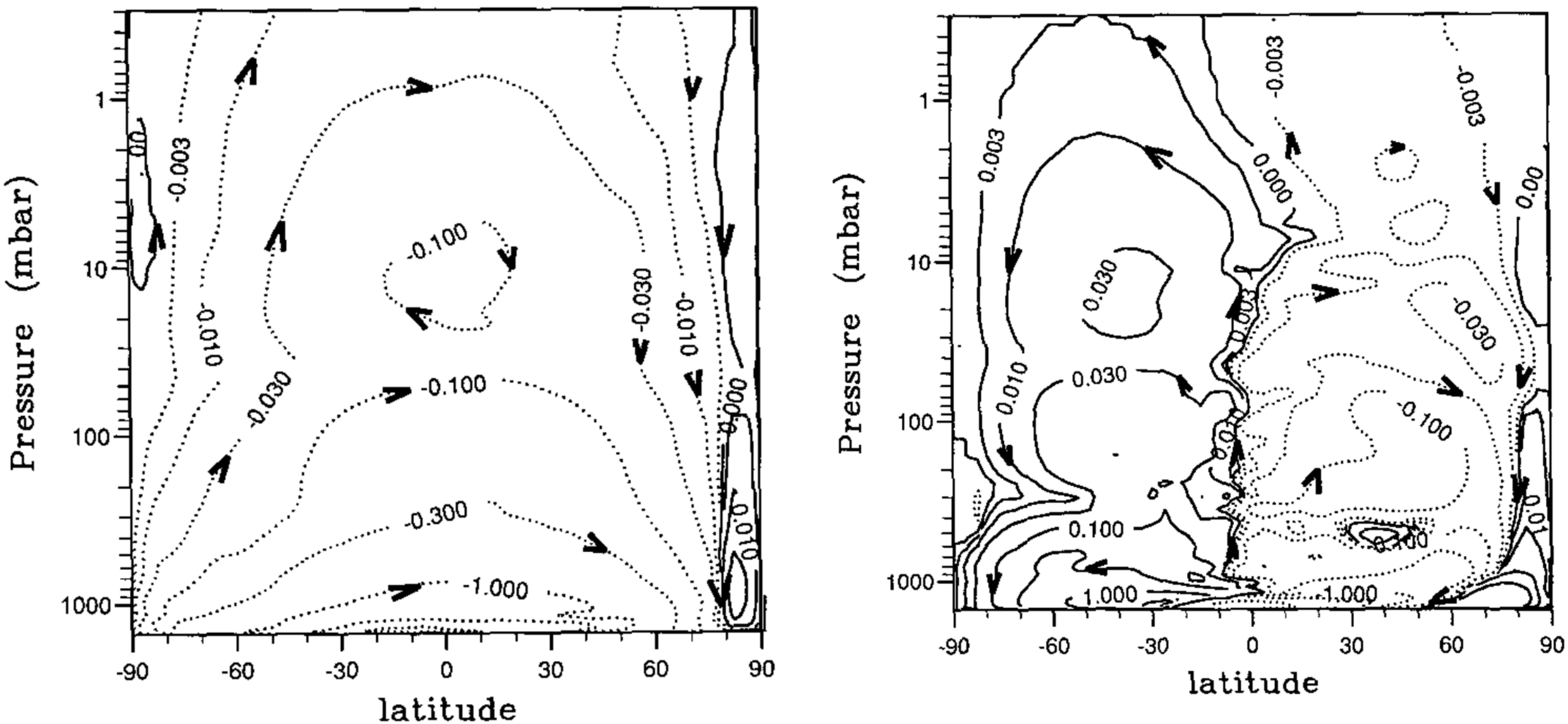

Hourdin 1995

Strong seasonal cycle in clouds (and precipitation)

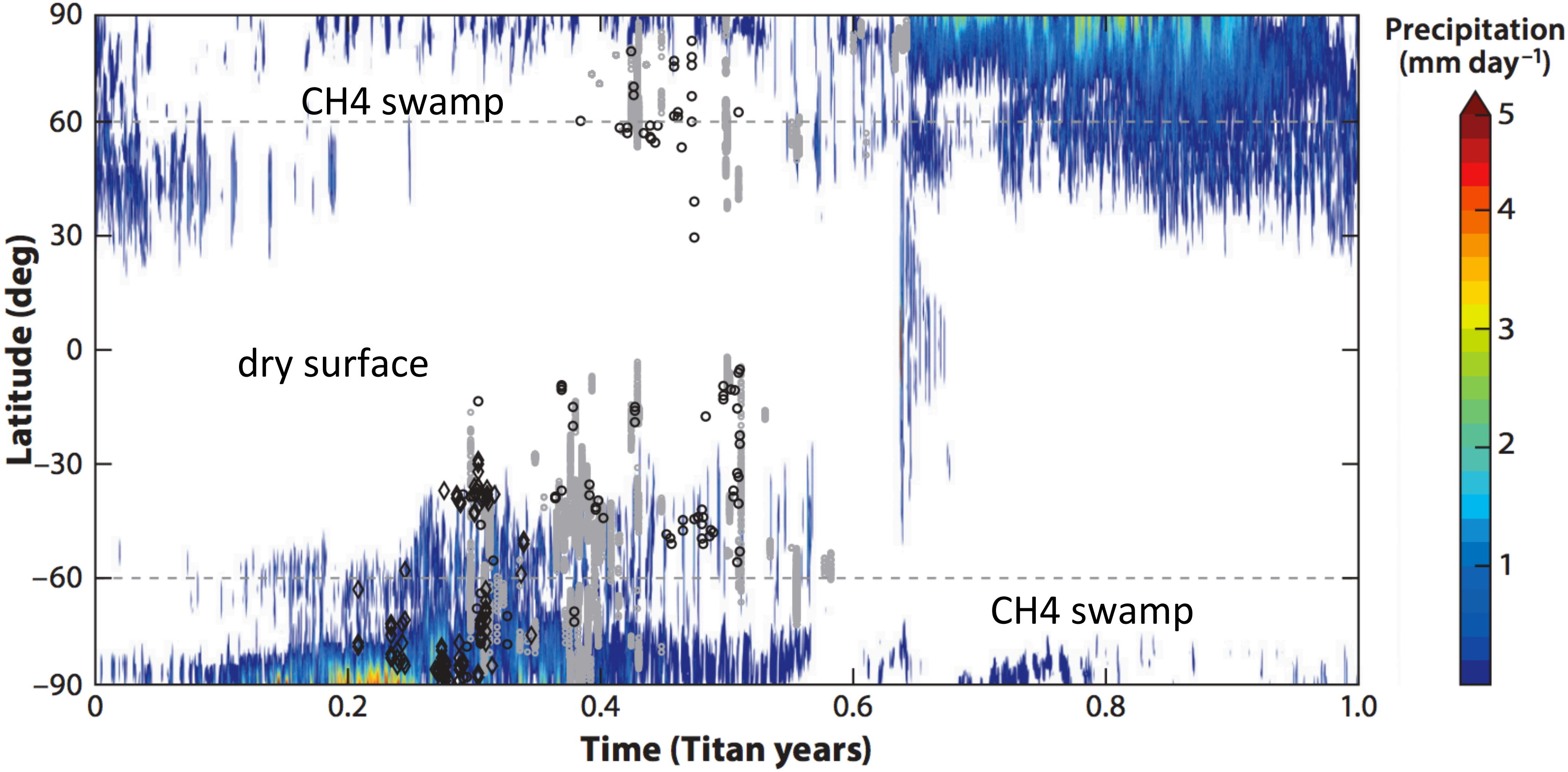

Figure 4

The precipitation distribution (*colors*) from the wetlands simulation with the Titan Atmospheric Model compared to tropospheric cloud locations as observed by the Imaging Science Subsystem (ISS), the Visual and Infrared Mapping Spectrometer (VIMS), and ground-based telescopes. The edges of the wetlands are shown by dashed lines.

Orbital cycles of Saturn (→ orbital cycles in insolation on Titan) may explain why lakes are mostly in the N Hemisphere

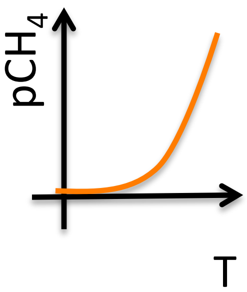

Nonlinear (Clasius-Clapeyron) increase in pCH4 with T

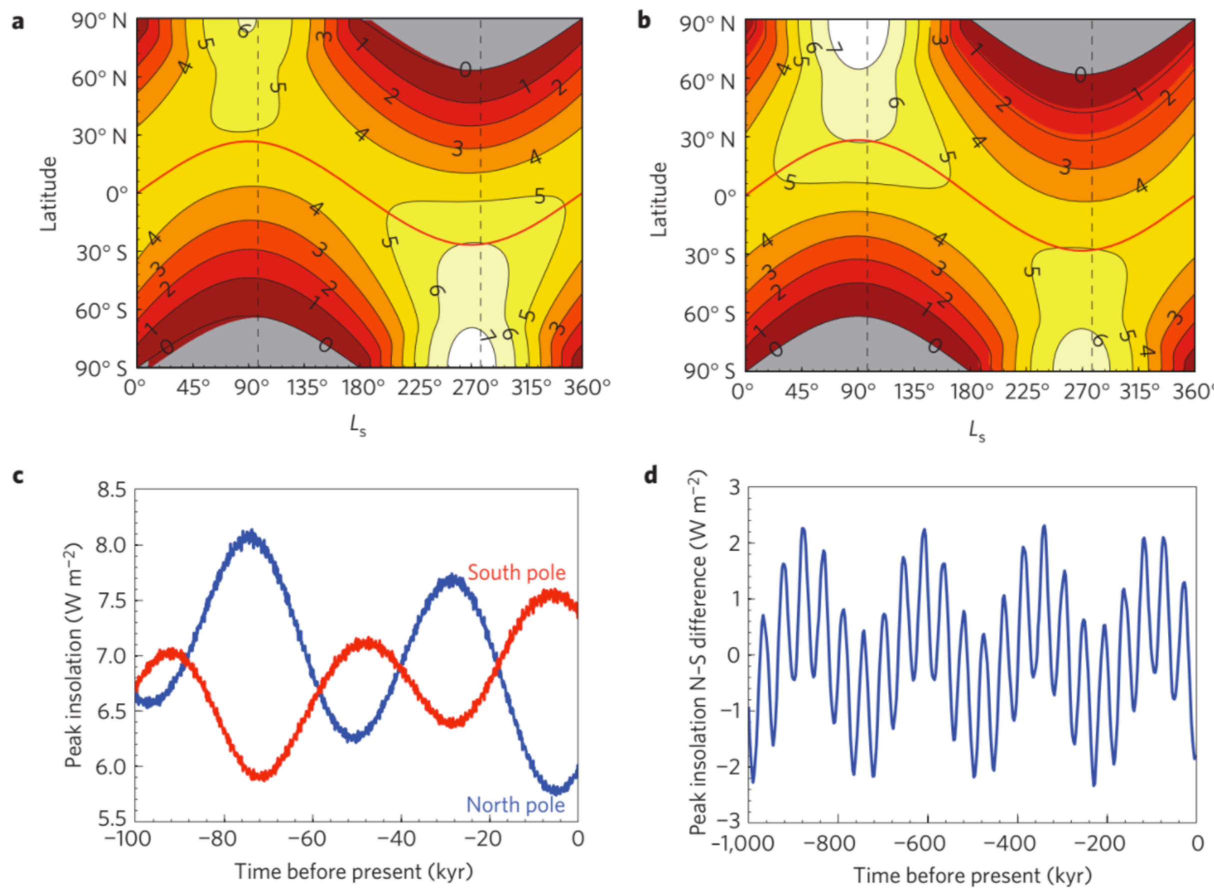

Figure 3 | Incoming solar radiation. a,b, The insolation function at the top of Titan's atmosphere (contours in W m^{-2}). Two cases are contrasted: **a**, the present day ($t = 0$, $L_{s,p} = 277.7°$, $e = 0.054$) and **b**, the time at which $L_{s,p}$ was 180° away from the present ($t = -31.5$ kyr, $L_{s,p} = 97.7°$, $e = 0.046$). **c**, Peak annual insolation incident at the top of the polar atmosphere over the past 100 kyr. **d**, Peak annular insolation difference between the north and south poles over the past 1 Myr.

Aharonson et al., Nature Geoscience 2009

Surface processes as a record of climate: Titan

EXPLORATION OF TITAN

CLIMATE DRIVERS

SURFACE PROCESS RESPONSE

Questions about Titan's valleys:

(1) Mechanical or chemical erosion?
(2) Incision of channelized surface flows, or erosion driven by sapping?
(3) Catastrophic flows, or sustained/repeated flows of smaller magnitude?
(4) Is fluvial erosion due to observed valleys superficial relative to total relief (like Mars' highland valley networks), or the dominant process that controls relief (like on Earth)?
(5) Bedrock channels or self-formed alluvial channels?

(1) Mechanical or chemical erosion?

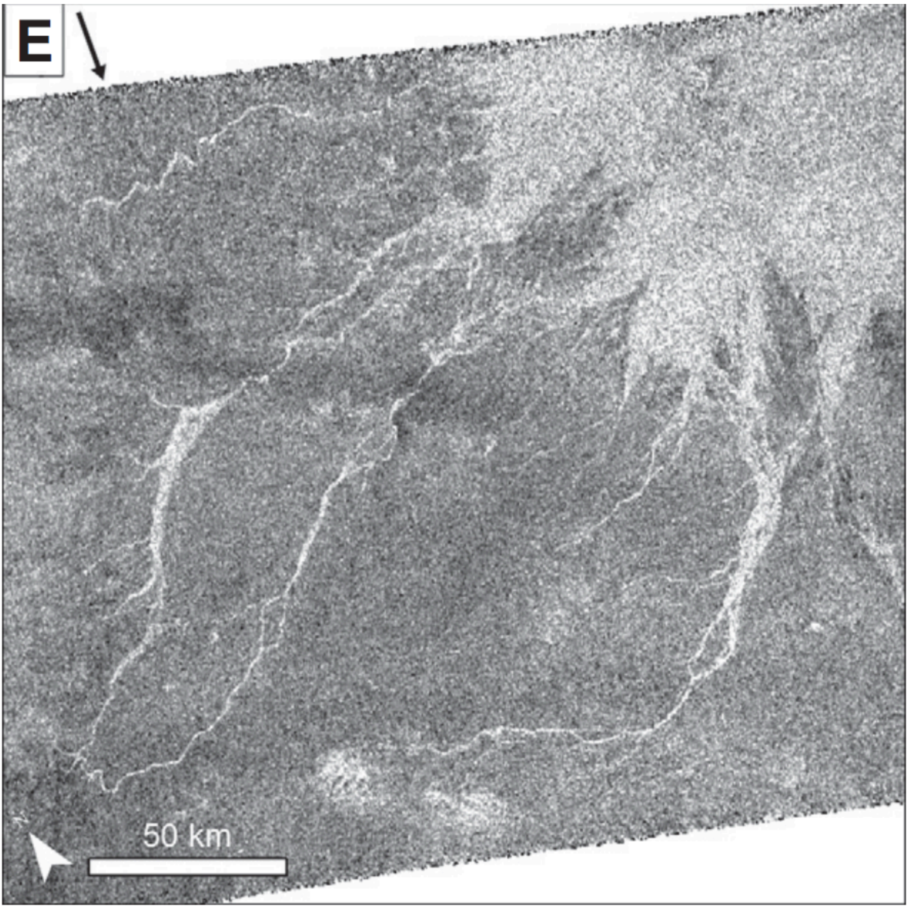

Burr et al. GSA Bulletin 2013

Ice is insoluble in liquid hydrocarbons

Titan's valleys form continuous networks that span hundreds of km

(2) Incision of channelized surface flows, or erosion driven by sapping?

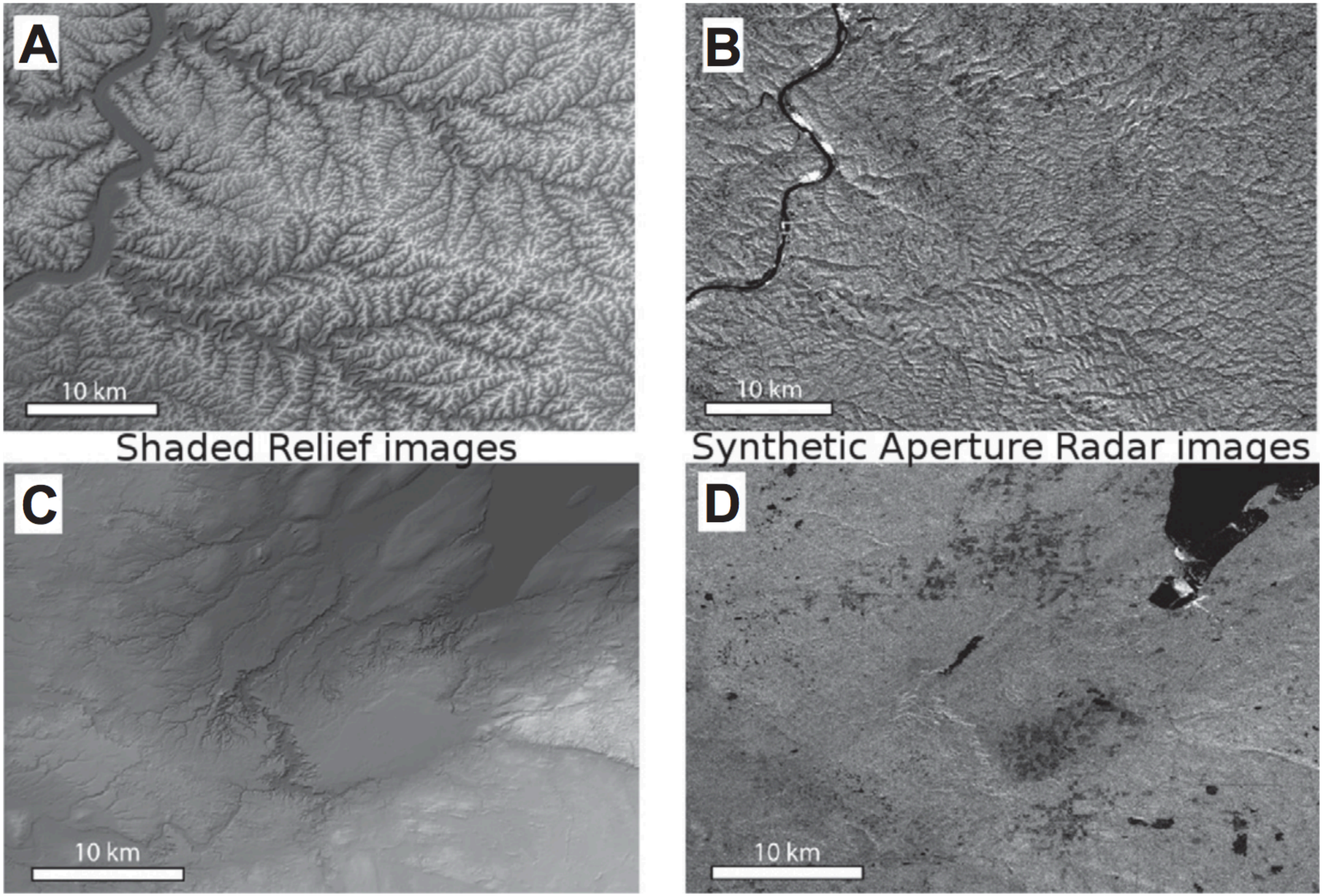

Junction angles of 72 degrees observed for groundwater sapping (Abrams et al., 2009)

Burr et al. 2013

Open question: bedrock channels or alluvial channels?

(3) Catastrophic flows, or sustained/repeated flows of smaller magnitude?

Uniform width, single-thread morphology, large length-to-width ratio

D.M. Burr et al./Icarus 226 (2013) 742–759

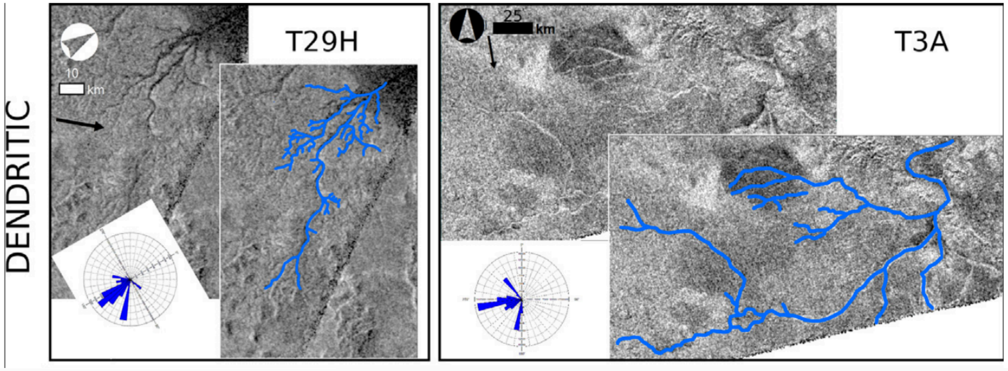

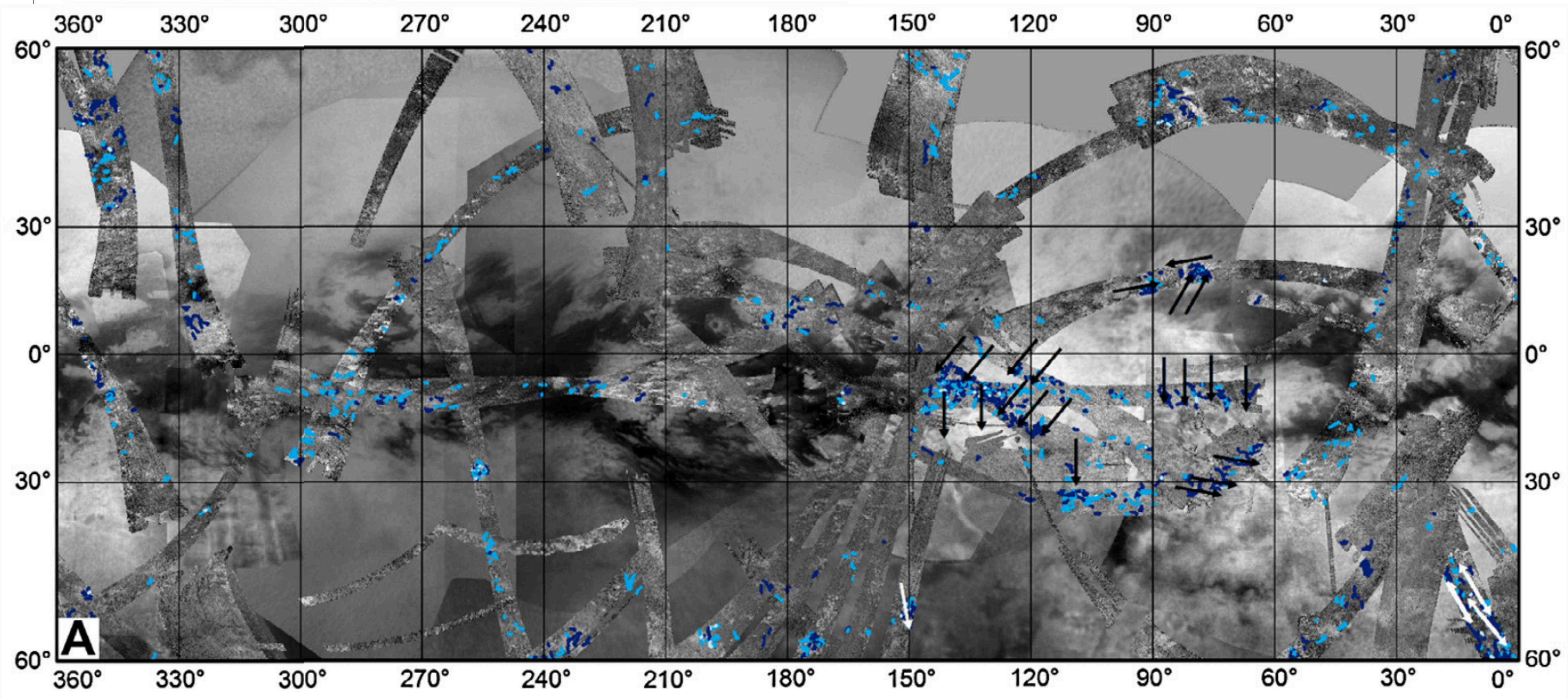

(4) Is fluvial erosion due to observed valleys superficial relative to total relief (like Mars' highland valley networks), or the dominant process that controls relief (like on Earth)?

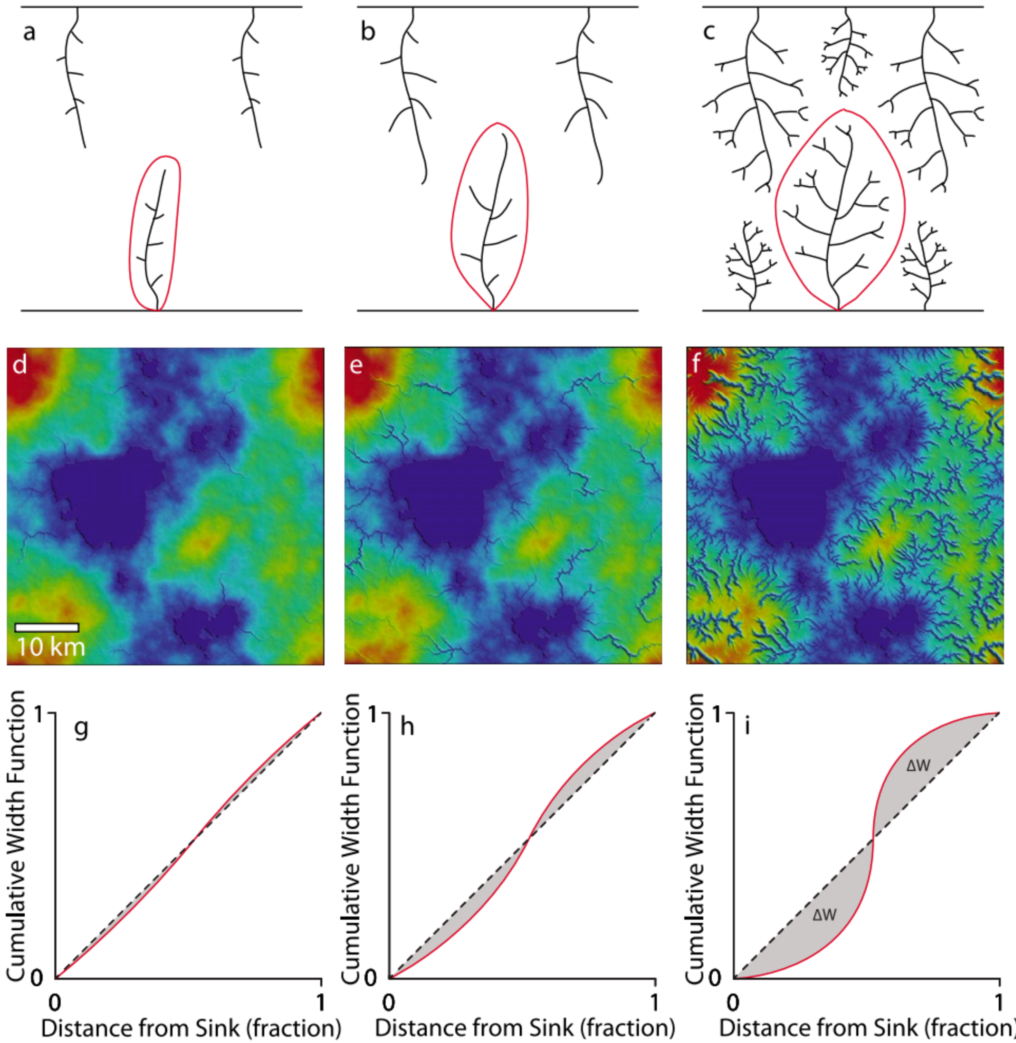

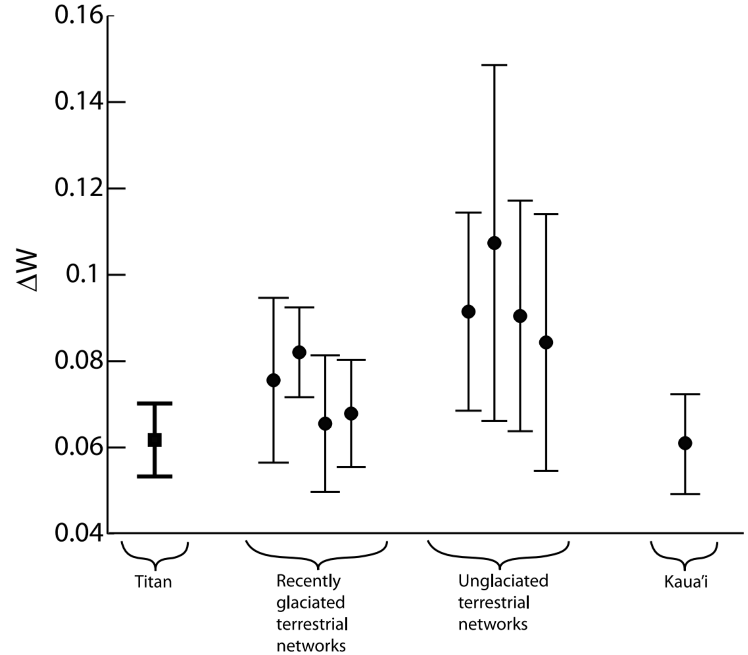

Drainage network morphology suggests modest fluvial exhumation (more similar to Mars than to Earth). Why?

Black et al. 2012

(a) Relatively recent climate change;
(b) Image resolution limits detection of river channels;
(c) Competing process resets landscape (cryovolcanism)?

Analysis of river widths on Titan (following Perron et al. 2006)

$$cPA = Q. \qquad (1)$$

The coefficient c has a value between zero and unity and

$$Q = whu.$$

$$u = \sqrt{\frac{8gRS}{f}}$$

$$\tau^* = \frac{\rho RS}{(\rho_s - \rho)D}$$

steady, uniform flow of Newtonian fluid

$$R = wh/(w + 2h)$$

$$R \approx h$$

$$\rho' = \rho_s/\rho - 1.$$

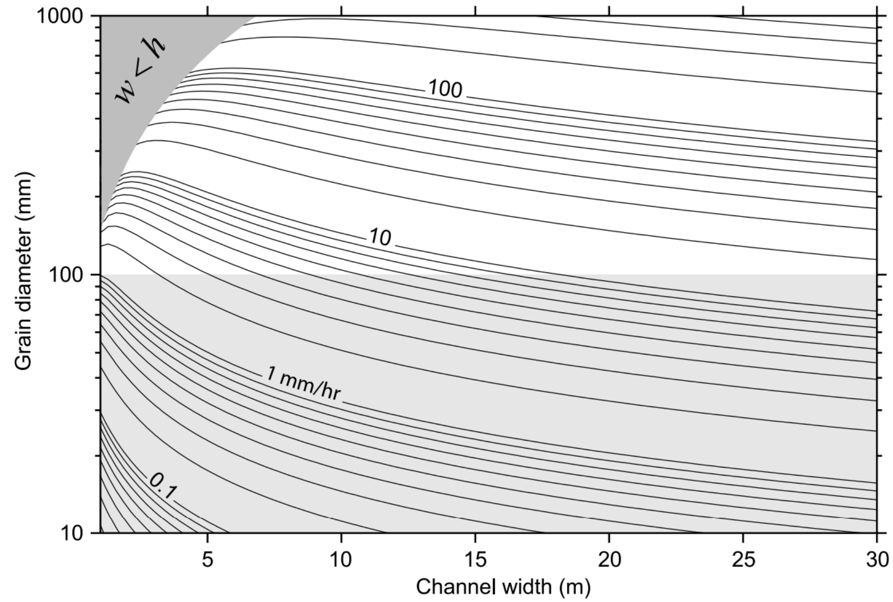

Figure 3. Contour map of the rate of methane precipitation (P_c) required to initiate sediment motion as a function of grain diameter (D) and channel width (w), calculated from equation (6). Contour units are millimeters per hour. The gray region in the upper left corresponds to parameter combinations for which flow depth exceeds channel width, a situation rarely observed in terrestrial rivers. The rectangular shaded region brackets the median grain diameter observed at the Huygens landing site (Figure 2).

$$P = \frac{1}{A}\frac{w^2 R}{w - 2R}\sqrt{\frac{8gRS}{f}}.$$

$$\boxed{P_c = \frac{w}{AS}\left(\frac{8g}{f}\right)^{\frac{1}{2}}(\rho' \tau_c^* D)^{\frac{3}{2}}}$$

Seas are up to 200m deep and mostly CH_4
→ 7×10^4 km^3 (15x Lake Michigan, 55x oil reserves on Earth)

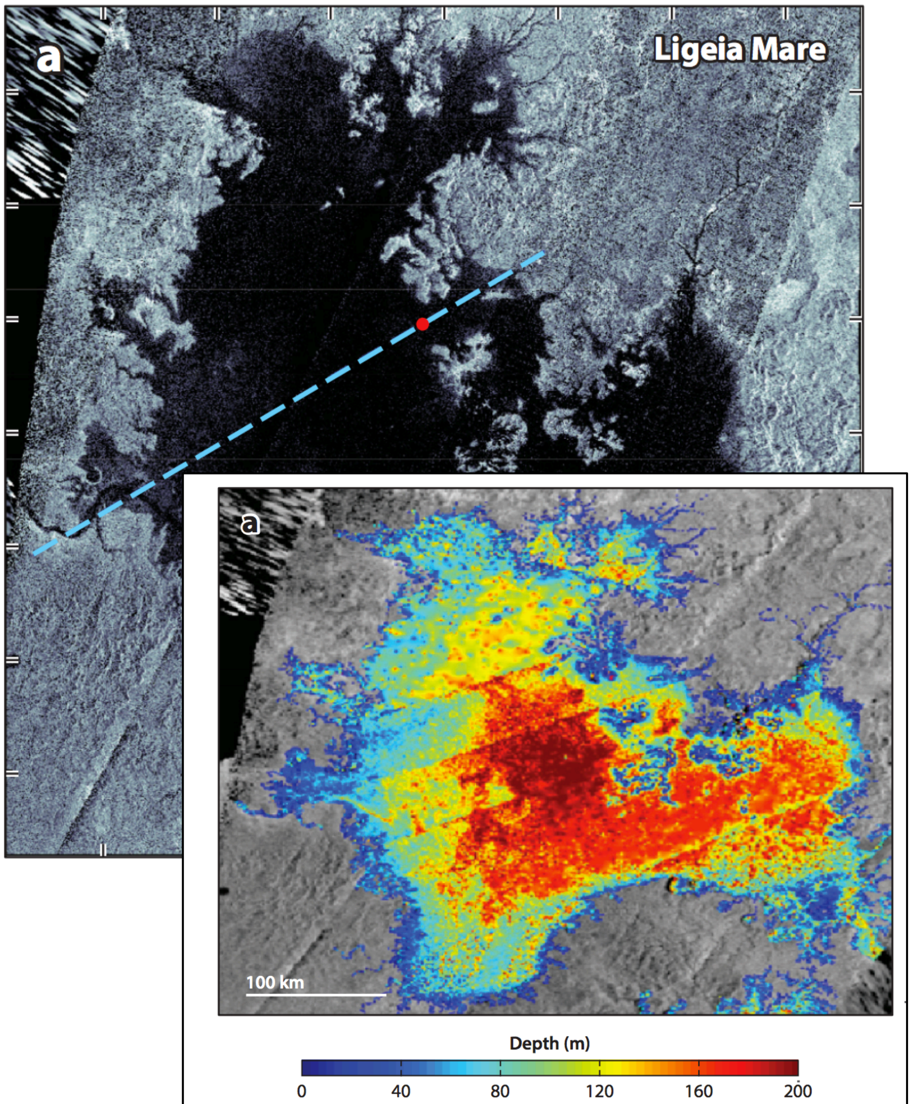

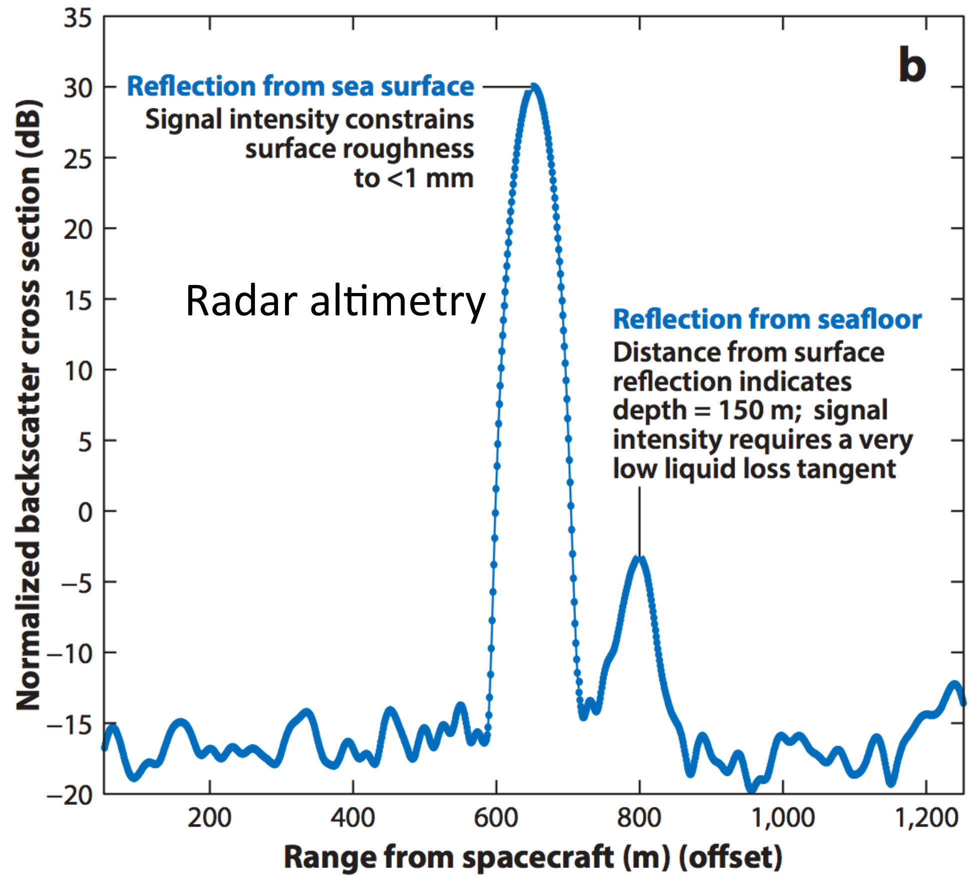

→ *time after radar pulse transmitted* →

Hayes 2016

Titan karst: is groundwater flow important in setting lake levels?

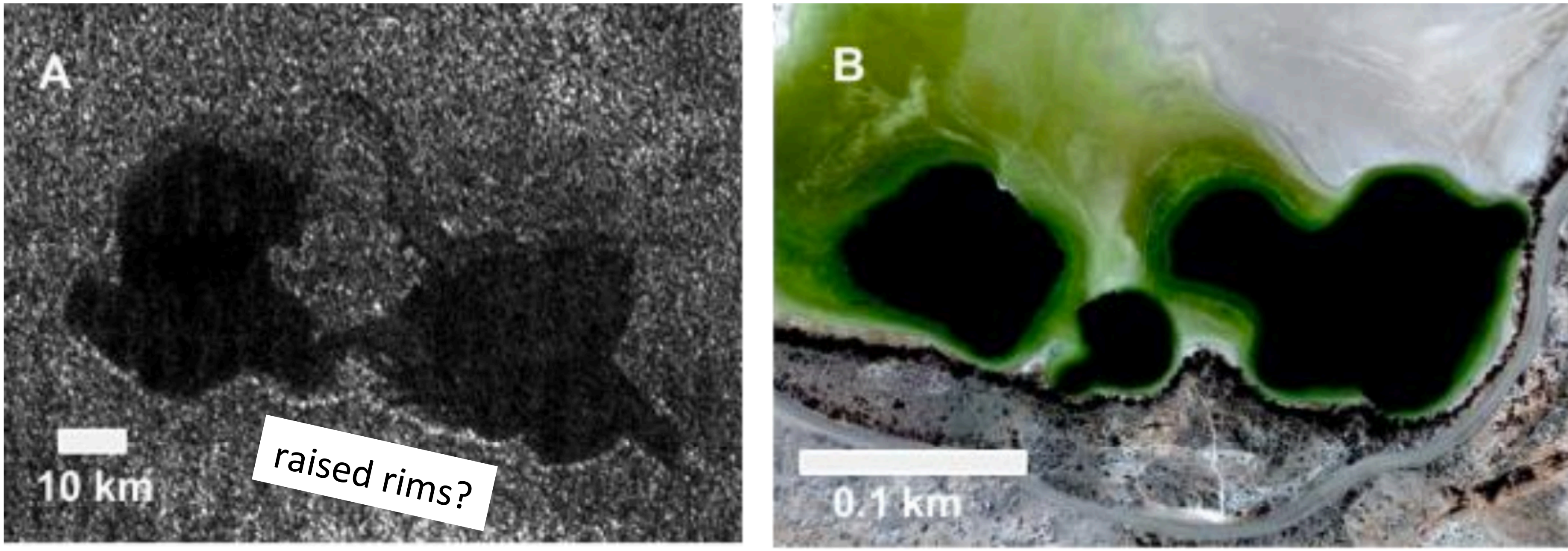

Figure 1. A) T16 SAR of Abeya Lacus, Titan (73°N, 47°W), radar illumination is from the top. B) Google Earth image of Lazy Lagoon, Bottomless Lakes State Park, New Mexico (33.3°N, 104.3°W).

Malaska et al., 2nd International Planetary Caves Workshop, 2015

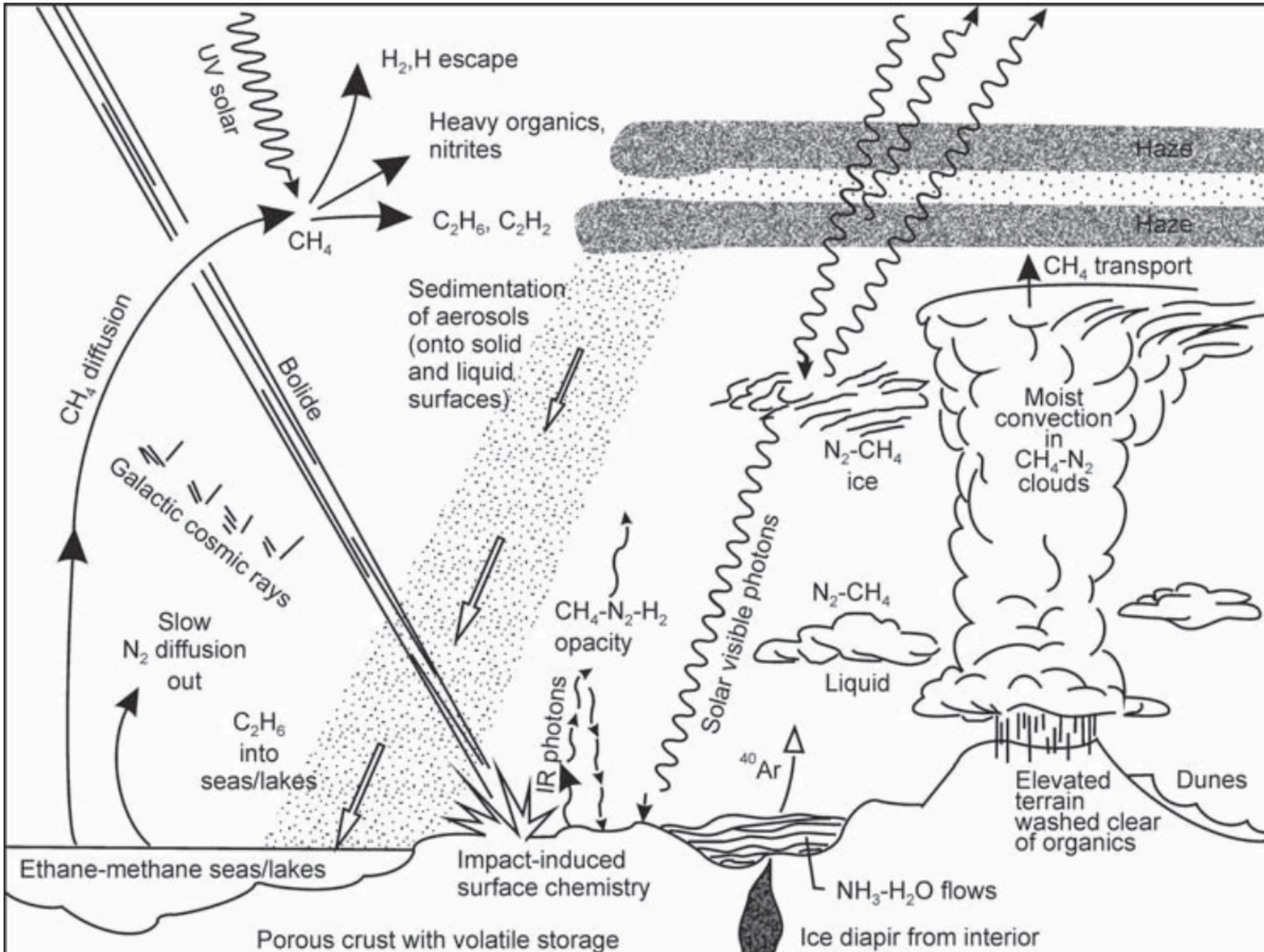
UV solar
H2,H escape
Heavy organics,
nitrites
C_2H_6, C_2H_2
CH_4
Haze
Haze
CH_4 transport
CH_4 diffusion
Bolide
Sedimentation
of aerosols
(onto solid
and liquid
surfaces)
Moist
convection
in
CH_4-N_2
clouds
N_2-CH_4
ice
Galactic cosmic rays
Solar visible photons
CH_4-N_2-H_2
opacity
N_2-CH_4
Liquid
Slow
N_2 diffusion
out
IR photons
C_2H_6
into
seas/lakes
^{40}Ar
Elevated
terrain
washed clear
of organics
Dunes
Ethane-methane seas/lakes
Impact-induced
surface chemistry
NH_3-H_2O flows
Porous crust with volatile storage
Ice diapir from interior

Lunine 1990

Unsolved:

Long term CH_4 cycle – resupply of CH_4?
(Lunine & Atreya, Nature Geoscience 2008)

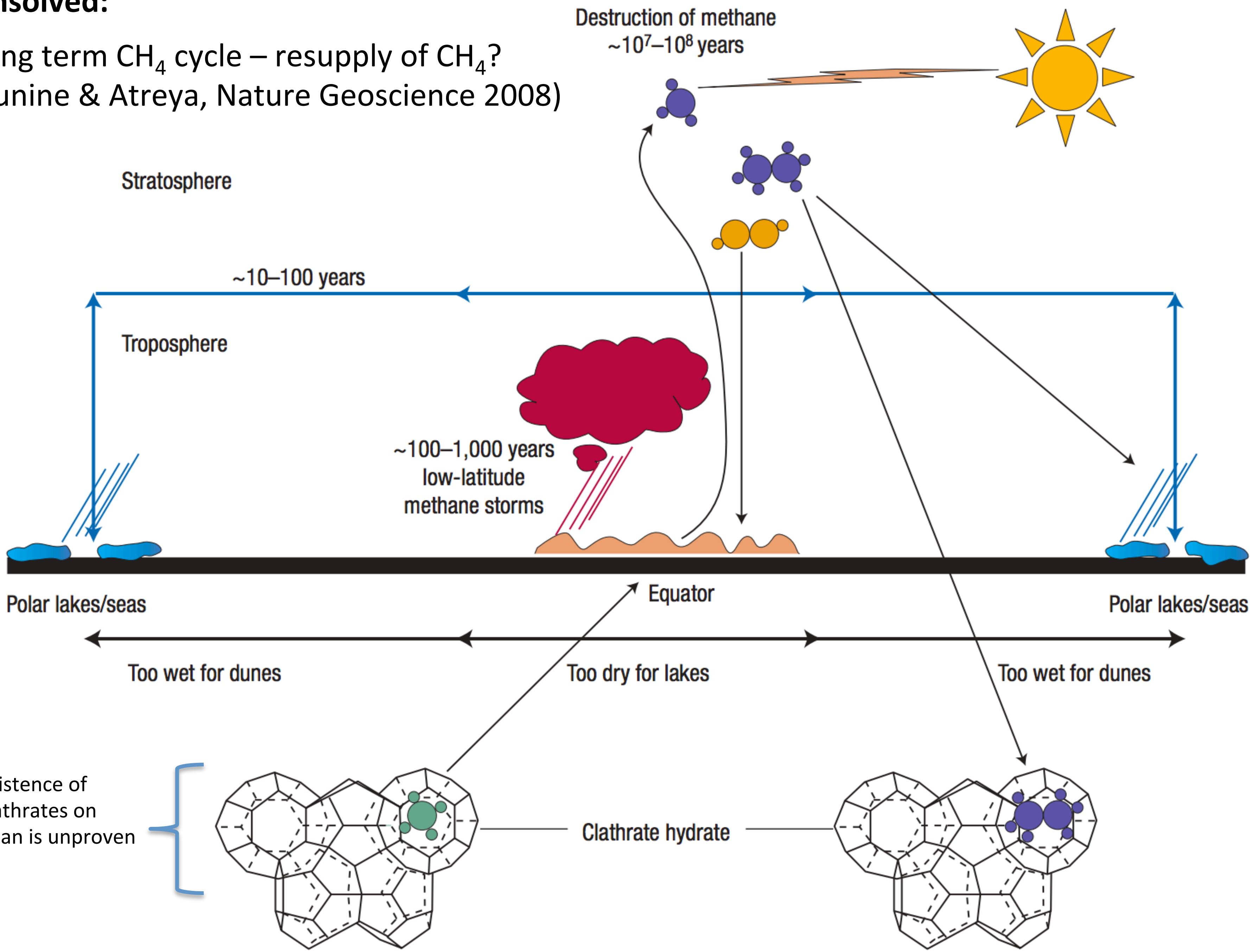

existence of
clathrates on
Titan is unproven

Key points

- Lines of evidence for a “hydrological” cycle on Titan
- Differences between climates of Titan and Earth and how these are reflected in surface geomorphology
- List and explain similarities and differences between the hydrological cycle of Earth and the methanological cycle of Titan

Backup slides

Transcient hillslope evolution

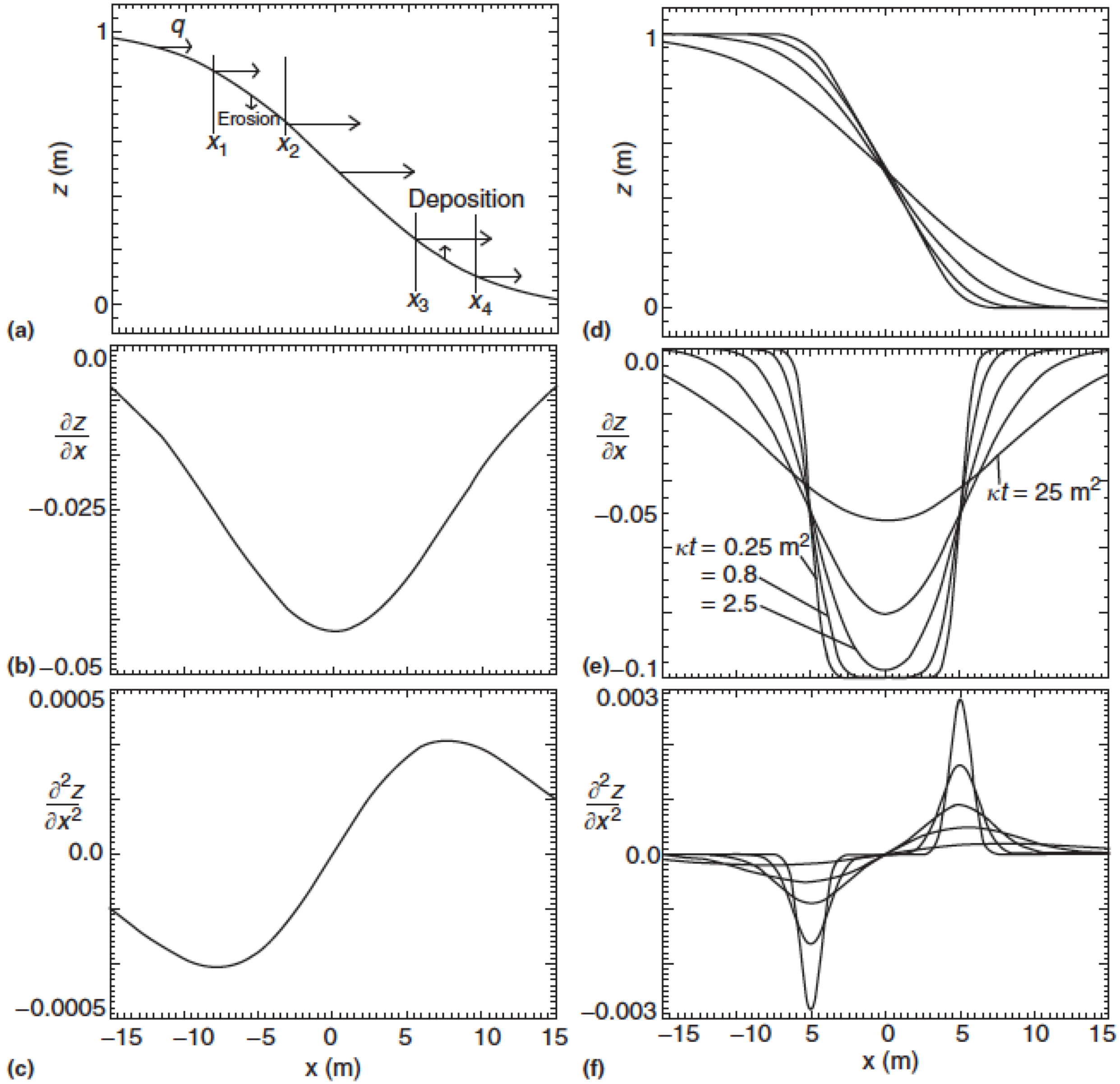

Figure 2 Evolution of a topographic scarp, illustrating (a) elevation, (b) slope, and (c) curvature. In (a), arrows of varying length represent the sediment flux at each point. In the diffusion model, the flux is proportional to the local slope, and the resulting raising or lowering rate of the surface is proportional to the change in flux per unit length, which, in turn, is proportional to the curvature. (d)–(f) Graphs of elevation, slope, and curvature for 5 times following scarp offset ($\kappa t = 0.25$, 0.8, 2.5, 8, and 25 m^2). Modified with permission from Pelletier, J.D., 2008. Quantitative Modeling of Earth Surface Processes. Cambridge University Press, Cambridge.

Pelletier, 2008, ch. 2; also Pelletier, 2013